SPECTROELECTROCHEMICAL STUDIES OF METALLOENZYMES AND POLYMER-COATED GRAPHITE TRANSPARENT ELECTRODES

Thesis by

Napapon Sailasuta Scott

In Partial Fulfillment of the Requirements

for the Degree of

Doctor of Philosophy

California Institute of Technology

Pasadena, California

1980

(Submitted July 1979)

ACKNOWLEDGMENTS

I owe a great deal to Professors Harry Gray and Fred Anson. Harry's support and enthusiasm at the beginning of my education at Caltech is deeply appreciated. Fred's willingness to discuss made the designing of spectroelectrochemical cells successful. The support, enthusiasm and encouragement during my education at Caltech from both Harry and Fred shall not be forgotten.

I also owe a great deal to my parents for providing me with the education and encouraging me to go on to graduate study. I realize the hard work they had to go through in order to put me through school. I only hope that my decision for my future will not disappoint them too much and hope that they will understand. I also thank my American parents, Carl and Melva Lee, for the enjoyable Christmas 1975 and summer of 1976.

I thank the members of the Gray and Anson groups both in the present and past for being there and for those delightful conversation both scientific and social.

Drs. Steve P. Cramer and Noboru Oyama deserve special thank for their collaboration--otherwise Chapters 2 and 3 would not be in this thesis. I also thank the members of the glass and mechanical shops for their helpful assistance.

Lastly, I thank my husband, Robert A. Scott, for his encouragement and companionship. His companionship made my last two years less painful and bearable. Without him I would not have stayed this long. He also taught me to analyze my kinetics data reported in this thesis. I am looking forward to our future together.

ABSTRACT

Thermodynamic parameters of metalloprotein electron transfer reactions, namely reduction potentials, enthalpies and entropies, are determined by means of spectroelectrochemical techniques. The studies concentrate on blue copper protein (Rhus vernicifera stellacyanin, Phaseolus vulgaris plastocyanin and Pseudomonas aeruginosa azurin), and c-type cytochromes (horse heart cytochrome c, Pseudomonas aeruginosa cytochrome c-551 and cytochrome oxidase). The results show that within the same class of metalloprotein studied, i.e., blue copper protein and cytochrome c, the observed enthalpy and entropy changes can be used as criteria for determining solvent access of the metal centers. The more access the metal center has to the solvent, the less negative enthalpy and entropy changes are associated with its reduction process. The increase in solvent access of the metal center is in the order cytochrome cd < cytochrome c-551 $\sim$ cytochrome c and azurin < plastocyanin < stellacyanin. The conclusions agree well with those from kinetic studies.

The reduction potentials of heme b_5 of liver sulfite oxidase have been determined. The potentials of the intact enzyme and those in which the molybdenum moeity has been removed are very similar, indicating that there is no interaction such as to alter the reduction potential of heme b_5 between the heme and molybdenum prosthetic groups. The reduction of the heme b_5 of chicken liver sulfite oxidase by $Fe(EDTA)^{2-}$ has also been investigated. The rate of electron transfer has been analyzed within the framework of the relative Marcus theory of outer sphere electron

transfer. The electrostatic corrected self-exchange rate constant is two orders of magnitude greater than the corresponding value of cytochrome c, indicating more accessibility of the heme of sulfite oxidase than in those of cytochrome c. The activation parameters have also been determined. It is proposed that electron transfer mechanism employed by heme b_5 of sulfite oxidase is very similar to that employed by cytochrome c, i.e., via exposed heme edge.

Spectroelectrochemical studies of the polymer-coated graphite transparent electrodes have been performed. The amount of polymer adsorbed on electrode surface was determined spectrally. The rates of attachment and detachment of Ru(III)(EDTA) to and from the pyridine group on the polymer backbone were studied. It was found that reactivity of the formation and detachment of Ru(EDTA) complex was less than the corresponding homogeneous reactions. The electrochemical properties of such electrodes were also reported.

TABLE OF CONTENTS

CHAPTER 1

THERMODYNAMIC STUDIES OF ELECTRON TRANSFER REACTIONS OF METALLOENZYMES AND SOME INORGANIC COMPLEXES

INTRODUCTION

Electron transfer properties of metalloenzymes have been subjected to current investigation [1,2]. Most of the investigations involved kinetics of electron transfer reactions in order to determine the mechanisms employed by metalloenzymes as well as small molecule reagents. The redox reaction mechanisms of inorganic complexes have been classified as outer and inner sphere electron transfers [3]. Each mechanism is characterized by the geometry of the nuclei in the transition state. Outer sphere reactions are those in which the complementary oxidation state change occurs via a path which does not involve the mutual sharing of a bridging ligand in the coordination spheres of both metals, while oxidation state change for inner sphere reactions involves the mutual sharing of a bridging ligand. The redox reaction mechanisms of metalloenzymes are expected to span a wider range due to their complexity. Marcus theory for outer sphere electron transfer reactions [4] has been used to interpret kinetics of electron transfer reactions of inorganic complexes with success [5-7].

In recent years the Marcus theory has been used by bio-inorganic chemists; application of the theory to the metalloenzymes kinetics resulted in a model for interpreted metalloenzyme electron transfer reactions [2,8]. In this model the electrostatic-corrected self-exchange rate constant (k_{11}^{corr}) for each metalloenzyme redox reaction based on cross reaction with inorganic reagent was calculated. Comparison of the calculated k_{11}^{corr} resulted in relative activity among metalloenzymes. The treatment has been applied successfully to blue copper proteins and cytochromes [8].

However, upon consideration of redox reactions of metalloenzyme-metalloenzyme and multi-site metalloenzymes (e.g., cytochrome oxidase), the measured rate constants are larger than would be expected based on Marcus theory [8]. It is conceivable that these protein-protein reactions might benefit from numerous interactions apart from those described in Marcus' treatment. Moreover, as free energy reactivity relationships are expected to exist, questions arise for the redox reactions of proteins with coupled redox sites, since they are designed to use the excess free energy available from an oxidation-reduction cycle.

Another method of arriving at the electron transfer mechanisms of metalloenzymes is the thermodynamic study of their electron transfer reactions. Thermodynamics, in a classical sense, deals with states of systems in energetic terms, and processes are involved only insofar as they let a system go from one state to another, i.e., it is independent of the path employed upon going from initial to final states. The state of a system is thermodynamically characterized by a fundamental equation which relates the internal energy of the system to its entropy, its volume, and its composition in terms of mole numbers [9]. This fundamental system can be transformed into quantities known as Gibbs free energy (G), enthalpy (H), and entropy (S). Gibbs free energy change (ΔG) of a system is directly proportional to oxidation-reduction potential E^0 of the system. The knowledge of E^0 of the system, especially those of metalloenzymes, will aid the understanding of mechanisms of electron transport in the physiological processes, e.g., oxidative phosphorylation and photosynthesis [10]. Accurate E^0 values are useful in determining

the sequence of electron transfers among enzymes in a particular chain since electrons are transferred successively to enzymes with increasingly positive redox potentials. Furthermore, it is also important in evaluating intermolecular interactions between enzymes, intramolecular interactions in enzymes with multiple redox centers, and effects of structural modifications [11].

As for enthalpy and entropy changes, the latter is known, for transition metal complexes, to be strongly dependent upon the charge and the nature of coordinated ligands [12]. It has been considered as the effect of structure-making and structure-breaking, due to surrounding solvent molecules [13]. Therefore, combination of free energy change and entropy change should allow the achievement of a better understanding of the structural factors affecting the reaction mechanisms.

This chapter will discuss the thermodynamic studies of metalloenzymes, namely stellacyanin, plastocyanin, azurin, and c-type cytochromes, i.e., horse heart cytochrome c, bacterial cytochrome c-551, and cytochrome cd. The special apparatus designed to be used in determining the temperature dependence of reduction potentials will be reported. The results will be compared, if possible, with those of inorganic complexes in order to understand processes involving the reduction. The attempt to use the Marcus and Sutin approach [14] to analyze activation parameters obtained kinetically by taking into consideration the observed thermodynamic parameters (Appendix I) will be reported.

A brief summary of metalloenzymes to be studied in this chapter is presented. Blue copper proteins to be studied function as electron

mediators between membrane bound proteins. French bean (Phaseolus vulgaris) plastocyanin oxidizes cytochrome f in the photosynthetic electron transport system between plastoquinone and P700, the primary donor of Photosystem I [15]. Pseudomonas aeruginosa azurin mediates electron transport between cytochrome c-551 and cytochrome oxidase (Figure 1) [16]. The physiological partner of Rhus vernicifera stellacyanin is yet to be identified [17].

The X-ray crystal structure analysis of poplar plastocyanin has been reported at 2.7 Å resolution [18]. The copper atom in plastocyanin has a highly distorted tetrahedral coordination geometry. It is coordinated by the sulfur atoms of cysteine 84 and methionine 92, and by the δ-nitrogen atoms of the imidazole groups of histidine 87 (Figure 2). It is also reported that in one direction access to the copper atom from the solvent is blocked only by the imidazole group of histidine 87 and the approach of solvent molecules to the copper center is limited to about 6Å. The coordination environment of the copper atom in azurin has not yet been identified due to poor resolution of electron density map [19]. It is proposed that the copper atom is probably bound to a cysteine, a methionine, and two histidine residues. A rough estimate of the shortest distance from the surface of the molecule to the copper atom is approximately 7.5 Å [19]. Recently, X-ray absorption spectroscopic studies reported the presence of a thiolate sulfur in the first coordination sphere of the copper in azurin [20]. The presence of nitrogen ligands and probably another sulfur ligand has also been established. Unfortunately, there is no X-ray crystal structure analysis for stellacyanin reported at this time. However, electron nuclear double resonance (ENDOR) studies suggest a presence of nitrogen ligand [21].

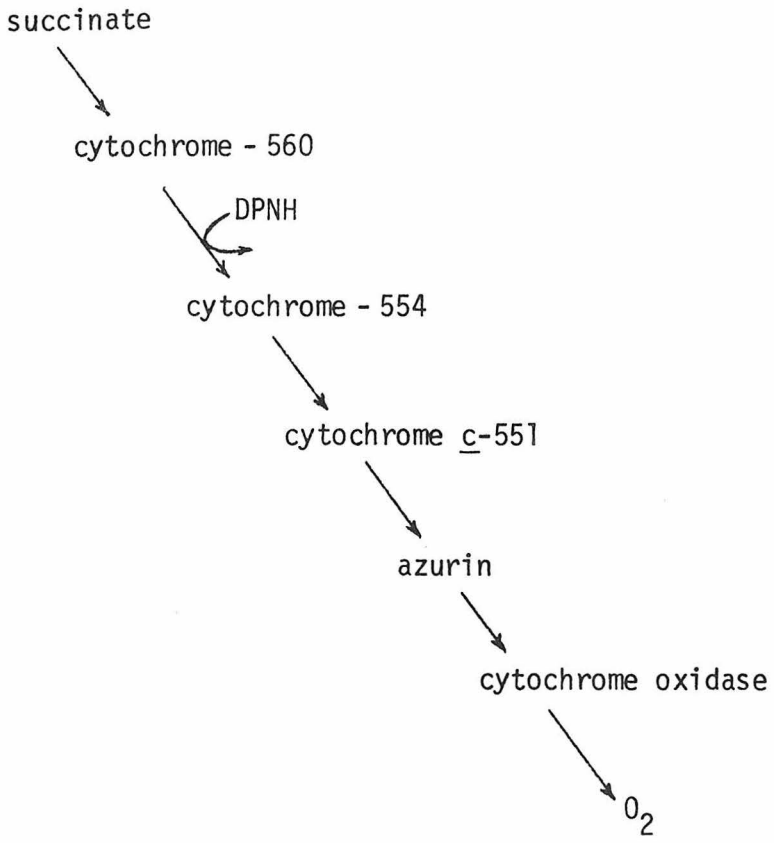

Figure 1. The position of cytochrome c-551, azurin, and cytochrome oxidase in the respiratory redox chain of Pseudominas aeruginosa.

Figure 2. The copper coordination of plastocyanin (taken from reference [18].)

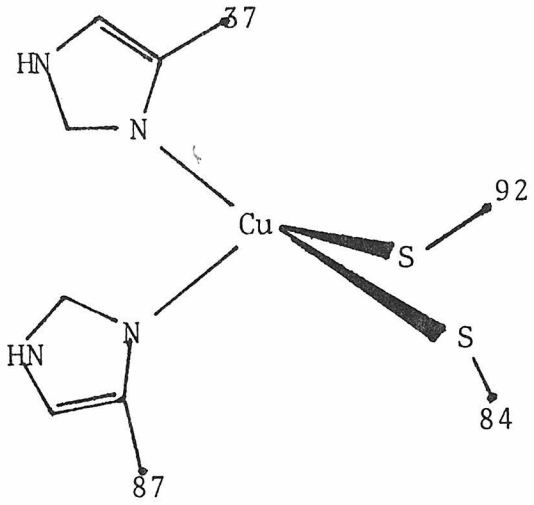
37
HN
N
92
Cu
S
N
HN
S
84
87

Resonance Raman spectral data indicate a four [22] or five [23] coordinate model for the blue copper site composed of one sulfur and three or four nitrogen ligands. The copper site (type 1) in these proteins exhibits a characteristic intense electronic absorption band system, which peaks at about 600 nm ($\varepsilon > 2 \times 10^3$) and an extremely small $A_{||}$ EPR spectral parameter [24]. Spectroscopic studies of cobalt(II) derivatives of these blue proteins have established that the 600 nm band is the ligand to metal charge transfer from cysteine [25,26].

The second type of electron transfer proteins to be studied is c-type cytochromes. Horse heart cytochrome c functions as an electron carrier between the membrane bound cytochrome c_1 and cytochrome oxidase [27]. Cytochrome c-551 is the physiological partner of azurin in the Pseudomonas aeruginosa respiratory chain in which cytochrome cd is the terminal protein [11]. Cytochromes of c-type are protein containing c-heme (Figure 3) covalently attached to the polypeptide chain by at least one thio-ether bond to a cysteine residue [27]. The heme c exhibits a characteristic visible absorption spectrum, an intense Soret band at about 400 nm ($\varepsilon \sim 10^5$), and bands at about 550 and 510 nm in the reduced form (Figure 4). Bacterial cytochrome cd is a dimer of two identical polypeptide chains, each containing a covalently bound heme c and a noncovalently bound heme d [28-30]. It has been established [30,31] that the enzyme functioned as a dimer, i.e., a four-electron system.

The X-ray crystal structure analysis of horse heart cytochrome c and cytochrome c-551 has been completed by Dickerson and coworkers [32, 33]. Their analysis revealed that they have the same basic folding

Figure 3. The structure of heme c

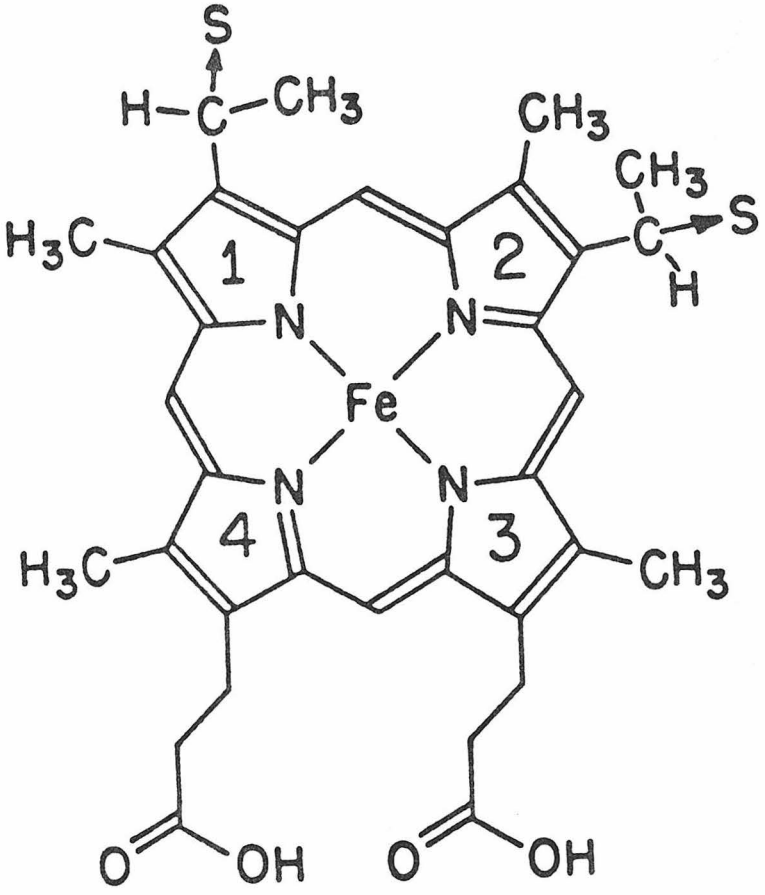
S
H–C–CH3
CH3
CH3
S
H3C
1
2
C
H
N
N
Fe
N
N
4
3
H3C
CH3
O
OH
O
OH

Figure 4. The reduced and oxidized cytochrome c spectra

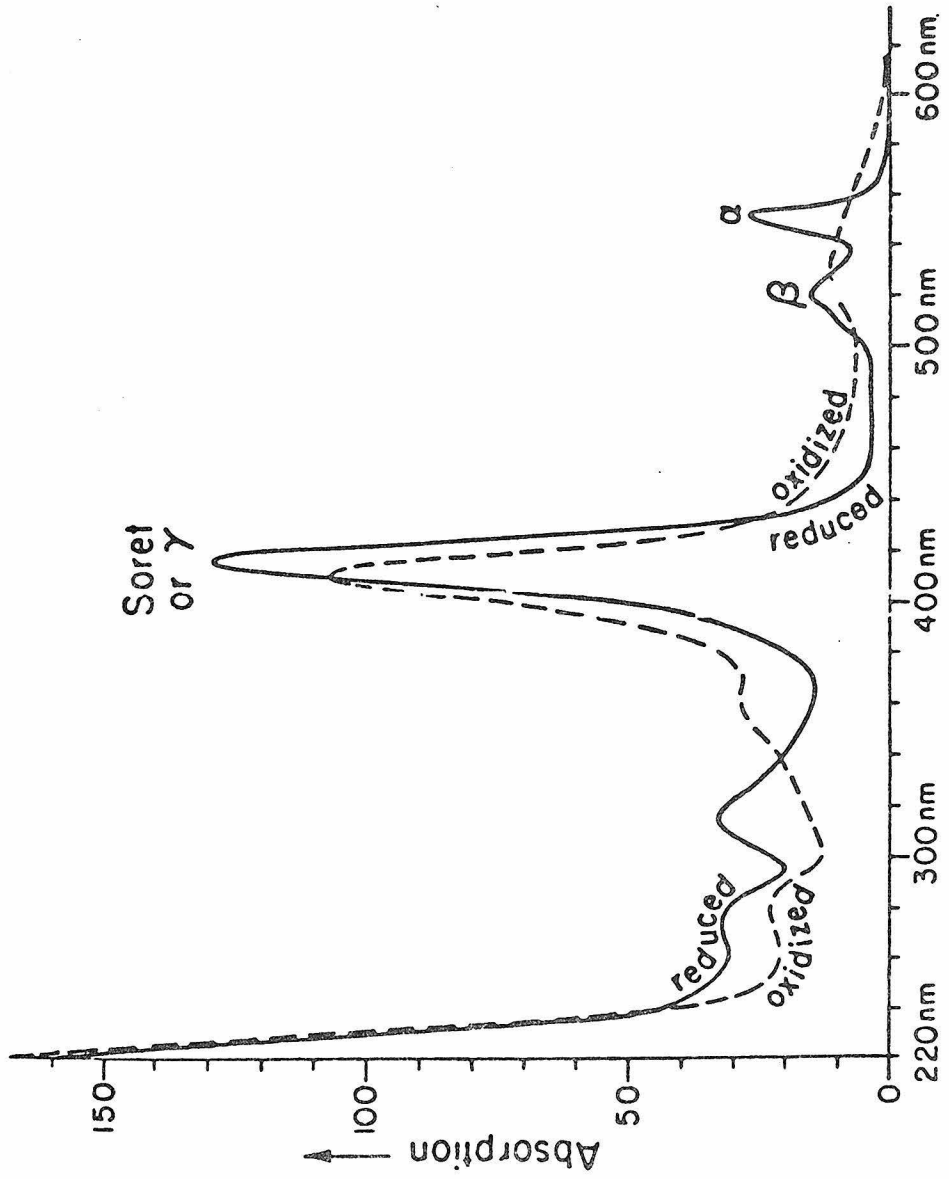
Absorption
150
100
50
0
220nm
300nm
400nm
500nm
600nm
Soret
or γ
reduced
oxidized
α
β
reduced
oxidized

pattern and hydrophobic heme environment except for a large deletion at the bottom of cytochrome c-551 heme crevice owing to the twenty fewer amino acid residues than horse heart cytochrome c [33]. Preliminary X-ray examination of the crystallized cytochrome cd confirmed that the enzyme is a dimer with two identical subunits [34].

SPECTROELECTROCHEMICAL TECHNIQUE

Spectroelectrochemical technique is a technique suitable for the study of the kinetics and mechanism of homogeneous chemical reactions associated with heterogeneous charge transition [35]. The technique involves electrochemical oxidation state change of the chemical species by addition or removal of an electron at an electrode. Spectral measurement on the solution adjacent to the electrode is made simultaneously with the electrogeneration process. There are several optical methods that have been coupled with electrochemistry [35,36] and the most common technique used is absorption spectroscopy. This technique has proven to be an effective method for studying the redox chemistry of inorganic, organic, and biological molecules. To be discussed in this section is the application to biological molecules. Review articles on spectroelectrochemistry are available elsewhere [35,36].

Application of spectroelectrochemical technique to biological molecules was first demonstrated by Heineman [37]. The technique combines the advantage of rapid equilibrium between electrode and redox species within thin layer cell with visible absorption spectroscopy, in order to determine the precise redox potential of metalloproteins. Metalloproteins often exchange electrons poorly with an electrode, presumably due to

insulation of the redox center from the electrode by the surrounding amino acid residues [37]. However, spectroelectrochemical measurement can be made by adding to the solution a small amount of another redox species, mediators. Mediators indirectly couple metalloprotein redox species with the electrode as illustrated by the scheme below:

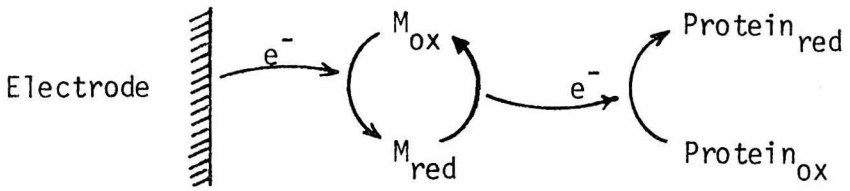

In a typical spectroelectrochemical experiment using an optically transparent thin layer cell (OTTLC)a series of potential, E_{app}, is sequentially potentiostated across the thin layer cell containing metalloprotein-mediator solution mixture. The mediator is first adjusted to its equilibrium (O)/(R) value by direct electrolysis at the electrode. It then, in turn, homogeneously oxidizes or reduces the protein in the solution until equilibrium between E_{app} at the electrode and all solution species is achieved. The equilibrium position is determined by means of cessation of the current flow and the stability of the absorption spectra of the product. The E^o and n values for the $M^{n+}/M^{(n+1)+}$ couple of the metalloprotein can then be calculated from the Nernst equation:

$$E_{app} = E^o + \frac{RT}{nF} \log \frac{(OX)}{(RED)}$$

Since selection of mediators used in the spectroelectrochemical experiments is very important in the precise determination of the reduction

potentials of metalloproteins, consideration of mediators is appropriate. The required properties of the mediators used and the criteria for the establishment of equilibrium as applied in spectroelectrochemical technique are summarized below:

1. The mediators must be able to readily oxidize and reduce the components to be determined and be able to interact readily with the electrode in order to establish their redox stages according to the applied potentials.

2. The mediators must have reduction potentials which allow them to span the required potential range (to a first approximation an active mediator is effective from 90% oxidation to 90% reduction, equivalent to ±60 mV (n = 1) on either side of the reduction potential.)

3. The mediators should not interact with the redox components so as to modify them chemically.

4. The mediators should not interfere with the measurements of the component of interest.

5. The measured values must be independent of the time allowed for measurement.

6. The same results must be attained by either oxidation or reduction processes.

7. The same results must be obtained using different mediators.

Lists of useful mediators are given in Table 1.

Table 1. Redox potentials and absorption maxima of organic and inorganic compounds useful as mediator-titrants for metalloenzyme electron transfer reactions

Compound	E^{o} [a] mV (NHE)	λ_{max}(nm), ε($cm^{-1}M^{-1}$)	Reference
$Fe(phen)_3^{3+}$	+ 1107	507(RED) (11,000)	b
$Fe(CN)_6^{3-}$	+ 420	420(OX) (1,100)	c
$Co(phen)_3^{3+}$	+ 360	330(OX) 4,680	d
$Ru(NH_3)_5py^{3+}$	+ 260	407(RED) (7,780)	e
2,6 dichlorophenol-indophenol	+ 227	600(OX) (2,060)	f
Bindschedler's Green	+ 216	700(OX)	g
$Fe(EDTA)^{2-}$	+ 120	258(OX)	h
$Ru(NH_3)_6^{3+}$	+ 51[i]	320 (100)	i
methyl viologen	- 358[j]	595(OX) (10,100)	k
		555(OX) (11,250)	
benzyl viologen	- 449[j]	605(OX) (12,400)	k

[a] E^{o} given at pH 7 (phosphate)

[b] P. George, G.I.H. Hanania, and D. H. Irvine, J. Chem. Soc., 3548 (1959).

[c] J. J. Alexander and H. B. Gray, J. Am. Chem. Soc. 90, 4260 (1968).

[d] F. Farina and R. G. Wilkins, Inorg. Chem. 7, 514 (1968), and this work.

[e] R. G. Gaunder and H. Taube, Inorg Chem. 9, 2627 (1970), and this work.

[f] W. R. Heineman, B. J. Norris, and J. F. Goelz, Anal. Chem. 47, 79 (1975).

[g] This work.

[h] H. J. Schugar, A. T. Hubbard, F. C. Anson, and H. B. Gray, J. Am. Chem. Soc. 91, 71 (1969).

[i] 0.1 M $NaBF_4$, H. S. Lim, D. J. Barclay, and F. C. Anson, Inorg. Chem. 11, 1460 (1972). P. Ford, F. P. Rudd, R. Gaunder, and H. Taube, J. Am. Chem. Soc. 90, 1187 (1968).

[j] E^o corresponds to $MV^{+2} + e^- = MV\cdot^+$

or $BV^{2+} + e^- = BV\cdot^+$

[k] E. Steckhan and T. Kuwana, Ber. Bunsenges. Phys. Chem. 78, 253 (1974).

Optically Transparent Thin Layer Cells (OTTLCS)

1. Aerobic Optically Transparent Thin Layer Cell. The transparent electrode was constructed as shown in Figure 5. A 500-line per inch gold minigrid (Buckbee Mears, St. Paul, Minn., 60% transmittance) cut into a 1x3 cm piece was placed between two microscope slides; each previously had two or three layers of 2 mil pressure sensitive Fluorofilm DF-1200 Teflon tape (Dilectrix Corp., Farmingdale, N.Y.) spacers placed around its periphery. The microscope slides were previously subjected to plasma cleaning (Harrick Scientific Corp., N.Y.) for 30 min. Gold wire of 0.1 mm diameter was placed on top of the gold minigrid at the side of the slide in order to bring the electrical contact to the upper part of the slide where it was held by a small socket slip. The minigrid was located within 4-5 mm of the cell bottom to minimize ohmic drop. The electrode was held together by epoxy along the vertical edges and part of the top. It was allowed to cure at 80°C for 24 hours.

Figure 5. The aerobic optically transparent thin layer cell

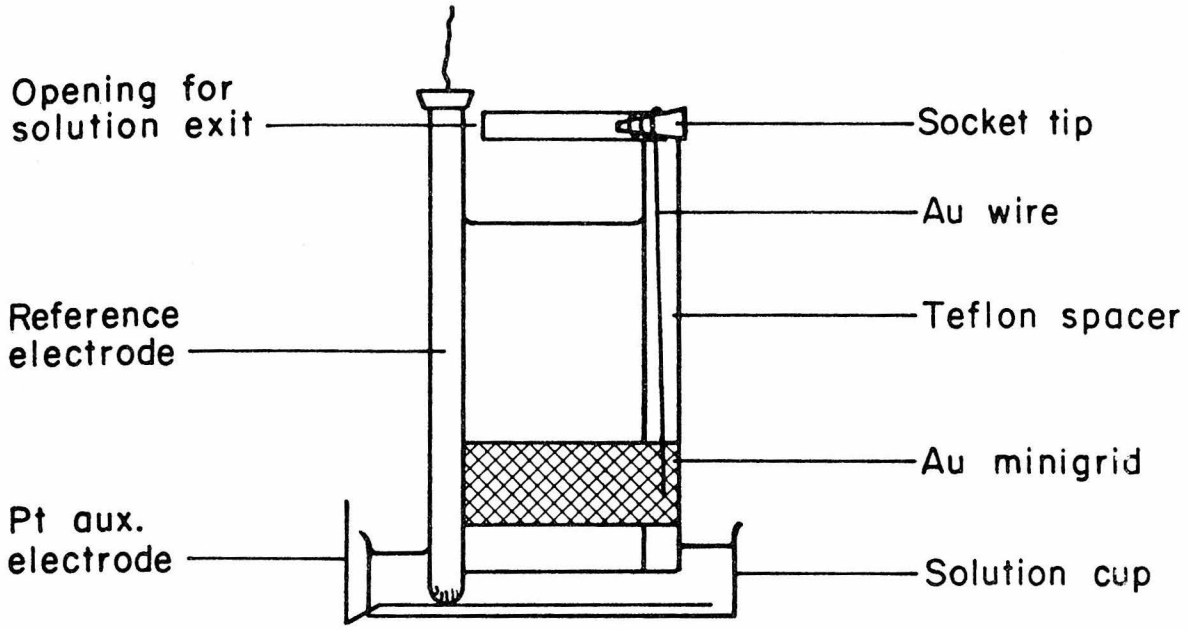
Opening for solution exit
Socket tip
Au wire
Reference electrode
Teflon spacer
Au minigrid
Pt aux. electrode
Solution cup

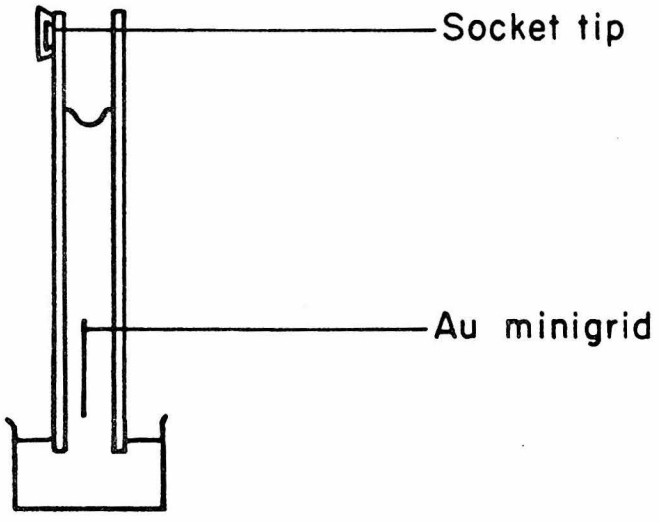
Socket tip
Au minigrid

In a typical experiment the transparent electrode was immersed to a depth of 1-2 mm in a 1.5 x 3.5 x 0.5 cm cup containing protein-mediator solution together with minisaturated calomel reference electrode and counter electrode as shown in Figure 5. The solution mixture was drawn into the thin layer cavity by small suction at the top opening and maintained by capillary action.

2. Anaerobic Optically Transparent Thin Layer Cells. Basically, the solution cup was eliminated and the auxiliary and reference electrodes were moved into the thin layer cavity. The reference electrode was located between the gold minigrid and auxiliary electrodes so that the potential control of the gold minigrid was best achieved. The cell is shown in Figure 6. The front face of the cell consisted of clear lucite, 4.5 x 2.5 x 0.4 cm. Two holes were drilled through the block onto which a two-holed block of 1 x 1 x 1 cm was attached. The holes were large enough to accommodate two Hamilton valves (No. 1MM2, Hamilton Co., Reno, Nevada). The back of the cell was a quartz slide of the same size as the front. Two or three layers of 2-mil Teflon tape were used as spacers. The working and auxiliary electrodes were 1 x 2.5 cm gold minigrids. They were placed 5 mm apart and sandwiched between lucite and quartz plates. Gold wires were used for electrical contacts similar to that of aerobic OTTLC. The cell was sealed around the edges with epoxy and was allowed to cure at 80°C for 24 hours.

In a typical experiment, the following procedure was used for oxygen removal from the solution and for filling the cell (Figure 6). With valve V_2 closed and valve V_1 opened to the vacuum degassing bulb A,

Figure 6. The anaerobic optically transparent thin layer cell

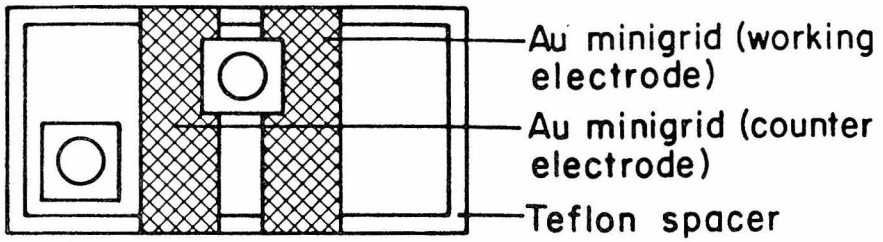
Au minigrid (working electrode)
Au minigrid (counter electrode)
Teflon spacer

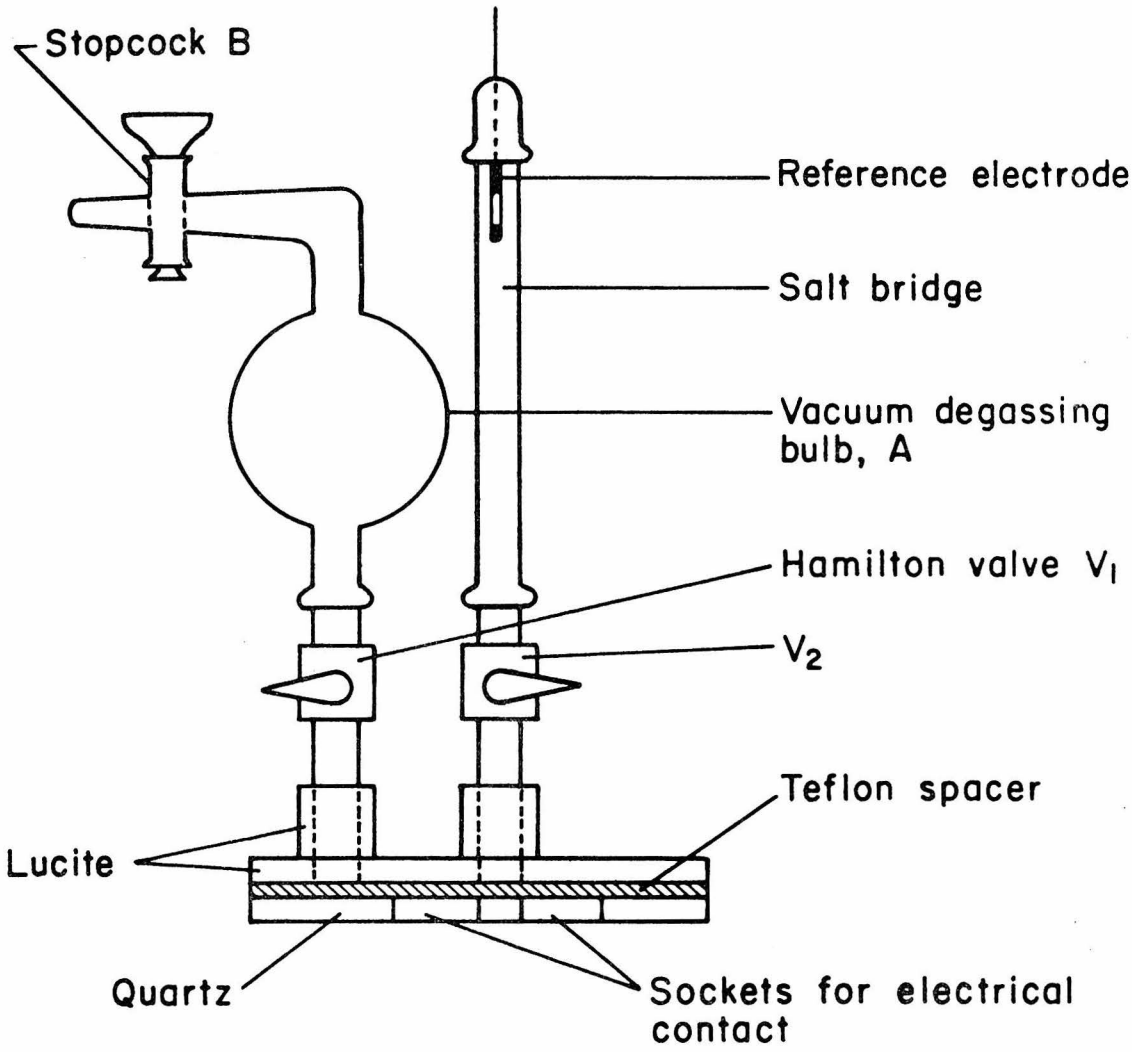
Stopcock B
Reference electrode
Salt bridge
Vacuum degassing bulb, A
Hamilton valve V_1
V_2
Teflon spacer
Lucite
Quartz
Sockets for electrical contact

the cell was connected to the nitrogen vacuum train by means of stopcock B. Three cycles of vacuum-nitrogen were applied to bulb A and thin layer cavity. Leaving the cell under nitrogen, the cell was disconnected from the train with valves and stopcock closed. Extreme care was taken to prevent the gold minigrids from tearing while vacuum was applied. A solution of previously degassed saturated KCl was added by means of Hamilton syringe to the reference tube and the calomel reference electrode was inserted (see figure). The cell was reattached to the train and vacuum-nitrogen-vacuum was applied to the cell and the bulb. Valve V_1 was closed and the cell left under vacuum. The bulb was filled with nitrogen and disconnected from the train. The mixture of protein-mediator solution was then added by Hamilton syringe to the bulb. The volume of protein solution necessary to fill the cell was approximately 0.75 ml. The cell was again connected to the train and four cycles of vacuum-nitrogen were applied to deoxygenate the protein solution. The stopcock was closed and the cell was disconnected from the train, leaving the bulb under nitrogen pressure. Valve V_1 was then carefully opened so that the protein solution filled in the thin layer cavity. While valve V_1 was still open, valve V_2 to the reference electrode was opened so that the protein solution filled in the Hamilton valve cavity and connected to the saturated KCl solution. To aid the flow of the protein solution into the Hamilton valve cavity, the cap of the reference electrode was barely opened.

This anaerobic transparent thin layer cell has proven to be very effective for anaerobic reduction of oxygen sensitive compounds, e.g., reduced methyl viologen. The dye showed no sign of reoxidation for a

period of two hours after being electrochemically reduced. It was found that the deoxygenation procedure was rather time consuming. Very often the minigrids were destroyed as a result of vacuuming. Therefore, the second type of anaerobic transparent thin layer cell was designed and constructed as shown in Figure 7. The cell was made from a clear lucite block of 7 x 2.5 x 2 cm. Two tapered holes were drilled from the top of the block into the opening of the cavity for reference and auxiliary ports. A thin layer cavity cell was formed in the lower half of the block (see figure) from which 4 and 1 cm^2 areas were cut out from the front and back, respectively. A 4 cm^2 quartz plate was glued in with epoxy to form the back of the thin layer cell onto which the Teflon spacers, gold minigrid, and gold wire were placed. The second 4 cm^2 quartz plate was placed on top and epoxied around the edges with pressure on the cell. A precalibrated thermocouple was glued into the thin layer cavity (care must be exercised to prevent the contact between thermocouple and gold minigrid) from the side of the block cell. The solution needed to fill the cell was approximately 0.5 ml.

It was found that filling the cell with previously degassed solution in a nitrogen glove bag and greasing the connections between reference, counter, electrodes, and the block cell with Apison grease was sufficient for electrochemically reduced methyl viologen to stay reduced for a period of two hours.

The exact thickness of the cells was calibrated spectrophotometrically at 530 ($\varepsilon = 1.1 \times 10^4 M^{-1} cm^{-1}$) and 600 nm ($\varepsilon = 2.06 \times 10^4 M^{-1} cm^{-1}$) with standard oxidized cytochrome c and 2,6-dichlorophenolindophenol solutions, respectively.

Figure 7. The anaerobic optically transparent thin layer cell (block cell).

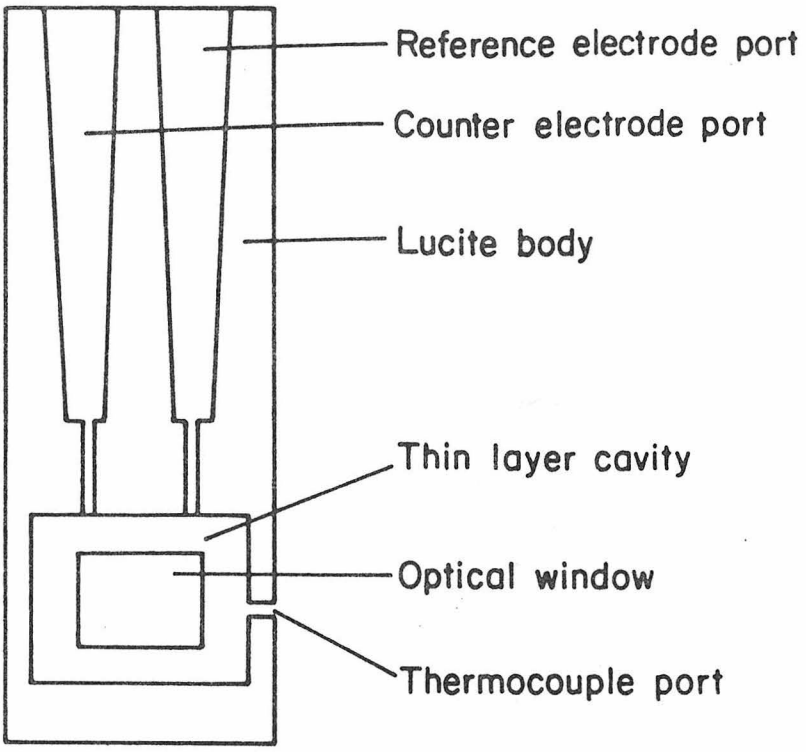
Reference electrode port
Counter electrode port
Lucite body
Thin layer cavity
Optical window
Thermocouple port

A.

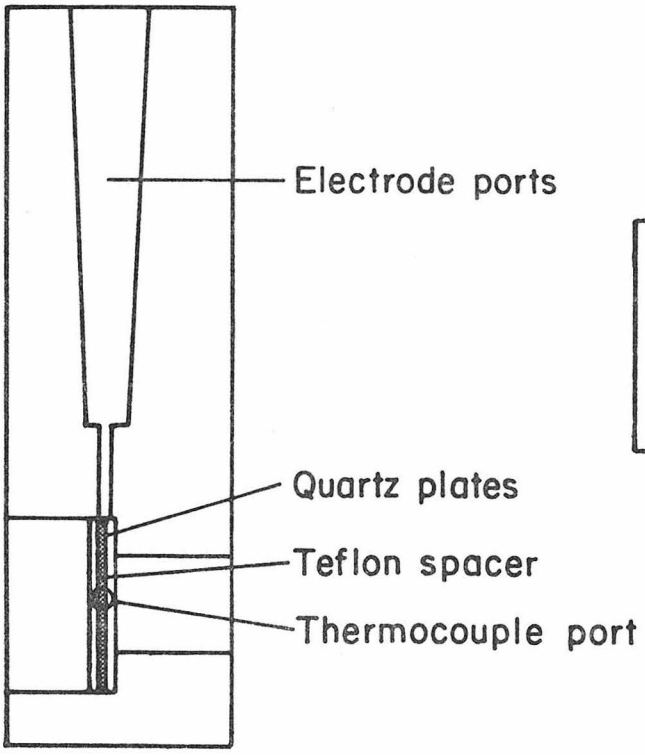
Electrode ports
Quartz plates
Teflon spacer
Thermocouple port

B.

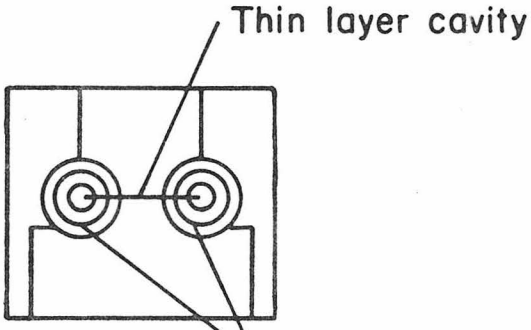
Thin layer cavity
Electrode ports

C.

3. Mini-Saturated Calomel Reference Electrode. The mini-electrode was composed of three parts: A) Hg/Hg_2Cl_2 (calomel), B) saturated KCl, and C) a salt bridge. These are shown in Figure 8. The Hg/Hg_2Cl_2 portion was made from a hair-thin tip of disposable pipette (approximately 2 cm long), large enough for 1 cm of the Pt-wire (3 cm total length) to be epoxied into it. A few drops of mercury were inserted from the bottom to cover the Pt-wire. A few drops of Hg_2Cl_2 suspended in saturated KCl were placed over the mercury. After the suspension settled, the surplus liquid was removed with a fine capillary. A fine needle was used to plug the capillary with asbestos in order to prevent the Hg and Hg_2Cl_2 from creeping out when turned upside down. The second part, B , was made of a 3 mm inside diameter pyrex tube (3.5 cm long) with a sealed cracked bottom. The cracked bottom was prepared from fusion of a soft glass bead onto the pyrex tube. The cracked glass bottom permits ionic contact between the electrolyte inside and outside the tubing, but prevents mixing. This part was filled with saturated KCl, and part A, which was held in the middle of a serum cap by a Pt wire, was placed into it. This assembly was placed inside the salt bridge C, which was previously filled with agar or saturated KCl. It was found that either agar or KCl worked equally well, except when the electrode was used with intensely colored solutions (e.g., dye) in which case saturated KCl was preferred because of the ease of the replacement with fresh solution. The salt bridge is necessary for the cell arrangement used throughout this report in order to keep the temperature of the calomel electrode constant while that of the thin layer cell is varied. The electrode was kept in saturated KCl solution when not in use, and the potential was

Figure 8. The mini-saturated calomel reference electrode.

A.

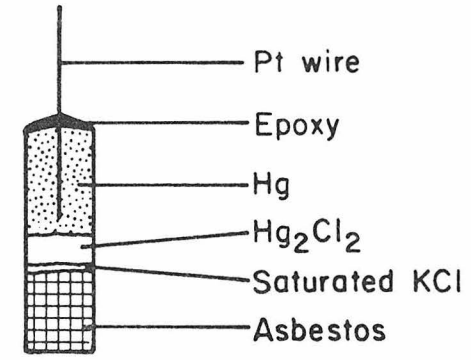
Pt wire
Epoxy
Hg
Hg_2Cl_2
Saturated KCl
Asbestos

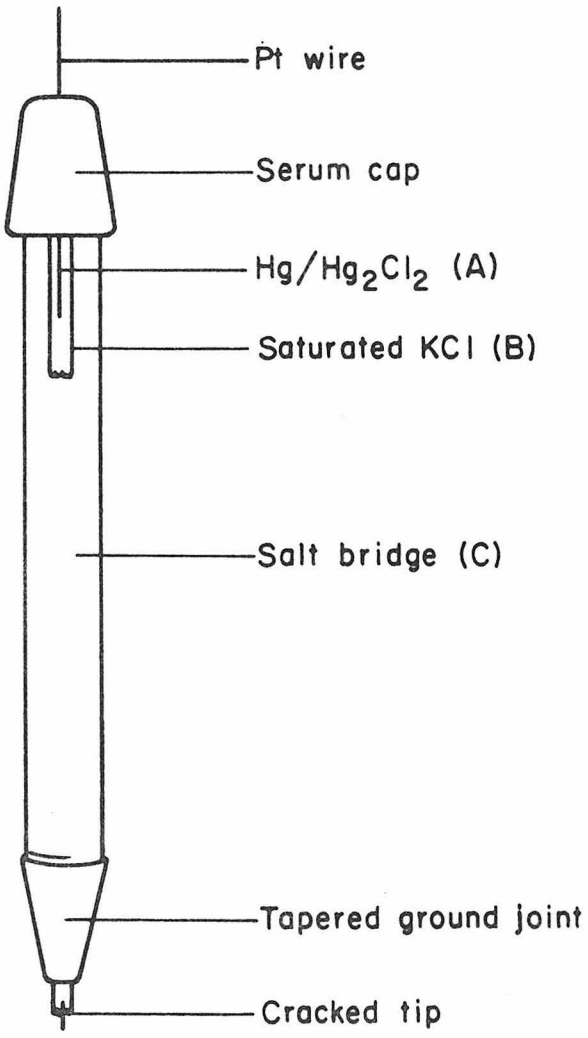
Pt wire
Serum cap
Hg/Hg_2Cl_2 (A)
Saturated KCl (B)
Salt bridge (C)
Tapered ground joint
Cracked tip

found to stay constant within ±5 mV versus several commercial calomel reference electrodes.

EDGE EFFECT

It is important to discuss here the edge effect which is intrinsic to the thin layer cell design employed in this study. A kinetic situation exists at the upper and lower edges of the transparent electrode (of the type shown in Figure 5 and only the upper edge for cells shown in Figures 6,7) due to diffusion of the redox components into the thin layer cell from the solution above and below. This diffusion is a result of concentration gradients which exist at the edges. The edges of the minigrid serve to maintain the equilibrium ratio of redox components in the bulk of the thin layer cell by electrolysis of incoming species. This edge effect is avoided by masking the light beam so that the observation window is at the center region of the transparent electrode where electrolysis has ceased. In this way, the thin layer region above and below the observation area (in the light path) serves as a buffer zone between the equilibrium condition in the thin layer portion and the kinetic phenomena at the edges.

A small residual current flows after equilibrium is reached in the bulk of the thin layer as a result of the continuing electrolysis at the edges. This current is sufficiently small that the true potential of the transparent electrode does not deviate from the applied potential. It has been shown that the difference between the applied potential and the true minigrid potential is only a few tenths of a millivolt [38].

METHODS

1. Spectroelectrochemical Experiments. Apparatus: The optically transparent thin layer cells used have been described in the previous section. For all protein experiments anaerobic OTTLC of the block type was used. Special care was exercised when oxygen-sensitive reduced proteins (stellacyanin and cytochrome oxidase) were used as described previously. In all experiments residual dissolved oxygen was removed from the thin layer cavity by maintaining electrode potential at -600 mV versus SCE for at least 15 min.

A Wenking model 6357 TR potentiostat was used to control the potential of the minigrid electrode. The precise values were measured with a Tektronix model DM 501 digital voltmeter.

The electrochemical cell was placed in a thermostated cell holder which fit in the cell compartment of Cary 17 or 15 spectrophotometer, where the optical measurements were performed.

Proteins and Mediators: Proteins studied and their criteria for purity are given in Table 2. 2,6-dichlorophenolindophenol (DCIP) of 99% purity was obtained from Fluka (Columbia Organic Chemical, Columbia, S.C.) and was used as received. [4-[[p-(dimethylamino)phenyl]-imino]-2,5-cyclohexadien-1-ylidene-]dimethyl-chloride],(Bindschedler's Green)(BG) was prepared according to a literature procedure [39] and was purified as suggested by Shine et al. [40]. Pentaaminepyridineruthenium(III), $Ru(NH_3)_5py^{3+}$ was prepared according to the method of Ford, et al. [41] as modified by Dr. Diane Cummins [42]. The $Ru(NH_3)_5py(PF_6)_2$ was a generous gift from Dr. Cummins. Tris cobalt complex of 1,10-phenanthroline was prepared by a method analogous to that of Pfeiffer and Werdelman [43].

Table 2. Sources and criteria of purity of proteins studied

Protein	Source	Criteria of Purity	Reference
Cytochrome c (type VI)	horse heart	$A_{550}/A_{280} = 1.2$	Sigma Chemical Co.
Cytochrome c551	Pseudomonas aeruginosa	$A_{551}/A_{280} = 1.2$	6
Cytochrome cd	Pseudomonas[a] aeruginosa	$A_{411}/A_{280} = 1.13$[b]	d
Stellaycanin	Rhus vernicifera[c]	$A_{604}/A_{280} = 0.18$	7
Plastocyanin	french bean leaves, Phaseolus vulgaris	$A_{597}/A_{280} = 0.90$	8
Azurin	Pseudomonos aeruginosa	$A_{625}/A_{280} = 0.58$	6

[a] American type culture collection #10145

[b] Gel electrophoresis in the presence of sodium dodicylsulfate revealed a very small amount of high molecular weight impurity.

[c] Japanese lacquer tree (from Saito and Co., Ltd., Tokyo).

[d] T. Horio, T. Higashi, T. Yamanaka, H. Matsubara, and K. Okunuki, J. Biol. Chem. 236, 944 (1961).

$Co(phen)_3(ClO_4)_3$ was a generous gift from Dr. J. McArdle.

All solutions were prepared immediately before use by dissolving an appropriate amount of mediator into the protein solutions. The concentration ratio of protein to mediator is 1:1 except for cytochrome c: DCIP as the ratio of 1:0.1 was used. Table 3 gives mediators used for each protein, together with wavelength monitored.

Table 3. Mediators used with each protein, and the wavelengths at which their protein concentrations were monitored

Protein	Mediator	E^o of Mediator (mV vs. NHE)	Species Monitored (λ_{nm})
Cytochrome c	BG DCIP	220 217	$Fe^{3+/2+}$ (550)
Cytochrome c551	BG	220	$Fe^{3+/2+}$ (551)
Cytochrome cd (c heme)	$Ru(NH_3)_5py^{3+}$	253	$Fe^{3+/2+}$ (553)
Cytochrome cd (d heme)	$Fe(EDTA)^{2-}$	120	$Fe^{2+/3+}$ (642)
Stellacyanin	$Ru(NH_3)_5py^{3+}$	253	$Cu^{2+/1+}$ (604)
Plastocyanin	$Co(phen)_3^{3+}$	360	$Cu^{2+/1+}$ (597)
Azurin	$Co(phen)_3^{3+}$	360	$Cu^{2+/1+}$ (625)

Spectral measurement: In a typical protein experiment, concentrations of reduced and oxidized protein corresponding to each applied potential to the transparent electrode were determined spectrophotometrically. The spectra were recorded after equilibrium among the electrode, mediator, and protein had been obtained as indicated by the cessation of current flow and the stability of the spectrum. Typical absorbance differences between solutions of fully oxidized and reduced protein was ca. 0.1 absorbance unit. For temperature dependence studies, thermal equilibrium was established by allowing the cell to equilibrate in the thermostated cell holder for approximately 45 min.

Data Analysis: The reduction potential of each protein was obtained from a plot of the applied potential (E_{app}) vs. the logarithm of the ratio of oxidized and reduced form of the protein:

$$E_{app} = E^{o} + \frac{RT}{nF} \log \frac{(O)}{(R)}$$

The E^{o} values reported are averages of at least three independent measurements. The error in E^{o} was estimated as given in Appendix 2.

The ionic entropy changes ($\bar{S}^{o}_{red} - \bar{S}^{o}_{ox}$) (Appendix 3) were obtained from the temperature dependence of the reduction potentials, $\bar{S}^{o}_{red} - \bar{S}^{o}_{ox} = \Delta\bar{S}^{o} = F/4.18[\Delta E/\Delta T]$. The enthalpy changes were calculated from the relation $\Delta G^{o} = \Delta H^{o} - T\Delta S^{o}$, where $\Delta S^{o} = \Delta\bar{S}^{o} - 20$ e.u. Standard deviations of ΔS^{o} and ΔH^{o} were obtained from linear least squares analysis.

2. Cyclic Voltammetry Experiments. A conventional two-compartment electrochemical cell was employed which isolated the saturated potassium chloride calomel reference electrode (Sargent Welch) from the gold wire working electrode. Cyclic voltammograms were obtained using a PAR model 173 Potentiostat/Galvanostat and were recorded on a Hewlett-Packard XY recorder. The E^{o} values were taken as half-way between cathodic and anodic waves.

RESULTS AND DISCUSSION

1. Inorganic Complexes. Reduction potentials of 2,6-dichlorophenolindophenol, Bindschedler's Green, $Co(phen)_3^{3+}$, and $Ru(NH_3)_5py^{3+}$ at 25°C were determined from both cyclic voltammograms (Figure 9) and thin layer spectra (Figure 10). The values obtained from both methods are in good agreement and are given in Table 4. The temperature dependence

Figure 9. Thin layer cyclic voltammograms of mediators, initial scans are cathodic.

i) 2,6-dichlorophenolindophenol 1.0×10^{-3}M in phosphate buffer, pH 7, ionic strength 0.1 M, scan rate 1 mV sec^{-1}.

(a) O_2 present

(b) O_2 removed by reduction to water

ii) Bindschedler's Green 1.0×10^{-3}M in phosphate buffer, pH 7, ionic strength 0.1 M, scan rate 1 mV sec^{-1}.

iii) $Co(phen)_3(ClO_4)_3$ 2.3×10^{-3}M, phosphate buffer, pH 7, ionic strength 0.05 M, scan rate 20 mV sec^{-1}.

iv) $Ru(NH_3)_5py(ClO_4)_3$ 2.3×10^{-3}M, phosphate 0.05 M, sulfate 0.05 M, pH 6.5, total ionic strength 0.1 M, scan rate 20 mV sec^{-1}.

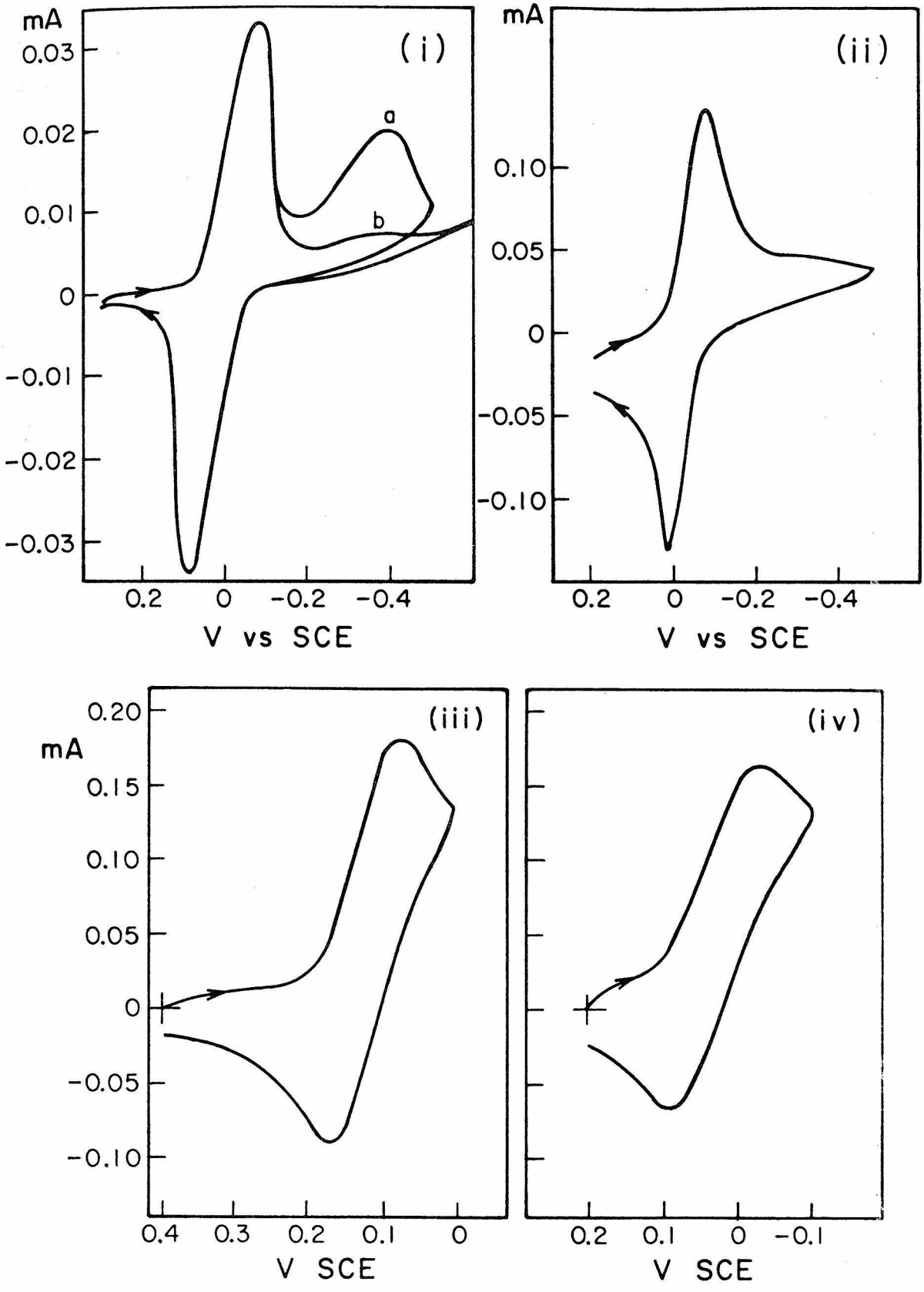
mA
0.03
0.02
0.01
0
-0.01
-0.02
-0.03
(i)
a
b
0.2
0
-0.2
-0.4
V vs SCE
mA
0.10
0.05
0
-0.05
-0.10
(ii)
0.2
0
-0.2
-0.4
V vs SCE
mA
0.20
0.15
0.10
0.05
0
-0.05
-0.10
(iii)
0.4
0.3
0.2
0.1
0
V SCE
(iv)
0.2
0.1
0
-0.1
V SCE

Figure 10. Thin layer spectra of mediators for different values of applied potential, E_{app} mV vs. SCE.

i) 2,6-dichlorophenolindophenol 1.0×10^{-3}M, cell thickness 0.048 cm.

a) -100 b) -14.8 c) -4.7

d) +4.7 e) +15.3 f) +25.5

g) +200

ii) Bindschedler's Green 1.0×10^{-3}M, cell thickness 0.048 cm

a) -150 b) -32 c) -24.6

d) -20.3 e) -15.2 f) -4.7

g) +1.5 h) +10.2 i) +24.8

j) +150

iii) $Co(phen)_3(ClO_4)_3$ 1.84×10^{-3}M, cell thickness 0.051 cm.

a) +250 b) +200 c) +180

d) +160 e) +140 f) +120

g) +100 h) +80 i) +60

j) 0

iv) $Ru(NH_3)py(ClO_4)_3$ 1.80×10^{-3}M. Cell thickness 0.051 cm

a) -150 b) -50 c) -25

d) -15 e) 0 f) +20

g) +40 h) +150

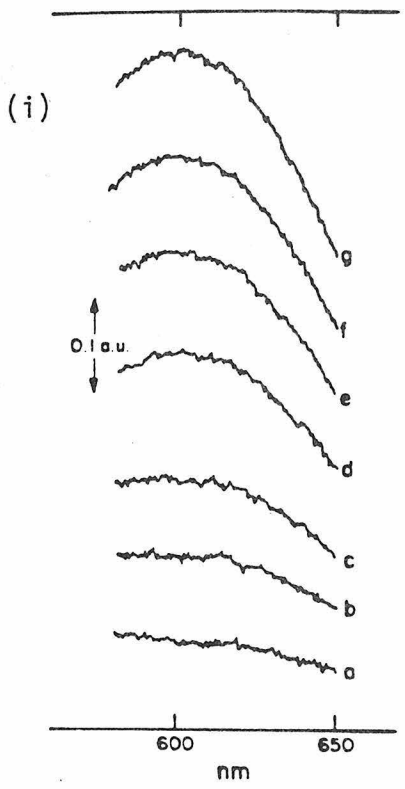
(i)
0.1 a.u.
g
f
e
d
c
b
a
600
650
nm

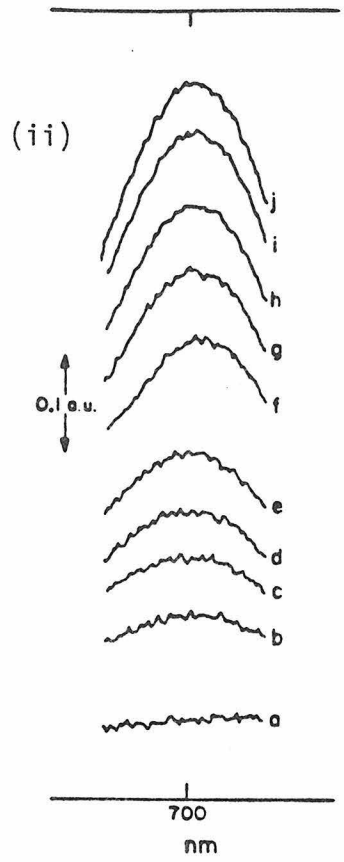
(ii)
0.1 a.u.
j
i
h
g
f
e
d
c
b
a
700
nm

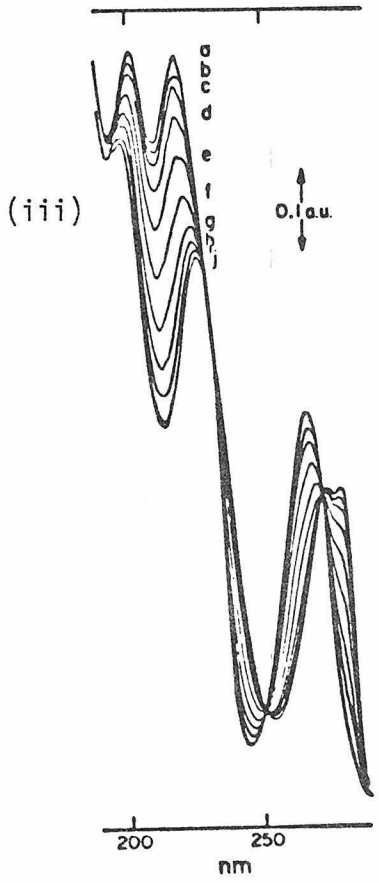
(iii)
0.1 a.u.
a
b
c
d
e
f
g
h
i
j
200
250
nm

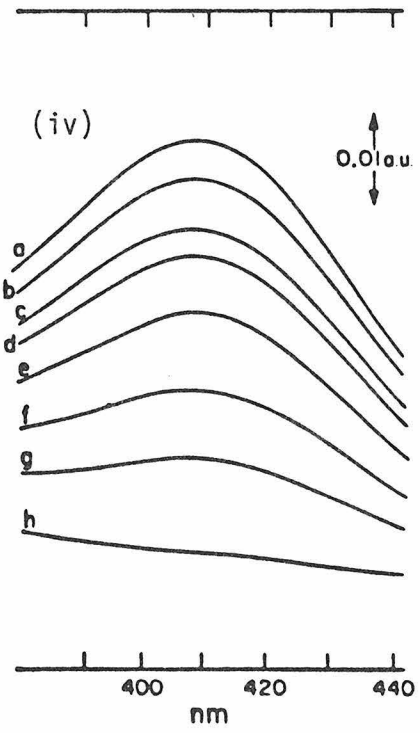
(iv)
0.01 a.u.
a
b
c
d
e
f
g
h
400
420
440
nm

of the reduction potentials of $Co(phen)_3^{3+}$ and $Ru(NH_3)_5py^{3+}$ were also determined and the calculated standard enthalpy and entropy changes are given, together with some other complexes, in Table 4.

Table 4. Reduction potentials and standard enthalpy and entropy changes of some organic and inorganic compounds obtained from this work and literature values

Reagent	E^o mV (NHE)	ΔH^o kcal mole^{-1}	ΔS^o e.u.	Reference
$Fe(OH_2)_6^{3+/2+}$	770	-10	27	a
$Fe(phen)_3^{3+/2+}$	1072	-32	-26	b
$Fe(CN)_6^{3-/4-}$	355	-27	-62	a
$Co(OH_2)_6^{3+/2+}$	1810	-16	44	c
$Co(phen)_3^{3+/2+}$	360	- 9	- 4	this work[d]
$Ru(NH_3)_5py^{3+/2+}$	253	-10	-15	this work[e]
$Ru(NH_3)_6^{3+/2+}$	51	- 7	-17	f
2,6-dichlorophenol indophenol	220	-	-	this work[g]
Bindschedler's Green	217	-	-	this work[g]

[a] G.I.H. Hanania, D. H. Irvine, W. A. Eaton, and P. George, J. Phys. Chem. 71, 2022 (1967).

[b] V. T. Taniguchi, unpublished result, and E. L. Yee, R. J. Cave, K. L. Guyer, P. D. Tyma, and M. J. Weaver, J. Am. Chem. Soc. 101, 1130 (1979)

[c] Encyclopedia of Electrochemistry, A. J. Bard, ed., vol. 3 (1976), p. 46.

[d] pH 7, phosphate buffer, ionic strength 0.05 M.

[e] pH 6.5, phosphate 0.05 M, sulfate 0.05 M, total ionic strength 0.1 M.

[f] D. K. Lavallee, C. Lavallee, J. C. Sullivan, and E. Deutsch, Inorg. Chem. 12, 570 (1968).

[g] pH 7, phosphate buffer, ionic strength 0.1 M.

It is evident that the reduction potentials of metal complexes vary considerably with the kind of ligand. Rock [44] has attempted to account for the observed shift in potentials with ligand by using ligand field theory. It is pointed out that the two effects of entropy and ligand field must be taken into account in order to understand the variations of reduction potentials with ligands. George and McClure [45] and Buckingham and Sargeson [46] treated the problem by setting up a thermodynamic cycle involving the ionization of the gaseous M(II) ions, the gaseous complexation reactions of M(II) and M(III), the dissolution of the gaseous complex ions, and the oxidation of the M(III) complex in solution. Both approaches, although complicated by the fact that terms necessary for the evaluation of E^o are frequently not available experimentally, have proven to give good agreement between the observed and calculated E^o of some inorganic complexes [44-46]. The E^o of $Fe(phen)_3^{3+}$ and $Co(phen)_3^{3+}$ is shifted in the opposite direction relative to the aquo couples. Buckingham [46] treated this difference as a result of ligand field effect, that is, the π-bonding ligand such as 1,10-phenanthroline, is a strongly stabilized metal ion which has a configuration t_{2g}^6. For cobalt this configuration occurs in the low spin Co(III) state, whereas for iron it occurs in the low spin Fe(II) state. This makes the Co(III) more stable than Co(II), and Fe(II) more stable than Fe(III), thus

shifting the E^o of $Co(phen)_3^{3+}$ to a more negative value while that of $Fe(phen)_3^{3+}$ shifts to a more positive value relative to their aquo couples. Moreover, the ΔS^o of the 1,10-phenanthroline complexes of cobalt and iron shift negatively when compared to their aquo complexes. The major contribution to the change in entropy upon reduction of the aquo complex is generally viewed as a decrease in the solvent ordering around the ion, due to partial charge neutralization. Specifically, reduction of $Fe(OH_2)_6^{3+}$ and $Co(OH_2)_6^{3+}$ decreases the charges within the inner spheres and expands their radii, thereby releasing a few water molecules from the outer sphere to the bulk water. The entropy change associated with this process is positive. In contrast to the aquo complexes, the ΔS^o values for the reductions of $Fe(phen)_3^{3+}$ and $Co(phen)_3^{3+}$, which possess hydrophobic ligands, are negative. In this case, the propellerlike configuration of the planar phenanthroline ligands provides open channels for water molecules to come into relatively close contact with the oxidized metal ions. The partial charge neutralization (+3 to +2) upon reduction causes a net rearrangement of these water molecules, resulting in the formation of cages of structure water of abnormally low entropy [47,48] in the hydrophobic phenanthroline channels. However, for $Fe(CN)_6^{3-}$, the reduction potential lies above that for the aquo couple even though cyanide ion is a strong π-bonding ligand. The ΔS^o is far more negative than the $Fe(phen)_3^{3+}$ couple. Rock [44] has treated the observed negative ΔS^o as a special effect due to a negatively charged cyanide ligand. The negative charge on the complex causes water molecules to rearrange themselves into a more ordered configuration. In the case of $Ru(NH_3)_6^{3+}$ and $Ru(NH_3)_5py^{3+}$ couples, the

reduction potentials shift positively as the sixth ammine ligand of $Ru(NH_3)_6^{3+}$ is replaced by pyridine to form $Ru(NH_3)_5py^{3+}$. As one would expect, the π-bonding capability of pyridine is much greater than that of ammine, causing the lower oxidation state, Ru(II), to be more stable than Ru(III).

It is important to point out here that the reduction potentials and the standard enthalpy and entropy changes of metal complexes are also controlled partly by solvent media. Gutman et al. [49] have studied the solvent effects on the E^o of $Fe(CN)_6^{3-}$ and proposed a model of acceptor-donor interactions between the ionic species and the solvent molecules in order to explain the shift of the E^o in various solvents. They concluded that the π-electron pair donor of the divalent iron complex is more stabilized by interaction with the solvent which has more acceptor property, which in turn will shift the E^o to a more positive value as the acceptor property of the solvents increases.

2. Blue Copper Proteins. Thin layer spectra of proteins with appropriate mediators are shown in Figure 11. Figure 12 shows Nernst plots at various temperatures. Their E^o and corresponding standard enthalpy and entropy changes (Appendix 3) are given in Table 5.

The reduction potentials of stellacyanin, plastocyanin and azurin obtained in this work are +184, +347, and +330 mV versus NHE, respectively. The value for bean plastocyanin is slightly lower than the value reported for spinach plastocyanin [50]. The potentials for stellacyanin and azurin are in good agreement with the values frequently cited [51].

Figure 11. Thin layer spectra of the proteins with mediators for different values of applied potential, E_{app}, mV vs. SCE.

i) Cytochrome c 2×10^{-4}M with 2,6-dichlorophenolindophenol 1.0×10^{-4}M. Cell thickness 0.047 cm.

a) -200 b) +10.9 c) +20.4

d) +35.9 e) +50.3 f) +75.5

ii) Cytochrome c 2×10^{-4}M with Bindschedler's Green 1.0×10^{-5}M. Cell thickness 0.018 cm.

a) -150 b) -1.5 c) +15.6

d) +28.3 e) +40.2 f) 60.4

g) +150

iii) Cytochrome c-551 2×10^{-4}M with Bindschedler's Green 2×10^{-5}M. Cell thickness 0.014 cm.

a) -600 b) -29.4 c) -6.1

d) +6.3 e) +24.6 f) +45.6

g) +67.3 h) +150

iv) Cytochrome cd (c heme) 2.5×10^{-4}M with $Ru(NH_3)_5py^{3+}$ 2×10^{-5}M. Cell thickness 0.045 cm.

a) -400 b) 0 c) +30.0

d) +50.0 e) +65.0 f) +75.0

g) +150.0

Figure 11 (contd.)

v) Cytochrome cd (d-heme) 0.55×10^{-3}M with $Fe(edta)^{2-}$ 6.6×10^{-3}M. Cell thickness 0.046 cm.

a) +100 b) +10 c) 0
d) -10 e) -20 f) -40
g) -60 h) -100

vi) Stellacyanin 2.7×10^{-3}M with $Ru(NH_3)_5py^{3+}$ 2.8×10^{-3}M, cell thickness 0.021 cm.

a) 0 b) -10 c) -20
d) -30 e) -50 f) -65
g) -80 h) -95 i) -150

vii) Plastocyanin 1.8×10^{-3}M with $Co(phen)_3^{3+}$ 2.0×10^{-3}M, cell thickness 0.051 cm.

a) +300 b) +190 c) +150
d) +120 e) +100 f) 0

viii) Azurin 1.0×10^{-3}M with $Co(phen)_3^{3+}$ 1.0×10^{-3}M, cell thickness 0.051 cm.

a) +300 b) +145 c) +120
d) +110 e) +100 f) +85
g) +65 h) 0

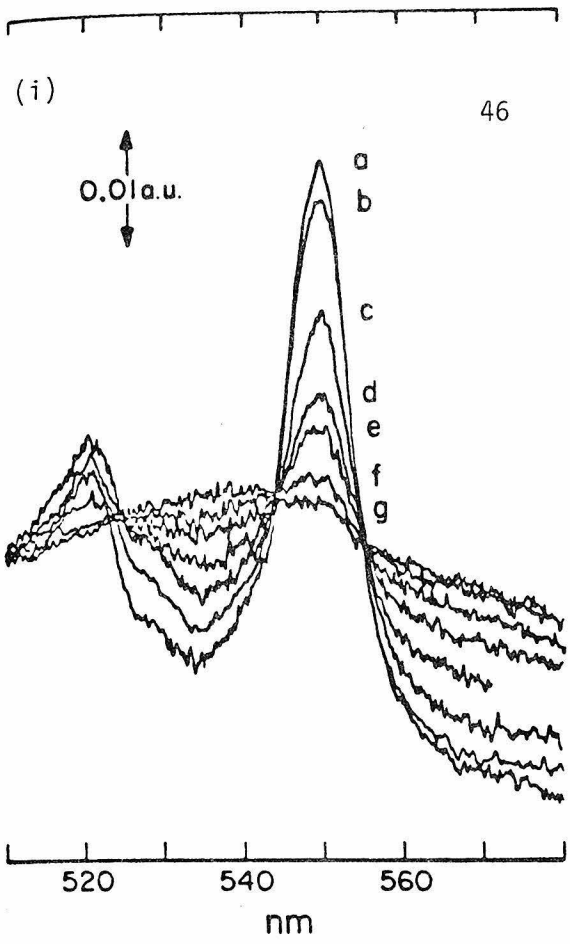
(i)
0.01 a.u.
a
b
c
d
e
f
g
520
540
560
nm

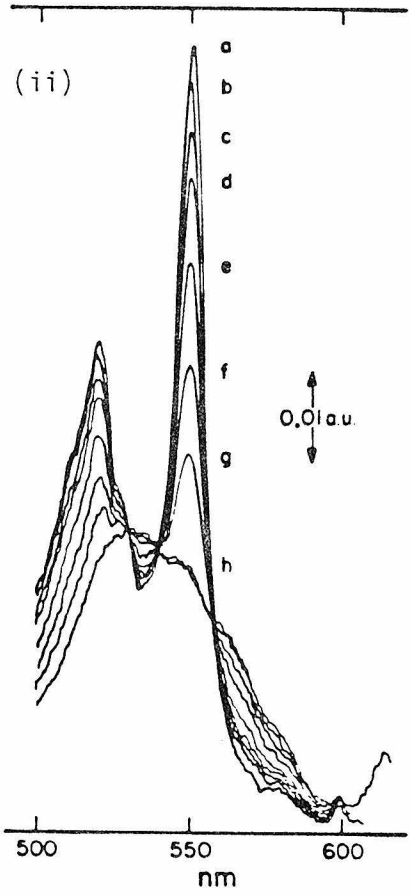
(ii)
a
b
c
d
e
f
g
h
0.01 a.u.
500
550
600
nm

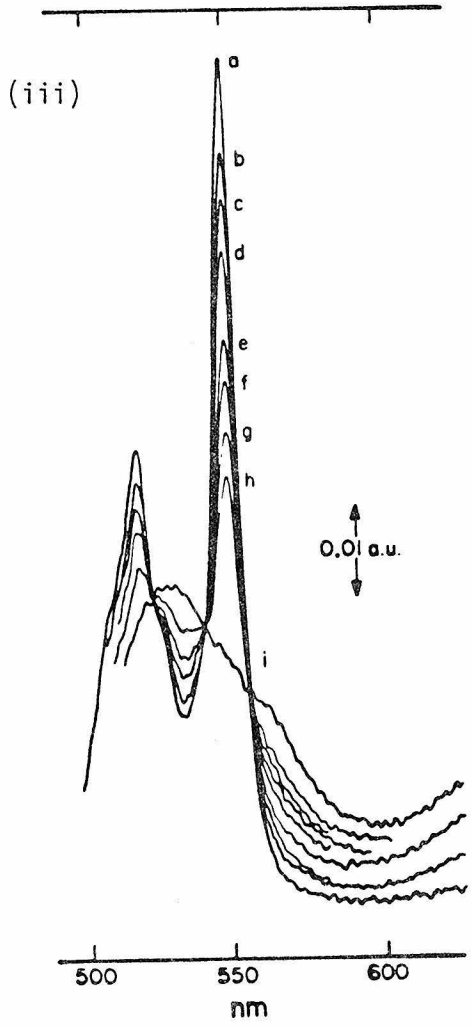
(iii)
a
b
c
d
e
f
g
h
i
0.01 a.u.
500
550
600
nm

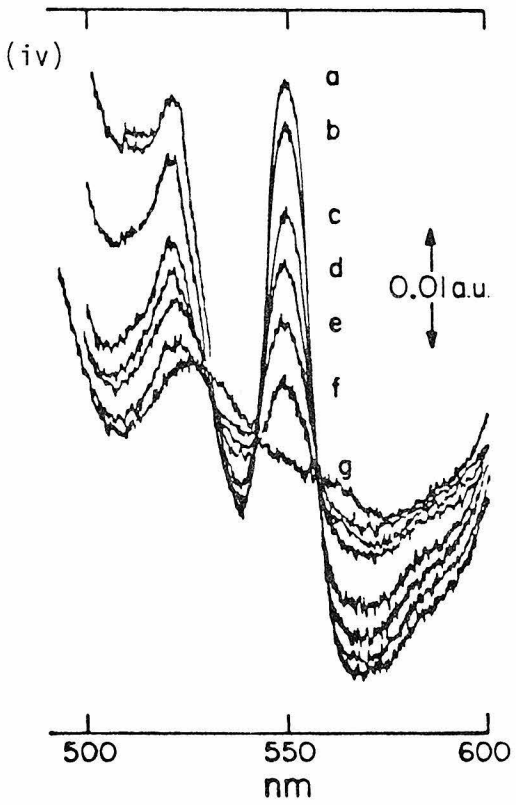
(iv)
a
b
c
d
e
f
g
0.01 a.u.
500
550
600
nm

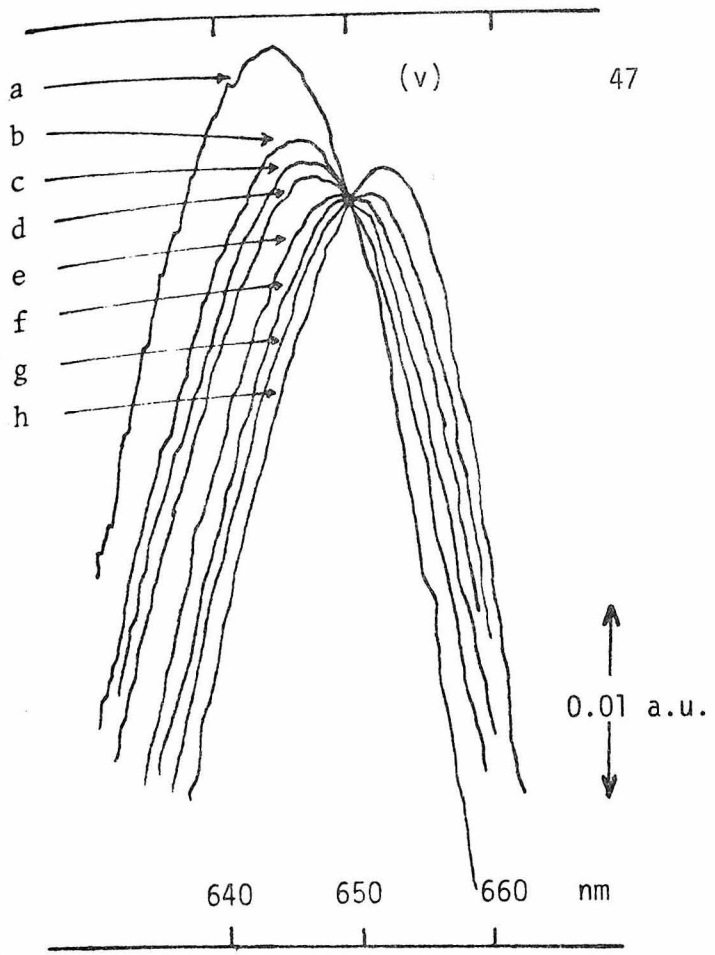
(v)
a
b
c
d
e
f
g
h
0.01 a.u.
640
650
660
nm

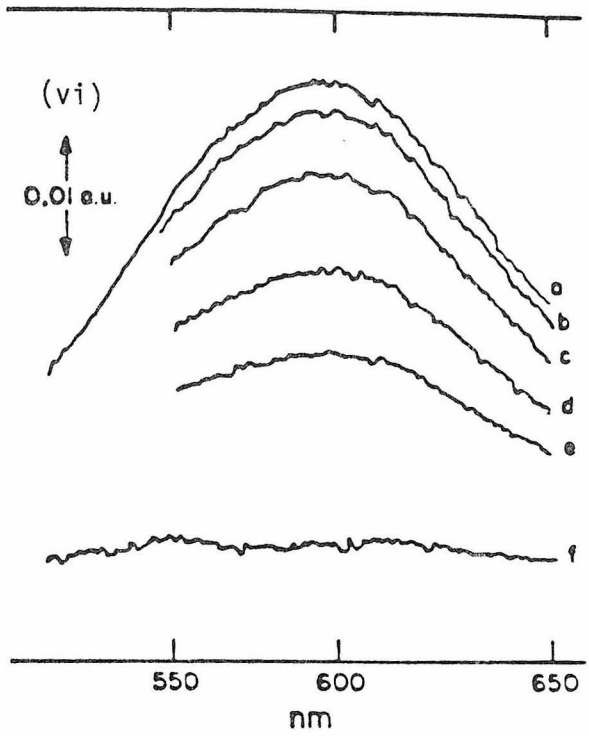
(vi)
0.01 a.u.
a
b
c
d
e
f
550
600
650
nm

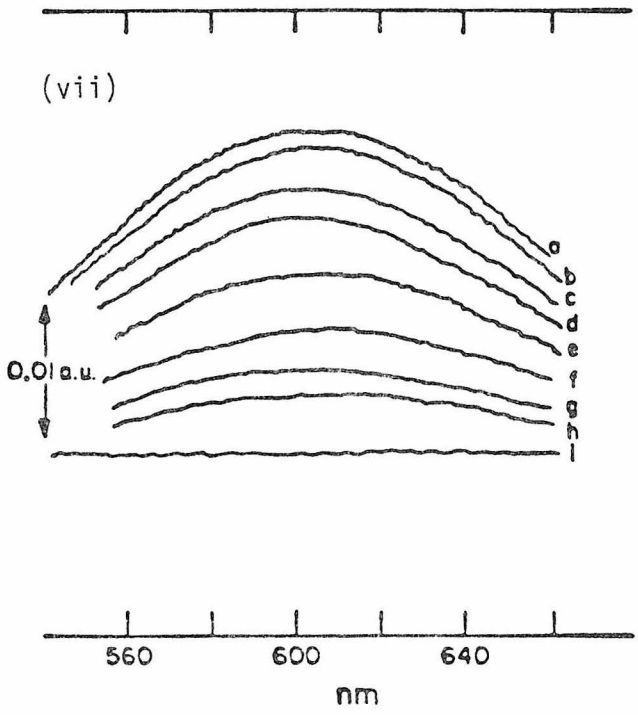
(vii)
0.01 a.u.
a
b
c
d
e
f
g
h
i
560
600
640
nm

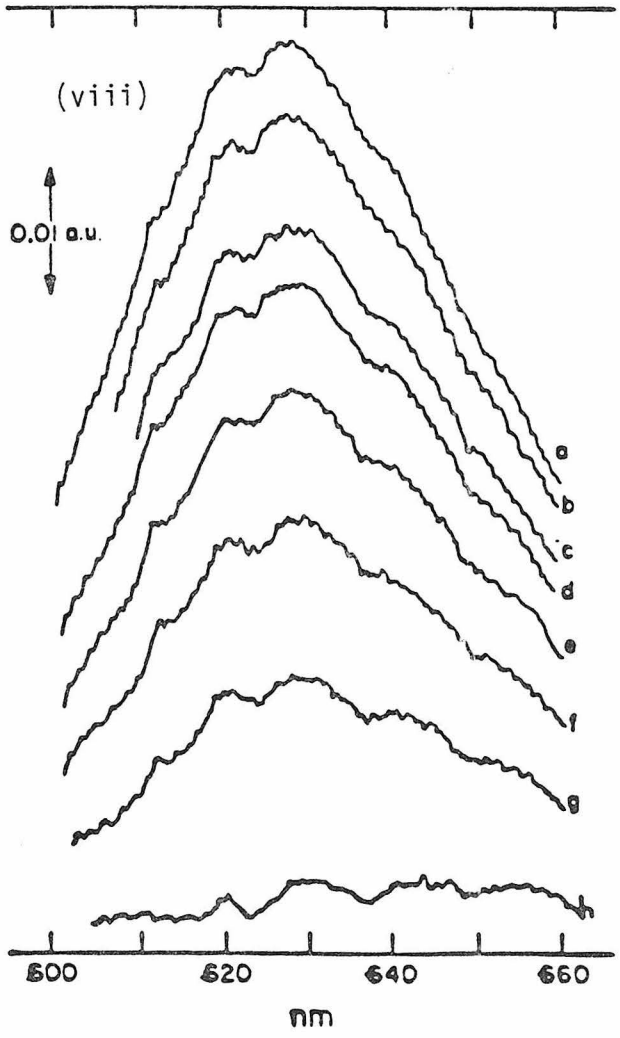
(viii)
0.01 a.u.
a
b
c
d
e
f
g
h
600
620
640
660
nm

Figure 12. Nernst plots (E_{app} vs. $\log\frac{[O]}{[R]}$) for the proteins at different temperatures (°C). Experimental conditions are the same as those given in Figure 11.

i) Cytochrome c

a) 8.8 b) 12.5 c) 16.4

d) 26.0

ii) Cytochrome c-551

a) 8.0 b) 11.5 c) 15.5

d) 20.5 e) 25.0

iii) Cytochrome cd (c-heme)

a) 4.0 b) 8.0 c) 16.0

d) 21.0 e) 24.0

iv) Stellacyanin

a) 6.5 b) 11.2 c) 16.2

d) 21.7 e) 25.0

v) Plastocyanin

a) 6.5 b) 15.0 c) 18.0

d) 23.0 e) 25.0

vi) Azurin

a) 12.2 b) 15.0 c) 19.0

d) 21.0 e) 24.2

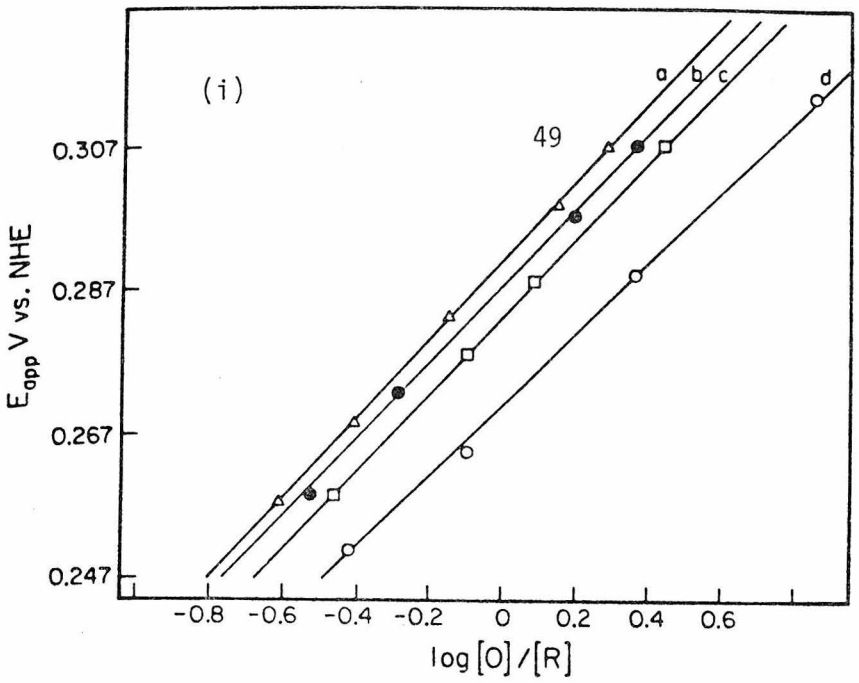
(i)
49
a
b
c
d
0.307
0.287
0.267
0.247
-0.8
-0.6
-0.4
-0.2
0
0.2
0.4
0.6
E_{app} V vs. NHE
log [O] / [R]

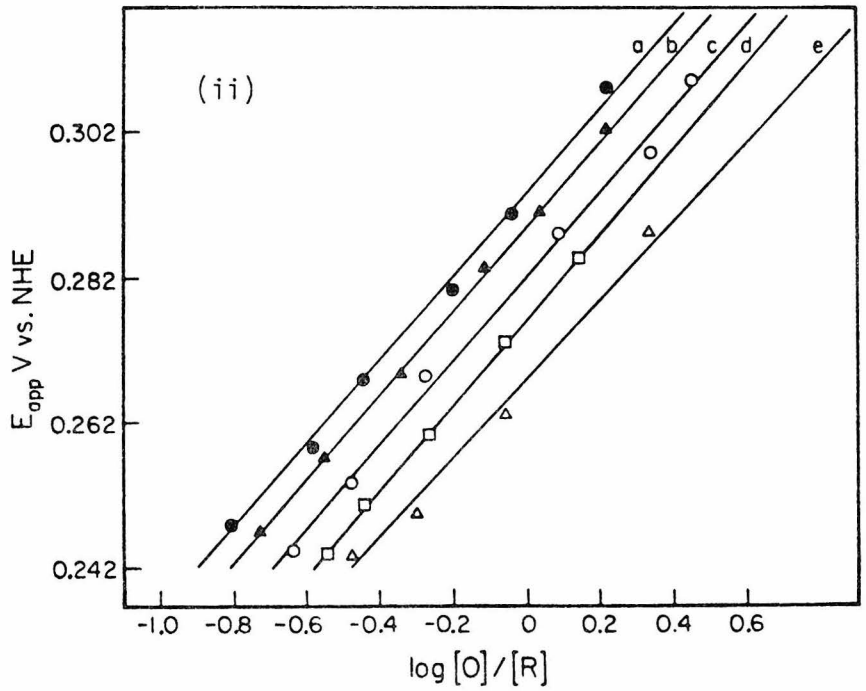
(ii)
a
b
c
d
e
0.302
0.282
0.262
0.242
-1.0
-0.8
-0.6
-0.4
-0.2
0
0.2
0.4
0.6
E_{app} V vs. NHE
log [O] / [R]

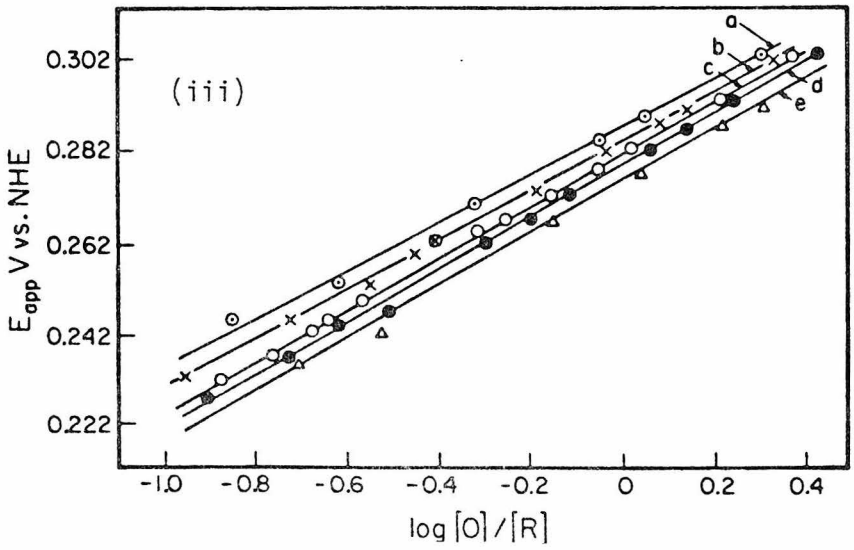
(iii)
a
b
c
d
e
0.302
0.282
0.262
0.242
0.222
-1.0
-0.8
-0.6
-0.4
-0.2
0
0.2
0.4
E_{app} V vs. NHE
log [O] / [R]

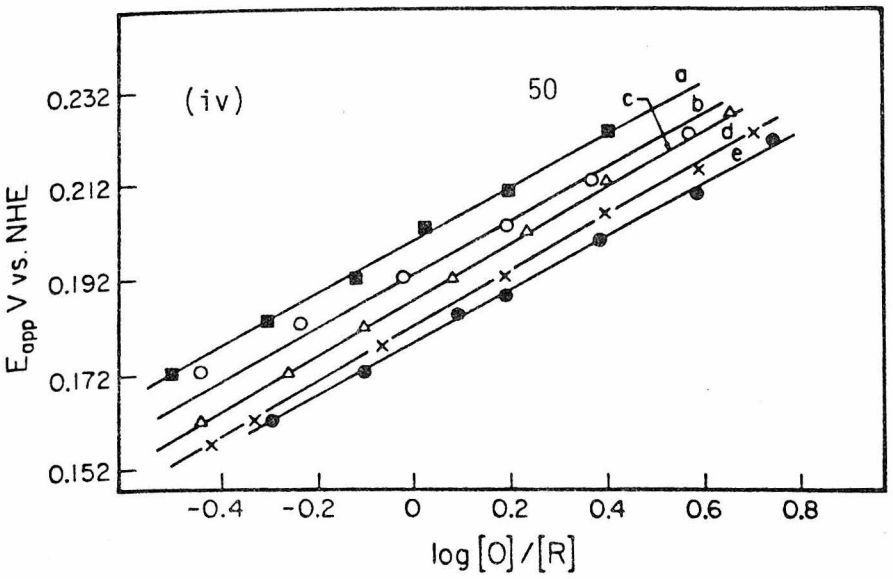
(iv)
50
a
b
c
d
e
0.232
0.212
0.192
0.172
0.152
-0.4
-0.2
0
0.2
0.4
0.6
0.8
E_{app} V vs. NHE
log [O]/[R]

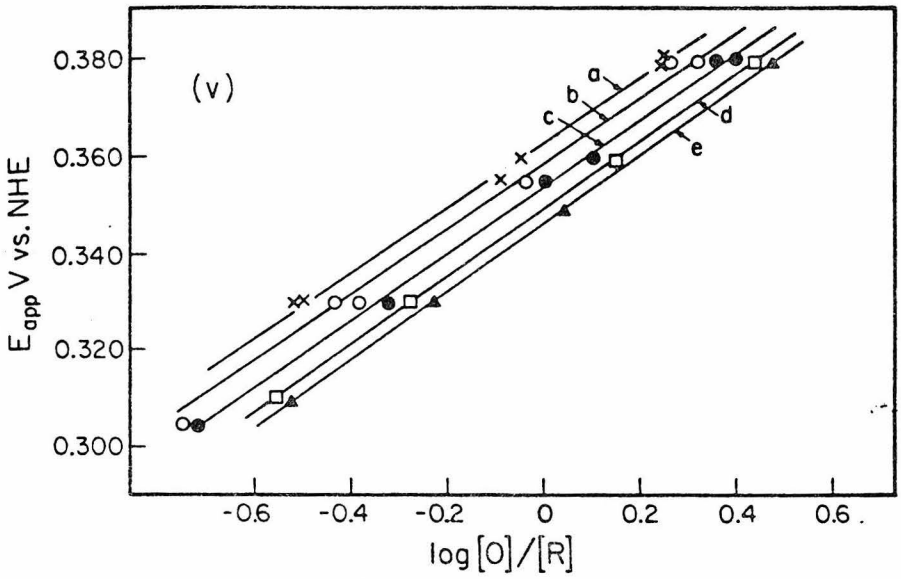
(v)
a
b
c
d
e
0.380
0.360
0.340
0.320
0.300
-0.6
-0.4
-0.2
0
0.2
0.4
0.6
E_{app} V vs. NHE
log [O]/[R]

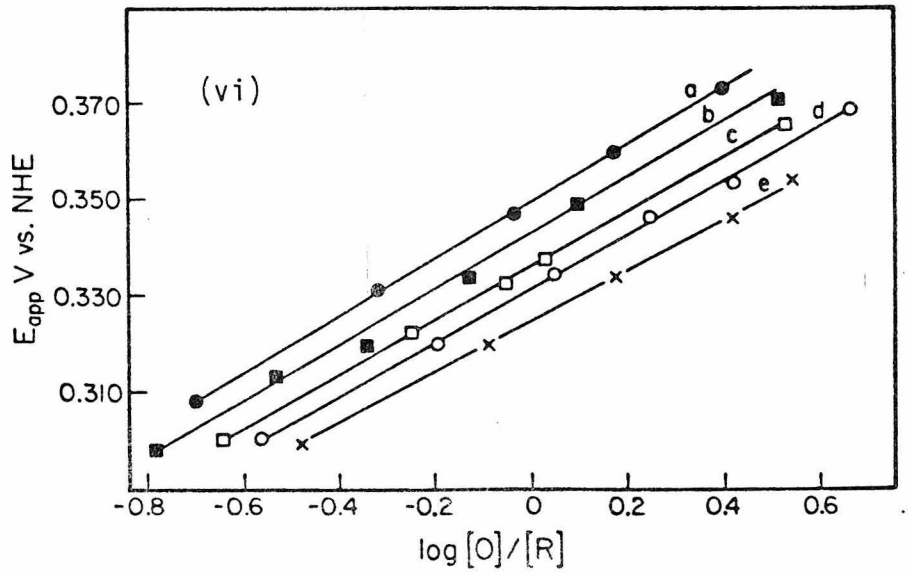
(vi)
a
b
c
d
e
0.370
0.350
0.330
0.310
-0.8
-0.6
-0.4
-0.2
0
0.2
0.4
0.6
E_{app} V vs. NHE
log [O]/[R]

Table 5. Ionic entropies, standard entropies, and standard enthalpies of the proteins studied

Protein	E^o mV [a] vs. NHE	$\bar{S}^o_{Red} - \bar{S}^o_{Ox}$ e.u.	ΔS^o [b] e.u.	ΔH^o [c] kcal mole^{-1}
Cytochrome c	+270	-17	-37	-17
Cytochrome c-551	+276	-12	-32	-16
Cytochrome cd (c heme)	+269	-57	-77	-29
(d heme)	+235	-	-	-
Stellacyanin	+184	-24	-44	-17
Plastocyanin	+347	-32	-52	-23
Azurin	+330	-43	-63	-26

[a] Standard deviation ±3 mV

[b] Standard deviation ±3 e.u.

[c] Standard deviation ±0.5 kcal mole^{-1}

The fact that plastocyanin and azurin have similar E^o values most likely reflects close structural similarities. Indeed, preliminary crystallographic results [52,53] in combination with spectroscopic data [54] indicate that the copper binding site in azurin is very much like that of plastocyanin. The crystal structure of oxidized poplar plastocyanin at 2.7 Å resolution shows that the copper(II) atom has a highly distorted tetrahedral coordination geometry [53]. The four copper coordination positions are occupied by the sulfur atoms of cysteine 84 and methionine 92, and the δ-nitrogen atoms of the imidazole groups of histidines 37 and 87. Furthermore, the copper site, which carries unit positive charge in the oxidized form, is located beneath a hydrophobic patch formed by a number of residues. Unfortunately, there is

no structural information concerning stellacyanin at this time.

The above suggestion that there may be some relationship between copper binding structure and the redox potential is all the more intriguing in view of the fact that stellacyanin, with a potential much less positive than any other blue protein, is known not to possess any methionine [55]. Thus ligand environment of the copper in stellacyanin must be at least slightly different from that of the plastocyanin structure. It is likely that one contributing factor to the unusually low potential of stellacyanin is in fact its different copper coordination environment.

The values of ΔS^o for the electron transfer reactions of the three blue proteins are large and negative. Interpretation of these results is facilitated if we first consider the corresponding thermodynamic parameter for the reduction of $Fe(H_2O)_6^{3+}$, which is ΔS^o = 27 e.u. [56]. The major contribution to the change in the entropy upon reduction of $Fe(H_2O)_6^{3+}$ is generally viewed as a decrease in the solvent ordering around the ion owing to partial charge neutralization. Specifically, reduction of $Fe(H_2O)_6^{3+}$ decreases the charge within the inner sphere and expands its radius, thereby releasing a few water molecules from the outer sphere to the bulk water. The entropy change associated with this process is positive. In contrast to $Fe(H_2O)_6^{3+}$, the value of ΔS^o for reduction of $Fe(phen)_3^{3+}$ which possesses hydrophobic ligands, is approximately -20 e.u. [57]. In the latter case, the propeller-like configuration of the planar phenanthroline ligands provides open channels that allow water molecules to come into relatively close contact with the Fe(III) in the oxidized complex. The partial charge neutralization

(+3 to +2) upon reduction causes a net rearrangement of these water molecules, resulting in formation of cages of structured water of abnormally low entropy [58,59] in the hydrophobic phenanthroline channels. We believe that the latter effect is important in the blue proteins, as the copper environment is hydrophobic and full charge neutralization of the redox center (+1 to 0) occurs upon reduction. Thus, any partially disordered water molecules near the +1 site will be converted to a highly ordered state (an internally hydrogen-bonded network of very low entropy) in the reduced protein.

We attribute the differences in ΔS^{o} among the three blue proteins to variations in the hydrophobic character of the copper redox centers. The results suggest, therefore, that the hydrophobicity of the metal site environment increases in the order stellacyanin < plastocyanin < azurin [60]. It should be noted that the proposed order is inversely related to the accessibility of the redox sites to hydrophilic inorganic agents thathave been derived [61] from kinetic experiments, as is reasonable. Further evidence that the blue copper center in stellacyanin is the least hydrophobic, and thus most kinetically accessible, is the fact that we were able to measure the reduction potential of this protein in the absence of a mediator and the resulting value was the same as that obtained in the presence of a mediator. The only difference was that the time required to reach equilibrium after each new potential applied was a few minutes longer. The other two blue proteins required a mediator in order to obtain stable potential readings.

It has been shown recently that self-exchange electron transfer rate constants calculated on the basis of relative Marcus theory provide

a useful framework for comparisons of the reactivity of metalloproteins with a variety of redox reagents [61-63]. The k_{11}^{corr} values calculated from the protein-$Fe(EDTA)^{2-}$ cross reactions have been used to define a "kinetic accessibility" scale due to the fact that $Fe(EDTA)^{2-}$ reagent is hydrophilic and there is a lack of extended π orbitals (in fact, the $Fe(EDTA)^{2-}$ complex is hydrophobic on one side, being mostly methelene hydrogen, and thus not likely to transfer electron effectively via this side). This makes effective orbital overlap sensitive to small changes in protein-reagent interaction and metal site accessibility. Therefore protein with high k_{11}^{corr} is thought to associate with a more accessible metal site. The kinetic accessibility order of the three blue proteins is: stellacyanin > plastocyanin > azurin [61]. Similar treatment is considered based on Marcus and Sutin framework [64]. The contribution of protein self-exchange ΔH_{11}^{corr} and ΔS_{11}^{corr} to the cross-reaction activa-parameters, ΔH_{12}^{*} and ΔS_{12}^{*} was calculated as given in Tables 6-8, and plots of log k_{11}^{corr} versus ΔH_{11}^{corr} and ΔS_{11}^{corr} are shown in Figure 13. The justification of the plots is as follows: The abscissa is the kinetic accessibility scale for the reason previously described. The ordinate, ΔH_{11}^{corr}, represents enthalpic energy for protein rearrangement, together with Frank-Condon barriers, while ΔS_{11}^{corr} represents the conformation change of the protein necessary to facilitate an electron transfer.

Inspection of Figure 13 gives immediate evidence that the ΔH_{11}^{corr} and ΔS_{11}^{corr} calculated based on $Fe(EDTA)^{2-}$ and $Co(phen)_3^{3+}$ and $Ru(NH_3)_5py^{3+}$ cross reactions are close together, indicating the independence of the redox reagents in the case of stellacyanin, but they span a wider range

Table 6. Protein-small molecule cross reaction rate, protein and small molecule self-exchange rate data*

Protein (1)	Reagent (2)	k_{12} $M^{-1}sec^{-1}$	ΔH_{12} kcal $mole^{-1}$	ΔS_{12} e.u.	μk_{12}	μk_{22} $M^{-1}sec^{-1}$	ΔH_{22} kcal $mole^{-1}$	ΔS_{22} e.u.	E^o_{11} mV NHE	ΔH^o_{11} kcal $mole^{-1}$	ΔS^o_{11} e.u.	E^o_{22} mV NHE	ΔH^o_{22} kcal $mole^{-1}$	ΔS^o_{22} e.u.
Stellacyanin	$Co(phen)_3^{3+}$	1.8×10^5	6	-13	0.1	4.17	5.1	-34	184	-17	-44	360	-10.3	-3.6
	$Fe(EDTA)^{2-}$	4.3×10^5	3	-21	0.5	3.0×10^4	4.0	-25				120	-20.1	- 58
	$Ru(NH_3)_5py^{3+}$	1.94×10^5	6.7	-12	0.1	4.3×10^5	8.0	-16				253	-10.3	- 15
Plastocyanin	$Co(phen)_3^{3+}$	4.9×10^3	14	5	0.1				347	-23	-52			
	$Fe(EDTA)^{2-}$	8.2×10^4	2.1	-29	0.2									
	$Ru(NH)_3)_5py^{3+}$	7.1×10^3	5.6	-22	0.5									
Azurin	$Co(phen)_3^{3+}$	3.2×10^3	14.3	7	0.2				330	-26	-63			
	$Fe(EDTA)^{3-}$	1.3×10^3	2.0	-37	0.2									
	$Ru(NH_3)_5py^{3+}$	2.0×10^3	8.8	-14	0.1									

*Taken from S. Wherland and H. B. Gray, Biological Aspects of Inorganic Chemistry, D. Dolphin, ed. (John Wiley, 1977, pp. 289-368).

Table 7. Work term and entropy term corrections for self-exchange and cross sections of protein and small molecules

Protein (1)	Reagent (2)	R_1 Å	R_2 Å	Z_1^*	Z_1'	Z_2	Z_2'	ω_{12} kcal mole^{-1}	ω_{21} kcal mole^{-1}	ω_{11} kcal mole^{-1}	ω_{22} kcal mole^{-1}	S_{12} e.u.	S_{21} e.u.	S_{11} e.u.	S_{22} e.u.
Stellacyanin	$Co(phen)_3^{3+}$	19.5	7.0	-2.4	-1.4	3.0	2.0	-.1354	-.0527	.0158	.5060	.6228	.2424	-.0727	-2.3276
	$Fe(EDTA)^{2-}$		4.0	-1.4	-2.4	-2.0	-1.0	-.0194	-.0166		.4931	-.0892	-.0764		-2.2683
	$Ru(NH_3)_5py^{3+}$		3.5	-2.4	-1.4	3.0	2.0	-.2159	-.0840		1.8489	.9931	.3864		-8.5049
Plastocyanin	$Co(phen)_3^{3+}$	15.8		-6.2	-5.1	3.0	2.0	-.5086	-.2789	.3097		2.3396	-1.2829	-1.4246	
	$Fe(EDTA)^{2-}$			-5.1	-6.2	-2.0	-1.0	.2493	.1515			-1.1468	-.6969		
	$Ru(NH_3)_5py^{3+}$			-6.2	-5.1	-3.0	2.0	-.2218	-.1216			1.0203	.5594		
Azurin	$Co(phen)_3^{3+}$	17.2		-2.4	-1.4	3.0	2.0	-.0884	-.0344	.0248		.4066	.1582	-.1141	
	$Fe(EDTA)^{2-}$			-1.4	-2.4	-2.0	-1.0	.0580	.0497			-.2668	-.2286		
	$Ru(NH_3)_5py^{3+}$			-2.4	-1.4	3.0	2.0	-.2736	-.1064			1.2586	.4894		

Table 8. Calculated protein self-exchange activation parameters, including electrostatic corrections

Protein (1)	Reagent (2)	k_{11}^{corr}	ΔG_{11}^{corr}	ΔG_{11}^{**}	ΔG_{22}^{**}	ΔG_{r}^{o}	ΔS_{r}^{o}	ΔS_{12}^{**}	ΔS_{22}^{**}	ΔS_{11}^{**}	ΔS_{11}^{corr}	ΔH_{11}^{**}	ΔH_{11}^{corr}	log k_{11}^{corr}
Stellacyanin	$Co(phen)_3^{3+}$	3.26×10^5	9.92	9.90	14.72	-3.97	40.02	-12.38	-31.67	-30.29	-30.36	.87	.87	
	$Fe(EDTA)^{2-}$	2.41×10^5	10.10	10.08	10.84	-1.48	14.01	-21.09	-22.73	-33.03	-33.11	.24	.23	5.38
	$Ru(NH_3)_5py^{3+}$	1.61×10^2	14.42	14.40	7.91	-1.46	28.39	-11.01	-7.49	-42.04	-42.12	1.87	1.87	
		2.04×10^5	10.20	10.18	12.13					-42.04	-42.12	-2.33	-2.35	
Plastocyanin	$Ca(phen)_3^{3+}$	2.33×10^4	11.48	11.46		.07	47.34	2.66		-10.29	-11.71	8.39	7.99	
	$Fe(EDTA)^{2-}$	2.68×10^1	15.50	15.48		-4.78	6.45	-27.85		-39.45	-40.77	3.72	3.35	1.42
	$Ru(NH_3)_5py^{3+}$	7.39×10^1	14.89	14.87		2.27	36.54	-23.02		-77.12	-78.55	-8.11	-8.52	
		9.35×10^4	10.66	10.64						-77.12	-78.55	-12.32	-12.75	
Azurin	$Co(phen)_3^{3+}$	2.57×10^4	11.42	11.40		- .64	59.15	6.59		-13.58	-13.70	7.35	7.34	
	$Fe(EDTA)^{2-}$	1.10×10^{-2}	20.10	20.08		-4.80	-4.96	-36.73		-46.57	-46.69	6.20	6.19	-1.96
	$Ru(NH_3)_5py^{3+}$	4.46	16.55	16.53		1.94	47.23	-15.26		-72.26	-92.37	-5.0	-5.02	
		5.64×10^3	12.32	12.30						-72.26	-72.37	-9.23	-9.25	

Figure 13. i) Plot of log k_{11}^{corr} $(Fe(EDTA))^{2-}$ vs. ΔH_{11}^{corr} of stellacyanin, plastocyanin, and azurin.

$\Delta \equiv Fe(EDTA)^{2-}$, $\square \equiv Co(phen)_3^{3+}$,

$o \equiv Ru(NH_3)_5py^{3+}$

ii) Plot of log k_{11}^{corr} $(Fe(EDTA))^{2-}$ vs ΔS_{11}^{corr} of stellacyanin, plastocyanin, and azurin

$\Delta \equiv Fe(EDTA)^{2-}$, $\square \equiv Co(phen)_3^{3+}$,

$o \equiv Ru(NH_3)_5py^{3+}$

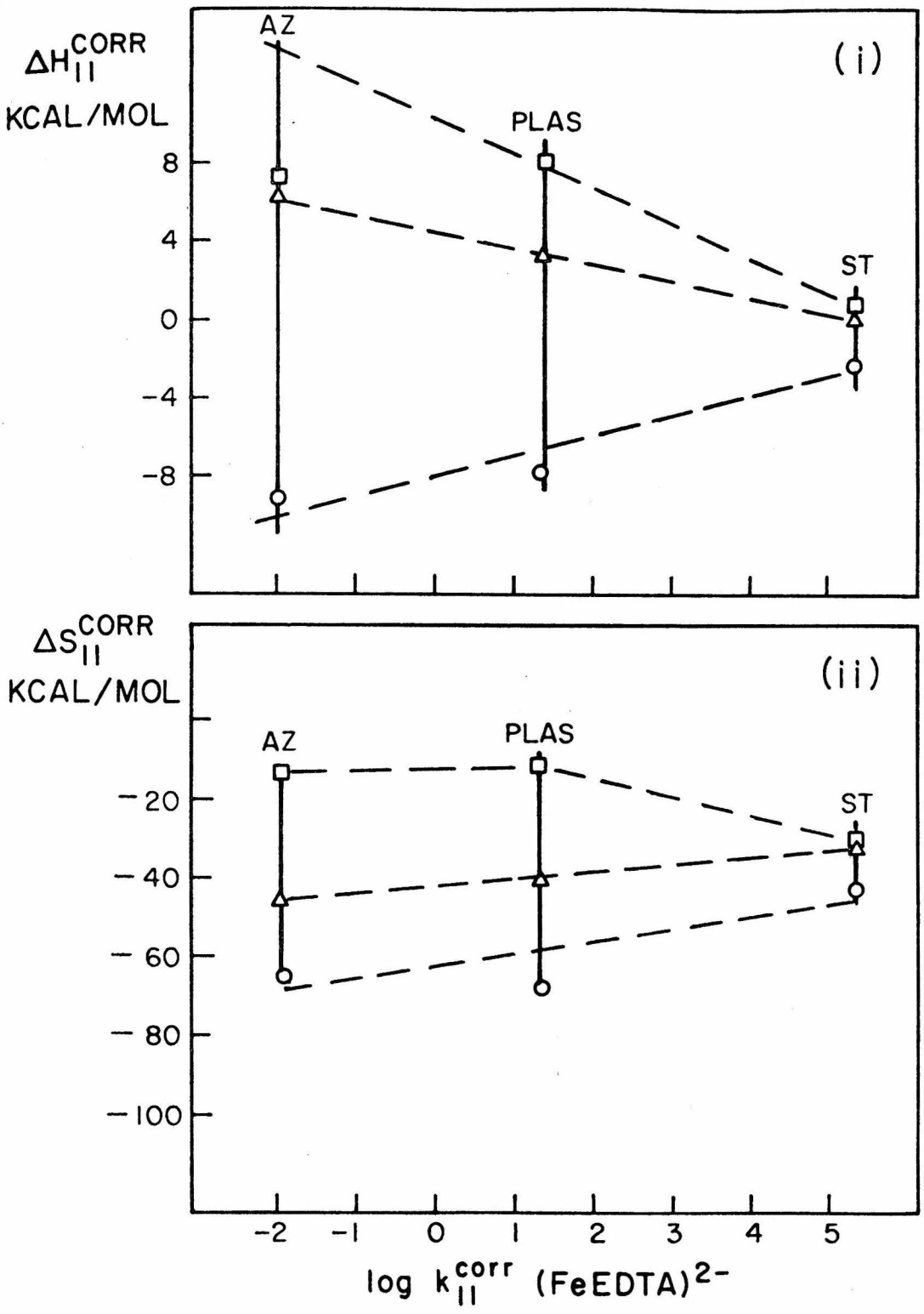
ΔH_{11}^{CORR}
KCAL/MOL
(i)
AZ
PLAS
ST
8
4
0
-4
-8
ΔS_{11}^{CORR}
KCAL/MOL
(ii)
AZ
PLAS
ST
-20
-40
-60
-80
-100
-2
-1
0
1
2
3
4
5
log k_{11}^{corr} $(FeEDTA)^{2-}$

for plastocyanin and azurin indicating a strong dependence on the redox reagents. The former observation is consistent with the hypothesis that the copper site in stellacyanin is highly kinetically accessible, that is, the copper atom must be near the surface of the protein within easy reach of the redox reagents [61]. The wide variation of ΔH_{11}^{corr} and ΔS_{11}^{corr} values for plastocyanin and azurin based on the three reagents is consistent with the idea that the copper center in each of these proteins is buried. It is apparent that the mechanistic pathways employed by plastocyanin and azurin depend strongly on the redox reagents.

Consider the calculated ΔH_{11}^{corr} based on $Fe(EDTA)^{2-}$ cross reactions for the three blue proteins; the value is slightly increased as the copper site in the protein becomes more buried. This suggests that the major contribution to the ΔH_{11}^{corr} is due to Frank-Condon activation of the oxidized and reduced copper centers and little enthalpic energy for protein rearrangement. The latter is supported by the evidence that there is very little change in ΔS_{11}^{corr} among the three blue proteins.

Comparison of the ΔH_{11}^{corr} $Ru(NH_3)_5py^{3+}$ reveals a decrease in the enthalpic energy as the copper site becomes more buried. This agrees with the original treatise [65] that the protruded hydrophobic edge of the pyridine in $Ru(NH_3)_5py^{3+}$ penetrated the hydrophobic pocket of the copper site sufficiently to effect optimal py-π copper-π overlap. Therefore, there is little, if any, enthalpic barrier for these proteins to overcome in order to transfer an electron. Furthermore, penetration of the pyridine ring into the protein hydrophobic pocket would generally be accompanied by conformation change, as evidenced from the

decrease in ΔS_{11}^{corr} from -42 e.u. of stellacyanin to -78 e.u. of plastocyanin. The similarity of ΔS_{11}^{corr} for plastocyanin and azurin suggested that the hydrophobicity of copper sites in both proteins were similar, such that they undergo similar conformation changes prior to electron transfer.

However, comparison of the ΔH_{11}^{corr} $Co(phen)_3^{3+}$ reveals completely opposite results from those of $Ru(NH_3)_5py^{3+}$. The ΔH_{11}^{corr} increases as the accessibility of the copper site decreases. As has been pointed out earlier [66], although $Co(phen)_3^{3+}$ is hydrophobic in nature, the planar propellerlike configuration of phenanthroline ligand restricts the correct orientation between the phen-π copper-π overlap. The steric effect is much too great, such that the enthalpic energy increases as the distance of protein penetration increases.

3. Cytochromes. The reduction potentials of the three c-type cytochromes are approximately the same. The measured value of horse heart cytochrome c is in good agreement with those reported earlier employing different methods [67-70]. The E^o value for bacterial cytochrome c-551 was reported to be the same as that of horse heart cytochrome c [71]. The reduction potential of the d-heme of cytochrome cd was found to be 34 mV less positive than that of c-heme (+269 mV versus NHE). This difference is in agreement with those reported earlier [50].

The similarity of the reduction potentials of the three c-heme cytochromes suggests that they possess the same type of heme coordination environment. In fact, the crystal structures of horse heart cytochrome c and bacterial cytochrome c-551 show that the heme coordination environments are similar [32,33]. The heme c is held in a hydrophobic pocket and is exposed to the external solvent only along one of its edges.

Recently, Kassner [73] has proposed a theoretical model for the effects of local nonpolar heme environments on the redox potentials of cytochromes. The model suggested that the nonpolarity of the local heme environment is directly proportional to the redox potential. Furthermore,Stellwagen and Shulman[76] has tested the above model by comparing the kinds of atoms contacting the heme in various heme-containing proteins. The results demonstrated that apolarity of the local heme environment of the proteins is virtually identical but that the reduction potential is inversely dependent on the exposure of the heme to an aqueous solvent. That is, the lower the reduction potential the more exposed the heme is to the aqueous solvent. It was concluded that the heme accessibility is increased in the order cytochrome c_2 < cytochrome c < cytochrome c-550 < hemoglobin < myoglobin. Therefore, application of the model to the cytochromes considered in this thesis would imply that the accessibility of the heme c to aqueous solvent is similar, that is, cytochrome c $\sim$ cytochrome c-551 $\sim$ cytochrome cd. However, this implication does not agree with the kinetic studies of these cytochromes with inorganic reagents [2]. Furthermore, the analysis of the kinetics of electron

transfer reactions of hemoglobin and myoglobin with inorganic complexes also revealed that the heme of myoglobin is more exposed to aqueous solvent than that of hemoglobin [74]. It is important to point out that there are two different types of heme-containing proteins considered by Stellwagen; they are, high spin (hemoglobin and myoglobin) and low spin (cytochromes c, c_2, and c-550) hemes. As has been pointed out earlier, they are different types of cytochromes and their reduction potentials are partly controlled by the spin states of the two oxidation states. Moreover, there are contributions to the reduction potentials of these cytochromes other than the local heme environment [75], namely, the axial ligands of the iron center. Therefore, it is felt that the reduction potentials cannot be directly related to the accessibility of the heme.

Among the thermodynamic parameters reported in this chapter, only those for horse heart cytochrome c have been previously reported. The value of the enthalpy change calculated for the redox reaction of horse heart cytochrome c (-17 ± 1 kcal mol^{-1}) is in agreement with those based on calorimetric data (-14.5 ± 1.5 kcal mol^{-1}) [67]. The difference is probably due to the fact that ferricyanide, which is known to bind to both oxidized and reduced forms of cytochrome c [76], was used as titrant in the determination of the previously published thermodynamic parameters.

Comparison of the thermodynamic parameters of the reduction of cytochrome c, cytochrome c-551, and cytochrome cd revealed that the reduction mechanisms for these proteins are similar, that is, they are all characterized by negatively large enthalpy and entropy changes. The

ΔH^o and ΔS^o changes are increasingly positive in the order cytochrome cd < cytochrome c < cytochrome c-551. The reduction of cytochrome cd is characterized by abnormally large enthalpy and entropy changes.

On the basis of the observed thermodynamic parameters, it is proposed that the difference in these values among the three cytochromes is attributable to the effect of solvent molecules surrounding the proteins and that they can be used as a criterion for the solvent accessibility of the heme sites. A plot of ΔH^o versus ΔS^o (Figure 14) reveals that a good extrathermodynamic relationship exists among these cytochromes. Thus ΔH^o varies linearly with ΔS^o, yielding value (slope) of 286 K (correlation coefficient 0.989) which lies in the range expected for the processes involving enzymic rate, equilibrium, and thermal denaturation [77,78]. The extrathermodynamic behavior has been attributed generally to the aqueous solvent surrounding the proteins [78]. The mechanism which each of the oxidized cytochromes undergoes to form the reduced proteins is similar. Also, it seems more likely that in each case variation in the thermodynamic parameters may be accounted for in terms of perturbation of water molecules surrounding the heme site on a common reduction mechanism. The fact that the ΔS^o value for the reduction of cytochrome cd is much more unfavorable than those of cytochrome c and cytochrome c-551 suggests that water molecules around the heme c site of cytochrome cd are much more perturbed than those around cytochrome c and cytochrome c-551. The perturbation of water molecules can be considered as a result of their hydrophobic environment. In fact, from the studies of inorganic complexes the reduction entropies

Figure 14. Compensation plot of cytochromes

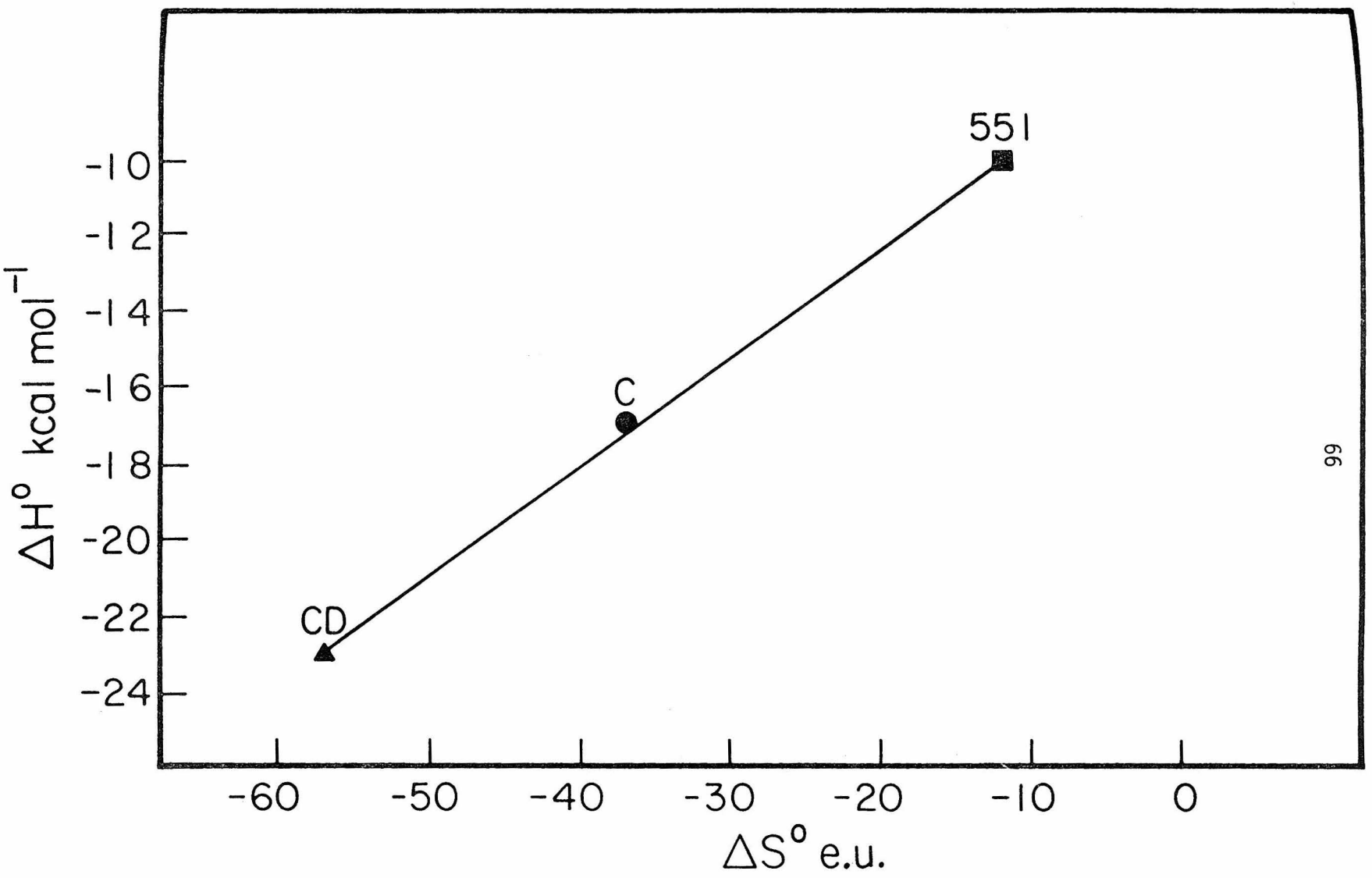
551
C
CD
-10
-12
-14
-16
-18
-20
-22
-24
ΔH° kcal mol⁻¹
-60
-50
-40
-30
-20
-10
0
ΔS° e.u.
99

of complexes with hydrophobic ligands are usually associated with large and negative enthalpy and entropy changes. Furthermore, the transfer of hydrocarbon from aqueous solvent into nonaqueous solvent is associated with losses of entropic driving force of 20 e.u. [29,30]. Therefore, it is concluded that the extrathermodynamic behavior is directly proportional to the degree of hydrophobicity of the heme sites for these cytochromes and is increased in the order cytochrome c $\sim$ cytochrome c-551 < cytochrome cd. It is interesting to note that the degree of hydrophobicity proposed is proportional to the kinetic accessibility scale, that is, based on the electrostatic corrected protein self-exchange rate constant calculated from cross-reaction with $Fe(EDTA)^{2-}$, the values for cytochrome c and cytochrome c-551 are not different by an order of magnitude (Tables 6-8), hence the kinetic accessibility of these two cytochromes do not differ much from each other. Unfortunately, there is no such treatment for cytochrome cd; however, it can be predicted that the kinetic access of cytochrome cd will be very small compared to cytochromes c and c-551.

It is interesting to consider the physical nature of oxido-reduction. Generally, it can be viewed as follows: The highly charged surface area of the enzyme (due to amino acid side chain) in aqueous solution will attract water molecules and counter ions. Upon reduction, the surface amino acid side chains rotate and translate with respect to the main polypeptide chain (breathing motion and rotation) resulting in the release of the bound water molecules around the surface to the bulk water. Whether the reduction process is accompanied by conformational

change is worth discussing. There exists an extensive body of physical and chemical data including studies on heme-ligand substituents [81), deuterium exchange [82,83], ion binding [84], and various denaturing conditions [85,86], which all indicate that the reduced form of cytochrome c possesses a more compact and structurally stable configuration than the oxidized form. The conformation change observed from the above mentioned solution studies has been suggested as being a dynamic type [88]. That is, it results from a change in either the frequency or the amplitude of the vibrational modes of the structure. This was justified as a result of lack of evidence from crystallographic data [87]. Recently, high resolution EXAFS results [89] supported this suggestion.

CONCLUSION

This chapter has been concerned with the standard enthalpy and entropy changes accompanying the reductions of the metal centers in metalloproteins. The metalloproteins studied include blue copper proteins and heme proteins. The standard enthalpy and entropy changes observed are large and negative. It has been proposed that they reflect the accessibilities of the redox sites to the solvent. Comparison of the distances of the edges of metal sites to the surface of the proteins obtained from available crystallographic data with the standard entropy changes shows a remarkable consistency among them as given in Table 9 . As the metal site becomes less accessible to the solvent, the entropy becomes more negative.

In the attempt to further characterize the activation parameters observed kinetically by means of the Marcus theory, only those for stellacyanin obey the theory. This is not surprising, since it is possible

that the electron transfer mechanism employed by metalloproteins are nonadiabatic as has been observed in inorganic complex electron transfer reactions [90,91]. Furthermore, the Marcus treatment does not take into consideration the precursor complex formations prior to the electron transfer step as it has been observed recently for electron transfer reactions involving metalloproteins [90-94].

Table 9. Distance of the edges of metal sites to the surface of the proteins and the corresponding standard entropy changes

Protein	Distance, Å	ΔS^o, e.u.
Cytochrome c-551	-	-32
Cytochrome c	2-3	-37
Stellacyanin	-	-44
Plastocyanin	3	-52
Azurin	5	-63
Cytochrome cd	-	-77

REFERENCES

1. L. E. Bennett, "Current Research Topics in Bioinorganic Chemistry," S. J. Lippard, ed. (Academic Press, New York, 1971).
2. S. Wherland and H. B. Gray, "Biological Aspects of Inorganic Chemistry," D. Dolphin, ed. (John Wiley, New York, 1976).
3. H. Taube, Adv. Inorg. Chem. Radiochem. 1, 1 (1959).
4. R. A. Marcus, Disc. Faraday Soc. 29, 21 (1960).
5. C. Creutz and N. Sutin, J. Biol. Chem. 249, 6788 (1974), and references cited therein.
6. C. T. Lin, W. Bottcher, M. Chau, C. Creutz, and N. Sutin, J. Am. Chem. Soc. 98, 6536 (1976), and references cited therein.
7. M. Chau, C. Creutz, and N. Sutin, J. Am. Soc. Chem. 99, 5615 (1977).
8. S. Wherland and H. B. Gray, Proc. Natl. Acad. Sci. USA 73, 2950 (1976).
9. H. B. Callen, in "Thermodynamics" (J. Wiley, New York, 1961).
10. a) H. R. Mahler and E. H. Cordes, in "Biological Chemistry" (Harper and Row, New York, 1971).
    b) N. I. Bishop, Ann. Rev. Biochem. 40, 197 (1971).
    c) D. F. Wilson, P. L. Dutton, M. Erecinska, J. G. Lindsay, and N. Sato, Accounts Chem. Res. 5, 234 (1972).
11. a) R. H. Tiesjema, A. O. Muijsers, and B. F. Van Gelder, Biochim. Biophys. Acta 305, 19 (1973).
    b) J. Vanderkooi and M. Erecinska, Arch. Biochem. Biophys. 162, 385 (1974).
12. a) R. E. Powell and W. M. Latimer, J. Chem. Phys. 19, 1139 (1951).
    b) J. W. Cobble, J. Chem. Phys. 21, 1446 (1953).
13. a) R. E. Powell, J. Phys. Chem. 58, 528 (1954).
    b) K. J. Laidler, Can. J. Chem. 34, 1107 (1956).
14. R. A. Marcus and N. Sutin, Inorg. Chem. 14, 213 (1975).

15. A. L. Lehninger, "Biochemistry" (Worth Publishers, Inc., New York, 1970).

16. T. Horio, I. Sekuzu, T. Higashi, and K. Okuniki, "Haematin Enzymes," J. E. Falk, R. Lemberg, and R. K. Morton, eds. (Pergamon Press, New York, 1961).

17. B. R. M. Reinhammar, Biochem. Biophys. Acta 275, 245 (1972).

18. P. M. Colman, H. C. Freeman, J. M. Guss, M. Murata, V. A. Norris, J.A.M. Ramshaw, and M. P. Venkatappa, Nature 272, 319 (1978).

19. E. T. Edman, R. E. Stenkamp, L. C. Sieker, and L. H. Jensen, Biochem. J. Mol. Biol. 123, 35 (1978).

20. T. D. Tullius, P. Frank, and K. O. Hodgson, Proc. Natl. Acad. Sci. USA 75, 4069 (1978).

21. G. H. Rist, J. S. Hyde, and T. Vanngard, Proc. Natl. Acad. Sci. USA 67, 79 (1970).

22. O. Siiman, N. M. Young, and P. R. Carey, J. Am. Chem. Soc. 98, 744 (1976).

23. V. Miskowski, S. P. Tang, T. G. Spiro, E. Shapiro, and T. H. Moss, Biochemistry 14, 1244 (1975).

24. R. Malkin and B. G. Malmstrom, Adv. Enzymol. 33, 177 (1970).

25. D. R. McMillin, R. A. Holwerda, and H. B. Gray, Proc. Natl. Acad. Sci. USA 71, 1339 (1974).

26. E. I. Solomon, P. J. Clendening, H. B. Gray, and F. I. Grunthaner, J. Am. Chem. Soc. 97, 3878 (1975).

27. R. E. Dickerson and R. Timkovich, "The Enzymes," P. Boyer, ed., 3rd edition, Vol. 11 (Academic Press, New York, 1975).

28. T. Horio, T. Higashi, H. Matsubara, and K. Okunuki, J. Biol. Chem. 236, 944 (1961).

29. T. Kuronen and N. Ellfork, Biochim. Biophys. Acta 275, 308 (1972).

30. T. Kuronen, M. Saraste, and N. Ellfork, Biochim. Biophys. Acta 393, 48 (1975).

31. M. Saraste and T. Kuronen, Biochim. Biophys. Acta 513, 177 (1978).

32. T. Takano, O. B. Kallai, R. Swanson, and R. E. Dickerson, J. Biol. Chem. 248, 5234 (1973).

33. R. J. Almassy and R. E. Dickerson, Proc. Natl. Acad. Sci. USA 75, 2674 (1978).

34. T. Takano, R. E. Dickerson, S. A. Schichman, and T. E. Meyer, submitted for publication.

35. T. Kuwana and N. Winograd," Electroanalytical Chemistry," A. J. Bard, ed., vol. 7 (Marcel Dekker, Inc., New York, 1974).

36. W. R. Heineman, Anal. Chem. 50, 390A (1978), and references cited therein.

37. W. R. Heineman, B. J. Norris and J. F. Goelz, Anal. Chem. 47, 79 (1975).

38. W. R. Heineman, personal communication.

39. H. Wieland, Ber. 48, 1078 (1915).

40. H. J. Shine, R. L. Snell, and J. C. Trisler, Anal. Chem. 30, 383 (1958).

41. P. Ford, D. F. P. Rudd, R. Gaunder, and H. Taube, J. Am. Chem. Soc. 90, 1187 (1968).

42. D. Cummins and H. B. Gray, J. Am. Chem. Soc. 99, 5158 (1977).

43. P. Pfeiffer and B. Werdelman, Z. Anorg. Allg. Chem. 263, 31 (1950).

44. P. A. Rock, Inorg. Chem. 7, 837 (1968).

45. P. George and D. S. McClure, Progr. Inorg. Chem. 1, 381 (1959).

46. D. A. Buckingham and A. M. Sargeson in "Chelating Agents and Metal Chelates," F. P. Dwyer and D. P. Mellor, eds. (Academic Press, Inc., New York, 1964), pp. 237-282.

47. R. Lumry in "Probes of Structure and Function of Macromolecules and Membranes," Vol. 2, B. Chance, et al., eds. (Academic Press, New York, 1971), p. 353.

48. C. Tanford in "The Hydrophobic Effect" (John Wiley, New York, 1973).

49. V. Gutmann, G. Gritzer, and K. Danksagmüller, Inorg. Chim. Acta 17, 81 (1976).

50. a) R. Malkin, D. B. Knaff, and A. J. Bearden, Biochim. Biophys. Acta 305, 675 (1973).
b) S. Katoh, I. Shivatori, and A. Takamiya, J. Biochem. 51, 32 (1962).

51. J. A. Fee, Struct. Bonding (Berlin) 23, 1 (1975).

52. E. T. Adman, R. E. Stenkamp, L. C. Sieker, and L. H. Jensen, J. Mol. Biol. 123, 35 (1978).

53. P. M. Colman, H. C. Freeman, J. M. Guss, M. Murata, V. A. Norris, J.A.M. Ramshaw, and M. P. Venkatappa, Nature (London) 272, 319 (1978).

54. E. I. Solomon, J. W. Hare, and H. B. Gray, Proc. Natl. Acad. Sci. USA 73, 1387 (1976).

55. C. Bergman, E. Grandoik, P. Nyman, and L. Strid, Biochem. Biophys. Res. Comm. 77, 1052 (1977).

56. G.I.H. Hanania, D. H. Irvine, W. A. Eaton, and P. George, J. Phys. Chem. 71, 2022 (1967).

57. Results from three independent measurements are as follows: -18(±2) (E. L. Lee, R. J. Cave, K. L. Guyer, P. D. Tyma, and M. J. Weaver, J. Am. Chem. Soc. 101, 1131 (1979); -25(±4) (V. T. Taniguchi, N. Sail Sailasuta, F. C. Anson, and H. B. Gray, to be submitted for publication); and -20(±2) e.u. (P. George, G.I.H. Hanania, and D. H. Irvine, J. Chem. Soc., 3548 (1959)). The first two values were calculated assuming that $S^{o}(H^{+}(aq) + e^{-} \rightarrow 1/2\ H_2) = 20$ e.u.

58. R. Lumry in "Probes of Structure and Function of Macromolecules and Membranes," Vol. 2, B. Chance, et al., eds. (Academic Press, New York, 1971), p. 353.

59. C. Tanford, "The Hydrophobic Effect" (John Wiley, New York, 1973).

60. The extent to which conformational changes contribute to S^o values is unknown. However, our interpretation in terms of rearrangement of water structure does not require accompanying conformational changes in the blue proteins.

61. R. A. Holwerda, S. Wherland, and H. B. Gray, Ann. Rev. Biophys. Bioeng. 5, 363 (1976).

62. S. Wherland, R. A. Holwerda, R. C. Rosenberg, and H. B. Gray, J. Am. Chem. Soc. 97, 5260 (1975).

63. R. C. Rosenberg, S. Wherland, R. A. Holwerda, and H. B. Gray, J. Am. Chem. Soc. 98, 6364 (1976).

64. R. A. Marcus and N. Sutin, Inorg. Chem. 14, 213 (1975).

65. D. Cummins and H. B. Gray, J. Am. Chem. Soc. 99, 5158 (1977).

66. J. V. McArdle, H. B. Gray, C. Creutz, and N. Sutin, J. Am. Chem. Soc. 99, 4141 (1977).

67. P. George, W. A. Eaton, and M. Trachtman, Fed. Proc. 27, 526 (1968).

68. R. Margalit and A. Schejter, FEBS Lett. 6, 278, (1970).

69. G. D. Watt and J. M. Sturtevant, Biochemistry 8, 4567 (1969).

70. R. Margalit and A. Schejter, Eur. J. Biochem. 32, 495, 500 (1973).

71. R. A. Morton, J. Overnell, and H. A. Harbury, J. Biol. Chem. 245, 4653 (1970).

72. H. Shimada and Y. Orii, J. Biochem. 80, 135 (1976).

73. R. J. Kassner, J. Am. Chem. Soc. 95, 2674 (1973).

74. A. Grant Mauk and H. B. Gray, Biochem. Biophys. Res. Comm. 86, 206 (1979).

75. G. R. Moore and R.J.P. Williams, FEBS Lett. 79, 229 (1977).

76. E. Stellwagen and R. G. Shulman, J. Mol. Biol. 80, 559 (1973).

77. R. Lumry and S. Rajender, Biopolymers 9, 1125 (1970).

78. R. Lumry in "Electron and Coupled Energy Transfer in Biological Systems," vol. 1A, T. E. King and M. Klingenberg, eds. (Marcel Dekker, New York, 1971), p. 1.

79. C. Tanford, J. Am. Chem. Soc. 79, 5340 (1957).

80. W. Kauzmann, Adv. Prot. Chem. 14, 1 (1959).

81. L. S. Kaminsky, P. E. Burger, A. J. Davison, D. Helfet, Biochem. 11, 3702 (1972).

82. D. D. Ulmer, J.H.R. Kagi, Biochem. 7, 2710 (1968).

83. J.H.R. Kagi and D. D. Ulmer, Biochem. 7, 2718 (1968).

84. For example, R. Margalit and A. Schejter, Eur. J. Biochem. 32, 500 (1973); E. Stellwagen and R. D. Cass, J. Biol. Chem. 250, 2095 (1975).

85. C. Greenwood and M. T. Wilson, Eur. J. Biochem. 22, 5 (1971).

86. C. Greenwood and G. Palmer, J. Biol. Chem. 240, 3660 (1965).

87. N. Mendel, G. Mendel, B. L. Trus, J. Rosenberg, G. Carlson, and R. E. Dickerson, J. Biol. Chem. 252, 4619 (1977).

88. F. R. Salemme, Ann. Rev. Biochem. 46, 299 (1977).

89. A. Labhardt and C. Yuen, Nature (London) 277, 151 (1979).

90. M. Chau, C. Creutz, and N. Sutin, J. Am. Chem. Soc. 99, 5615 (1977)

91. G. M. Brown and N. Sutin, J. Am. Chem. Soc., in press.

92. G. S. Yoneda and R. A. Holwerda, Bioinorg. Chem. 8, 139 (1978).

93. M. G. Segal and A. G. Sykes, Chem. Comm., 764 (1977).

94. M. Goldberg and I. Pecht, Biochemistry 15, 4197 (1976).

Appendix 1. Marcus Theory for Outer-Sphere Electron Transfer Reactions

Marcus theory predicts a relationship between the rate constant, k_{12}, for an electron transfer reaction, and K_{12}, the equilibrium constant for the reaction, and k_{11} and k_{22}, the self-exchange rate constants for the reductant and oxidant couples:[1]

$$k_{12} = [k_{11}k_{22}K_{12}f_{12}]^{1/2} \qquad (1)$$

where $$\log f_{12} = \frac{(\log K_{12})^2}{4 \log(k_{11}k_{22}/Z^2)}$$

(Z is a collision frequency, generally taken as $10^{11} M^{-1} sec^{-1}$), and

$$\Delta G^*_{12} = \frac{\Delta G^*_{11}}{2} + \frac{\Delta G^*_{22}}{2} + \frac{\Delta G^o_{12}}{2}(1 + \alpha) \qquad (2)$$

$$\alpha = \frac{\Delta G^o_{12}}{4(\Delta G^*_{11} + \Delta G^*_{22})}$$

There are many assumptions[2] made in deriving equations (1) and (2) and the more important ones are: 1) the stabilities of the precursor and successor complexes (including work terms for bringing the reactants together and separating the products) of various reactions has been neglected; 2) it has been assumed that the reactions involved in the rate comparisons are adiabatic, that is, $(\log K_{12})^2$ and/or $k_{11}k_{22}$ is sufficiently small; 3) no very rapid pre-equilibrium changes (e.g., spin changes) take place prior to the electron transfer step; and 4) nuclear

[1] R. A. Marcus, Disc. Faraday Soc. 29, 21 (1960).

[2] R. A. Marcus and N. Sutin, Inorg. Chem. 14, 213 (1975).

tunneling contributions have been neglected.

The theory has proven successful in predicting rate constants of inorganic complex electron transfer reactions when compared to those observed experimentally.[3-4] In general, the observed and calculated k_{12} agree within a factor of ten.[5] Recently, it has been reported,[2,6] that a better agreement between the observed and calculated rate constants can be achieved when corrections for electrostatic interactions are included. The work term correction for the observed rate constant is expressed according to equation (3)

$$W = 2.1175 \frac{Z_a Z_b}{R_a + R_b} \left[\frac{e^{-\kappa R_b}}{1 + \kappa R_a} + \frac{e^{-\kappa R_a}}{1 + \kappa R_b}\right] \qquad (3)$$

where $\kappa = 0.329 \mu^{1/2} \rho \text{ Å}^{-1}$

Z_a, Z_b = charges of reactants

R_a, R_b = radii of reactants

A detailed consideration of these corrections is available.[6] The activation parameters can be estimated using the equations derived by Marcus and Sutin:[2]

---

[3] M. H. Ford-Smith and N. Sutin, J. Am. Chem. Soc. 83, 1830 (1961).

[4] G. Dulz and N. Sutin, Inorg. Chem. 2, 917 (1963).

[5] M. Chan, C. Creutz, and N. Sutin, J. Am. Chem. Soc. 99, 5615 (1977).

[6] S. Wherland and H. B. Gray, "Biological Aspects of Inorganic Chemistry," D. Dolphin, ed. (John Wiley, New York, 1976).

$$\Delta H^*_{12} = \left[\frac{\Delta H^*_{11} + \Delta H^*_{22}}{2}\right](1 - 4\alpha^2) + \frac{\Delta H^o_{12}}{2}(1 - 2\alpha)$$

$$\Delta S^*_{12} = \left[\frac{\Delta S^*_{11} + \Delta S^*_{22}}{2}\right](1 - 4\alpha^2) + \frac{\Delta S^o_{12}}{2}(1 - 2\alpha) \qquad (4)$$

These activation parameters are not the same as those calculated normally from temperature dependence data which was assumed in the Marcus treatment.[1] Therefore the following corrections are necessary (assuming that $Z = 10^{11} M^{-1} sec^{-1}$, $T = 298°K$):

$$\Delta G^{\neq} = \Delta G^* - RT \ln(hZ/kT)$$

$$= \Delta G^* - 2.44 \qquad \text{kcal mole}^{-1}$$

$$\Delta H^{\neq} = \Delta H^* - \frac{1}{2} RT$$

$$= \Delta H^* + 0.3 \qquad \text{kcal mole}^{-1}$$

$$\Delta S^{\neq} = \Delta S^* + R \ln(hZ/kT) - \frac{1}{2} R$$

$$= \Delta S^* - 9.19 \qquad \text{e.u.}$$

The corrections for electrostatic interactions to entropy of activation can be obtained by differentiating the free energy with respect to temperature:

$$\Delta S = - \frac{\partial(\Delta W)}{\partial T}$$

assuming $\kappa = 50.3(\mu/\varepsilon T)^{1/2}$

and $\varepsilon T = a_0 + a_1 T + a_2 T^2$

where ε = dielectric constant of water. Hence,

$$\Delta S = -\frac{W}{\varepsilon}\left(\frac{a_o}{T^2} - a^2\right) - \frac{e^2 Z_a Z_b \kappa}{2(R_a+R_b)\varepsilon^2}\left(\frac{a_1}{2T} + a_2\right)$$

$$\times \left[R_a\left(\frac{e^{-\kappa R_a}}{1+\kappa R_b} + \frac{e^{-\kappa R_b}}{(1+\kappa R_a)^2}\right) + R_b\left(\frac{e^{-\kappa R_b}}{1+\kappa R_a} + \frac{e^{-\kappa R_a}}{(1+\kappa R_b)^2}\right)\right]$$

and the expression $\Delta h = \Delta W + T\Delta S$ can be used for correction of enthalpy component.

Appendix 2. Estimation in the Propagation of Error in the Nernst Plot

$$E_{applied} = E^{o} + \frac{0.059}{n} \log \frac{[O]}{[R]}$$

where $[O]/[R] = \frac{A_i - A_R}{A_o - A_i}$

A_i = absorbance

A_R = absorbance of the totally reduced enzyme

A_o = absorbance of the totally oxidized enzyme

Define $X_i = \frac{1}{2.303} \ln \frac{A_i - A_R}{A_o - A_i}$

$Y_i = E_i$

σ_A = standard deviation in measuring absorbance and assumed constant for all absorbances

Define $B \equiv A_o - A_i$

Then $\sigma_B^2 = (\sigma_{A_o})^2 + (\sigma_{A_i})^2$ *

$\sigma_B = \sqrt{2}\, \sigma_A$

Define $C \equiv A_i - A_R$

$\sigma_e = \sqrt{2}\, \sigma_A$

---

*P. R. Bevington, "Data Reduction and Error Analysis of the Physical Sciences," (McGraw-Hill, New York, 1969), Ch. 4.

Define $D = C/B$

$$\left(\frac{\sigma_D}{D}\right)^2 = \left(\frac{\sigma_C}{C}\right)^2 + \left(\frac{\sigma_B}{B}\right)^2$$

$$\sigma_D^2 = D^2\left(\frac{\sigma_C}{C}\right)^2 + D^2\left(\frac{\sigma_B}{B}\right)^2$$

$$= \left(\frac{\sigma_C}{B}\right)^2 + D^2\left(\frac{\sigma_B}{B}\right)^2$$

$$= [1 + D^2]\left(\frac{\sigma_B}{B}\right)^2$$

$$= 2\left[1 + \left(\frac{A_i - A_R}{A_o - A_i}\right)^2\right]\frac{\sigma_A^2}{(A_o - A_i)^2}$$

$$\sigma_D = \sqrt{2}\,\frac{\sigma_A}{A_o - A_i}\left[1 + \left(\frac{A_i - A_R}{A_o - A_i}\right)^2\right]^{1/2}$$

So

$$x = \frac{1}{2.303}\,\ell n\, D$$

$$\sigma_x = \frac{1}{2.303}\,\frac{\sigma_D}{D}$$

$$\sigma_y = \sigma_E$$

Let there be error in the Y axis so

$$[\sigma_y']^2 = \sigma_y^2 + \sigma_x^2$$

So $$[\sigma_y']^2 = \sigma_E^2 + \left[\frac{1}{2.303}\,\frac{\sigma_D}{D}\right]^2$$

$$= \sigma_E^2 + \left[\frac{1}{2.303}\cdot\frac{\sqrt{2}\,\sigma_A}{A_o - A_i}\left[1 + \left(\frac{A_i - A_R}{A_o - A_i}\right)^2\right]^{1/2}\frac{A_o - A_i}{A_i - A_R}\right]^2$$

$$= \sigma_E^2 + \left[\frac{1}{2.303} \cdot \frac{\sqrt{2}\,\sigma_A}{A_i - A_R} \left[1 + \left(\frac{A_i - A_R}{A_o - A_i} \right)^2 \right]^{1/2} \right]^2$$

Appendix 3. Theoretical Consideration of Reduction Potential and Its Temperature Dependence

Consider two complex ions ML_x^{n+} and $ML_x^{(n+1)+}$ of the same chemical composition, which differ only in their charges. The potential E for the reversible cell

$$Pt\left|ML_x^{n+}, ML_x^{(n+1)+}\right|\left|H^+_{a(H+)=1}\right|H_2(1\ atm)\ (Pt)$$

at constant temperature, pressure, and without any liquid junctions, is related to standard thermodynamic potential, E^o, by the expression

$$E = E^o - \frac{RT}{nF} \ln \frac{(a_{ML_x^{(n+1)+}})(a_{H_2})^{1/2}}{(a_{ML_x^{n+}})(a_{H+})} \qquad (1)$$

where R is the gas constant, T the absolute temperature, n the number of eletrons, F the Faraday, a_i the activity of the ion i, and E^o the potential of the system when all constituents involved in the cell reaction are unity activity.

It is convenient to regard E as resulting from two separate redox half cells

$$ML_x^{n+} \longrightarrow ML_x^{(n+1)+} + e^- \quad , \quad E_1^o$$

$$H^+ + e^- \longrightarrow \frac{1}{2} H_2 \quad , \quad E_2^o$$

Equation (1) may be rewritten as

$$E = \left(E_1^o - \frac{RT}{F} \ln \frac{a_{ML_x^{(n+1)+}}}{a_{ML_x^{n+}}}\right) - \left(E_2^o - \frac{RT}{F} \ln \frac{a_{H+}}{(a_{H_2})^{1/2}}\right) \qquad (2)$$

At unit activity of H^+ and one atmospheric pressure of hydrogen, the potential of the reversible hydrogen electrode is defined as zero at all temperatures. Equation (2) becomes

$$E = E_1^o - \frac{RT}{F} \ln \frac{a_{ML_x^{(n+1)+}}}{a_{ML_x^{n+}}} \tag{3}$$

For convenience it is assumed that concentrations and activities are equal; equation (3) can be rewritten as (Nernst equation)

$$E = E_1^o - \frac{RT}{F} \ln \frac{C_{ML_x^{(n+1)+}}}{C_{ML_x^{n+}}} \tag{4}$$

The temperature coefficient of electrode potentials can be defined experimentally in two ways, either as an "isothermal" or as "non-isothermal."[1] The isothermal temperature coefficient $(\frac{\partial E}{\partial T})_{iso}$ is the derivative of the electrode potential E of the isothermal cell

$$\text{SHE} \,\|\, \text{Electrolyte} \,|\, \text{Electrode} \tag{5}$$

where SHE is a standard hydrogen electrode and the temperature of both electrodes is varied in the same way. The nonisothermal temperature coefficient $(\frac{\partial E}{\partial T})_{noniso}$ is the derivative of the electrode potential E of the nonisothermal cell

$$\begin{aligned} &M(T_1)\,|\,\text{Electrode}(T_1)\,|\,\text{Electrolyte}(T_1)\,|\,\text{Electrolyte}(T_2)\,| \\ &\quad |\,\text{Electrode}(T_2)\,|\,\text{Electrode}(T_1)\,|\,M(T_1) \end{aligned} \tag{6}$$

---

[1] J. N. Agar, Rev. Pure and Appl. Chem. 8, 1 (1958).

In this arrangement, the temperature (T_1) of the half-cell containing the redox couple of interest is varied, while the temperature (T_2) of the other half-cell containing reference electrode is held constant.

The standard entropy and enthalpy of the isothermal cell reaction can be calculated from equations (7)[2] and (8):

$$\Delta S^o = \frac{F}{4.18} \left(\frac{\partial E}{\partial T}\right)_{iso} \tag{7}$$

$$\Delta G^o = \Delta H^o - T\Delta S^o \tag{8}$$

The overall entropy change for the cell reaction is

$$\Delta S^o = \overline{S}^o_{ML_x^{(n+1)+}} - \overline{S}^o_{ML_x^{n+}} + \frac{1}{2} S^o_{H_2(g)} - \overline{S}^o_{H^+(aq)}$$

At unit activity $\overline{S}^o_{H^+(aq)} = 5$ e.u.,[3] and at one atmospheric pressure, $S^o_{H_2(g)} = 31.2$ e.u.[4] Then

$$\Delta S^o = \overline{S}^o_{ML_x^{(n+1)+}} - \overline{S}^o_{ML_x^{n+}} + 20.6 \text{ e.u.}$$

The $\left(\frac{\partial E}{\partial T}\right)_{noniso}$ of a nonisothermal cell can be separated into three components:[5] ϕ_{tc}, a metallic thermocouple potential difference between the hot and cold region of the working electrode; ϕ_f^m, the corresponding

---

[2] G. M. Barrow, "Physical Chemistry," (McGraw-Hill, New York, 1961).

[3] R. W. Gurney, "Ionic Processes in Solution" (McGraw-Hill, New York, 1953).

[4] G.I.H. Hanania, D. H. Irvine, W. A. Eaton, and P. George, J. Phys. Chem. 71, 2022 (1967).

Galvani metal-solution potential difference at the working electrode; $\phi_{t\ell_j}$, Galvani potential difference across the thermal liquid junction within the KCl salt bridge, then

$$\frac{dE_f^{ni}}{dT} = \frac{d\phi_{tc}}{dT} + \frac{d\phi_f^m}{dT} + \frac{d\phi_{t\ell_j}}{dT} \tag{9}$$

since $\frac{d\phi_{tc}}{dT}$ [6] and $\frac{d\phi_{t\phi_j}}{dT}$ [5] are known to be negligibly small compared to most experiments where a precision of only $\pm 50\ \mu V\ deg^{-1}$ could be reliably achieved.[5] Therefore, equation (9) can be rewritten as

$$\frac{dE_f^{ni}}{dT} \simeq \frac{d\phi_f^m}{dT} \tag{10}$$

The temperature dependence of the potential, $\frac{dE^{ni}}{dT}$ could be identified with the coefficient $\frac{d\phi_f^m}{dT}$, which gives ΔS^o from equation (11) similar to those of equation (7).

$$\Delta\bar{S}^o = \frac{F}{4.18}\frac{d\phi_f^m}{dT} \tag{11}$$

where $$\Delta\bar{S}^o = \bar{S}^o_{RED} - \bar{S}^o_{OX}$$

$\Delta\bar{S}^o$ has been referred to as the absolute ionic entropy[5] or partial molar entropy.[4]

---

[5] E. L. Yee, R. J. Cave, K. L. Guyer, P. D. Tyma, and M. J. Weaver, J. Am. Chem. Soc. 101, 1131 (1979).

[6] J. N. Agar, Adv. Electrochem. Eng. 3, 31 (1963).

CHAPTER 2

STUDIES OF REDUCTION POTENTIALS AND ELECTRON TRANSFER KINETICS OF SULFITE OXIDASE

INTRODUCTION

Sulfite oxidase is an enzyme catalyzing the oxidation of inorganic sulfite to sulfate, the terminal step in sulfur catabolism in higher organisms [1]. The enzyme has been observed in bacteria [2,3], plants [4,5], and in mammalian tissues [6,7], especially in liver [1]. Sulfite oxidase exists as a dimer of 55,000 dalton polypeptide subunits and contains two b_5-like hemes and two molybdenums as prosthetic groups. The enzyme is present in the intermembrane space of mitochondria and is capable of reducing cytochrome c present in the inner mitochondrial membrane. The enzyme thereby couples the two-electron oxidation of sulfite with two one-electron reductions of cytochrome c, and the following catalytic cycle of the enzyme is shown in Figure 1. Sulfite oxidase from rat and beef livers can be proteolytically cleaved to give molybdenum and heme domains, each of which preserves the essential features of the particular metal site [8,9]. The chicken liver enzyme can also be cleaved, but only the heme domain remains intact [10]. Apart from being readily available and cleavable into functional domains, sulfite oxidase is also the smallest and simplest known molybdenum enzyme.

Structural information of both prosthetic groups in sulfite oxidase is available. The characteristic absorption spectra of the enzyme is similar to that of cytochrome b_5 [11]. The oxidized enzyme exhibits a broad low intensity band at 530 nm, a shoulder at 560 nm, and a Soret band at 413 nm. Upon reduction by sulfite or dithionite, the spectrum features peaks at 555, 526, 423, and 325 nm (Figure 2). The coordination environment of the iron is thus similar to that of cytochrome b_5, that is,

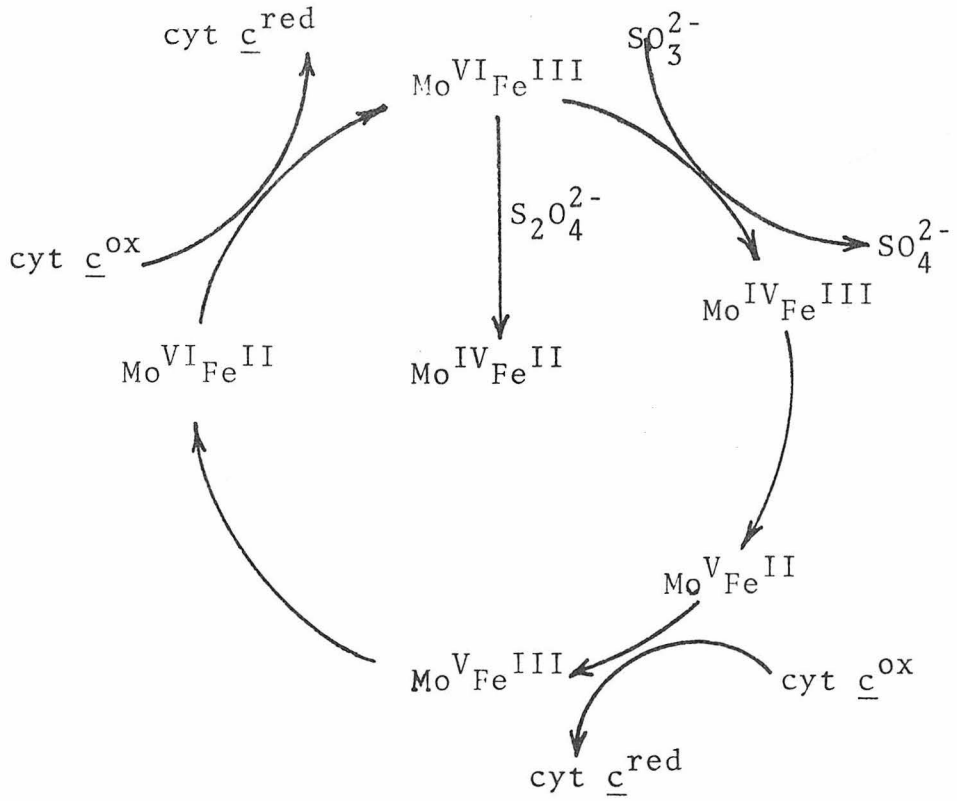

Figure 1. Catalytic cycle of sulfite oxidase.

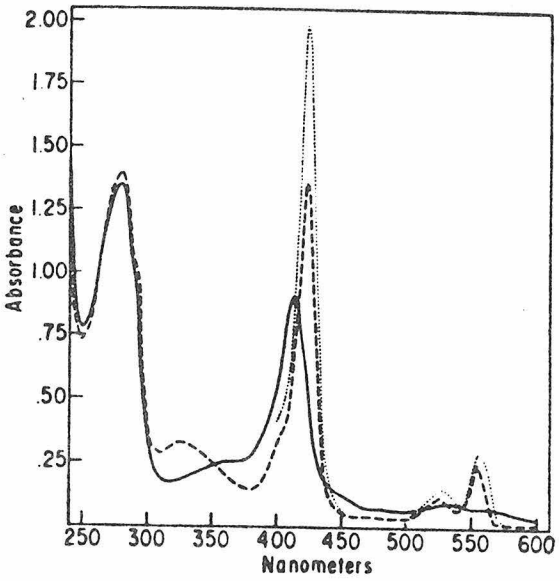

Figure 2. Absorption spectra of sulfite oxidase and of cytochrome b_5. The solid line represents the spectrum obtained from 0.75 mg per ml of sulfite oxidase in 0.05 M potassium phosphate at pH 7.8. The dashed line is the spectrum observed when sodium sulfite was then added to the final concentration of 1 mM. The dotted line represents the spectrum of microsomal cytochrome b_5 reduced by DPNH plus catalytic amounts of DPNH- cytochrome b_5 reductase. (from reference 1).

both the iron (III) and iron (II) centers are low-spin at neutral pH, being coordinated to protoporphyrin IX and two axial histidines [12,13]. Recently, structural information of the molybdenum coordination environment has become available through X-ray absorption spectroscopic studies [14]. They have established that the molybdenum is bound to a mixture of oxo and sulfur-donor ligands. Upon combination of EXAFS data and crystallographic results of model compounds, it has been established that the Mo(IV) of sulfite oxidase is coordinated to two cis oxo groups, two sulfurs with relatively short bond lengths trans to each other, one long distance sulfur trans to Mo = O, and a final intermediate distance sulfur, also trans to Mo = O.

Kinetics of the electron transfer reactions of sulfite oxidase have not been well studied except those in which both electron donors and electron acceptors are present [10,11]. It has been proposed that the enzyme employs a ping-pong mechanism in these reactions [15].

This chapter concerns the kinetic studies of the reduction of heme moiety in sulfite oxidase by $Fe(EDTA)^{2-}$ and in separate experiments the reduction potentials of the heme moiety have also been determined under a variety of conditions. Furthermore, in order to observe interaction, if any, between the two prosthetic groups, the reduction potentials of the heme moieties were determined in both native enzyme and those from which the molybdenum fragment has been removed. The results reported in this chapter were performed in collaboration with Dr. S. Cramer.

EXPERIMENTAL SECTION

Enzyme Preparation

Sulfite oxidase was prepared from fresh beef and chicken livers by a modification of the methods of Cohen and Fridovich [1] and of Kessler and Rajagopalan [13]. Typical samples used had a ratio $A_{413}:A_{280}$ of 0.5 - 0.7 for beef enzyme and 0.98 for chicken enzyme. The specific activity of the sulfite-cytochrome assay [1], assuming 2 hemes per molecular weight of 110,000 dalton and ε_{413} of 100 $mM^{-1}cm^{-1}$ per oxidized heme, was typically about 1200 and 1600 units per milligram of beef and cnicken enzyme, respectively. Sulfite oxidase concentrations were determined by measuring the 555 nm absorbance change accompanying full reduction with dithionite ($\Delta\varepsilon_{555}$ = 19.8 $mM^{-1}cm^{-1}$).

The cleavage of beef liver sulfite oxidase into molybdenum and heme domains was done by a method similar to Johnson and Rajagopalan [8] using either trypsin or papain as cleaving agents. Proteolysis was conducted until the enzyme had less than 2% of its original cytochrome c reductase activity, at which point the reactions were quenched with trypsin inhibitor or iodoacetamide. Separation of the domains was then accomplished by gel chromatography using Sephacryl S-200.

Reduction Potential Studies

Spectroelectrochemical technique using optically transparent thin layer electrode was employed in the measurements of the reduction potentials as described in Chapter 1. $Ru(NH_3)_6Cl_3$ or 2,6-dichlorophenolindophenol was used as a mediator. The experiments were performed using a

Cary 15 spectrophotometer.

The reduction potentials were calculated from the linear least squares fitting of the applied potential to the logarithm of the ratio of concentrations of oxidized and reduced heme, according to the Nernst equation.

Kinetic Studies

For kinetic measurements, reagent grade chemicals were used throughout, and deionized distilled water was used in the preparation of solutions. Ferrous EDTA solutions were prepared according to the literature procedure [16].

The measurements were performed using a modified Durrum D-110 stopped-flow spectrophotometer. Removal of oxygen from enzyme solution was done by using vacuum-nitrogen cycles where no denaturation process was observed. A special anaerobic set-up for kinetic measurements was employed in the studies and nitrogen was carefully bubbled through all reagent solutions. Solutions were allowed at least 45 minutes to come to temperature equilibrium prior to mixing. Temperature was controlled to ±0.1°C by a Forma scientific temperature bath.

Data were sent to a Tektronix 564B storage oscilloscope and to an A/D converter in conjunction with a PDP-10 computer. Data from the reduction with $Fe(EDTA)^{2-}$ (followed at 423 nm) were analyzed as pseudo first order in enzyme with the $Fe(EDTA)^{2-}$ in 100-fold excess.

RESULTS

Spectroelectrochemical Experiments

A typical spectroelectrochemical redox titration of the heme of sulfite oxidase is shown in Figure 3a, while Figure 3b illustrates the Nernst plot obtained from the data. The reduction potentials for the heme of sulfite oxidase under a variety of conditions are given in Table 1. The heme potentials of the beef liver enzyme were relatively insensitive to pH or the presence of the molybdenum domain. At pH 7.0 the intact chicken enzyme had a significantly higher potential (+84 mV) than the beef enzyme (+61 mV) under the same conditions.

Table 1. Reduction potentials of the heme of sulfite oxidase at different experimental conditions

Protein System	Conditions	E^o mV vs. NHE
beef, intact	0.1 M Tris pH 9	+55(±3)
beef, cleaved	0.1 M Tris pH 9	+66(±3)
beef, intact	0.1 M P_i pH 7	+61(±3)
beef, cleaved	0.1 M P_i pH 7	+57(±3)
chicken, intact	0.1 M P_i pH 7	+84(±3)

Figure 3. a) Thin layer spectra of beef liver sulfite oxidase 5.6×10^{-5}M with 1×10^{-3}M $Ru(NH_3)_6^{3+}$ as mediator for different values of applied potentials, E_{app} (mV vs. NHE), (a) -350, (b) 21.5, (c) 35.7, (d) 52.2, (e) 64.4, (f) 77.4, (g) 92.3, (h) 194.4

b) Nernst plot of the above data at 23°C.

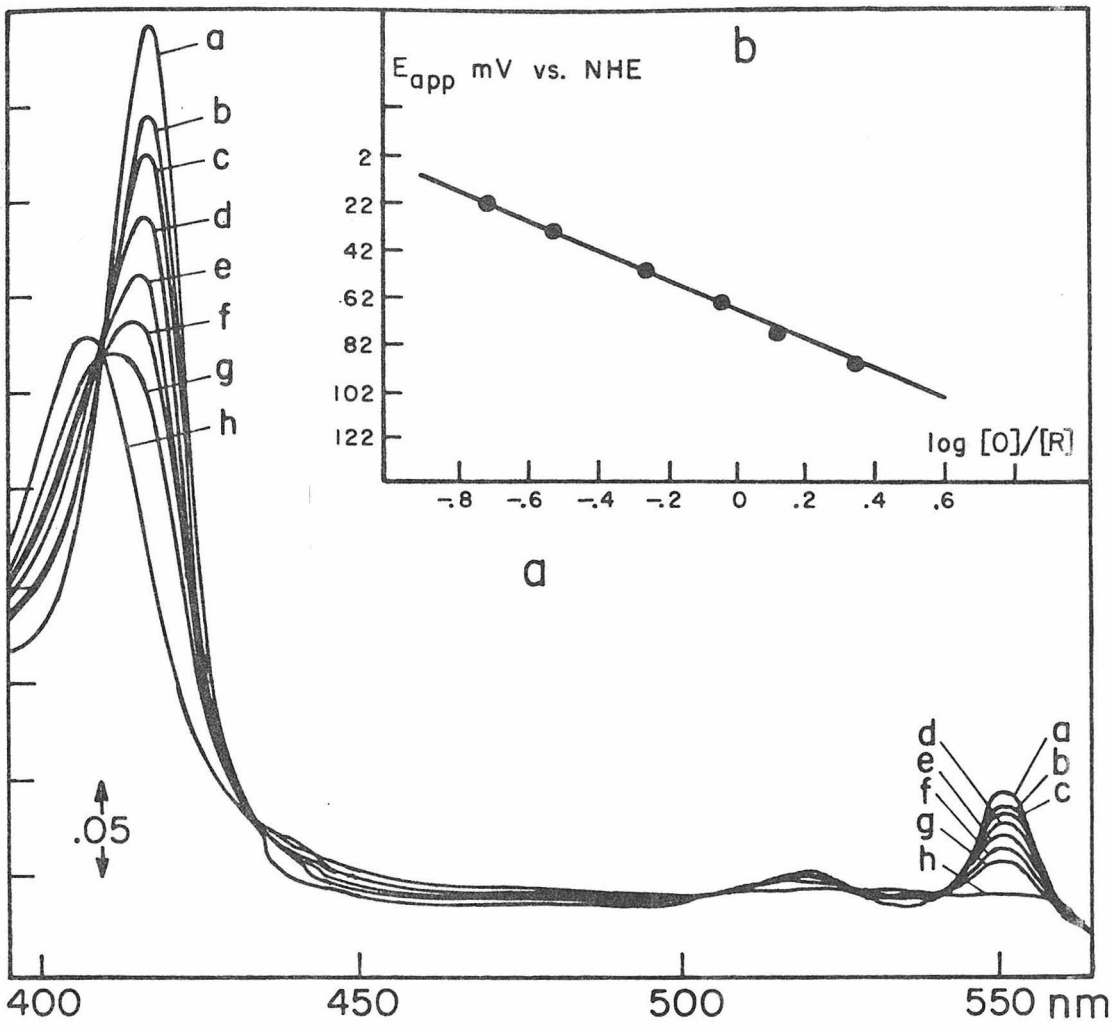
a
b
c
d
e
f
g
h
b
E_{app} mV vs. NHE
2
22
42
62
82
102
122
log [O]/[R]
-.8
-.6
-.4
-.2
0
.2
.4
.6
a
.05
400
450
500
550 nm

Kinetic Experiments

$Fe(EDTA)^{2-}$ reduction of chicken liver sulfite oxidase.

First order plots of absorbance changes with time were linear for greater than 90% of the reduction of sulfite oxidase. The concentration dependence of the observed rate constants is shown in Figure 4. Rate saturation was not observed over the concentration range of reductants employed. The weight least square fit of the data yields $k = 1.4 \times 10^3 M^{-1} S^{-1}$ (25°C, μ = 0.2 M, pH = 7 (phosphate)). The Eyring plot (Figure 5) gives $\Delta H^{\neq}$ = 5 kcal $mole^{-1}$ and $\Delta S^{\neq}$ = -28 e.u.

The reduction rate of sulfite oxidase by $Fe(EDTA)^{2-}$ increases with increasing ionic strength at pH 7 (Figure 6). The data were fitted to an equation derived from Marcus theory [17,18]:

$$\ln k = \ln k_o - 3.576 \left[\frac{\exp(-\kappa R_1)}{1 + \kappa R_2}\right] + \left[\frac{\exp(-\kappa R_2)}{1 + \kappa R_1}\right]\left[\frac{Z_1 Z_2}{R_1 + R_2}\right]$$

The best fit to data is obtained by assuming a charge on the enzyme of -20.

DISCUSSION

Reduction Potentials of Sulfite Oxidase Heme

The formal reduction potentials, E^o of b_5-like heme in both intact and heme fragment of sulfite oxidase from beef liver were determined at two different experimental conditions: a condition where the enzyme has maximum activity (tris buffer, pH 9, ionic strength 0.1 M) and at its physiological condition (phosphate buffer, pH 7, ionic strength 0.1 M). The E^o values for the former condition increase as the molybdenum fragment is removed, while for the latter condition the values remained approxi-

Figure 4. Plot of k_{obsd} vs $[Fe(EDTA)^{2-}]$ for the reduction of sulfite oxidase (observed at 423 nm)(25°, pH 7 (phosphate), $\mu = 0.2$.

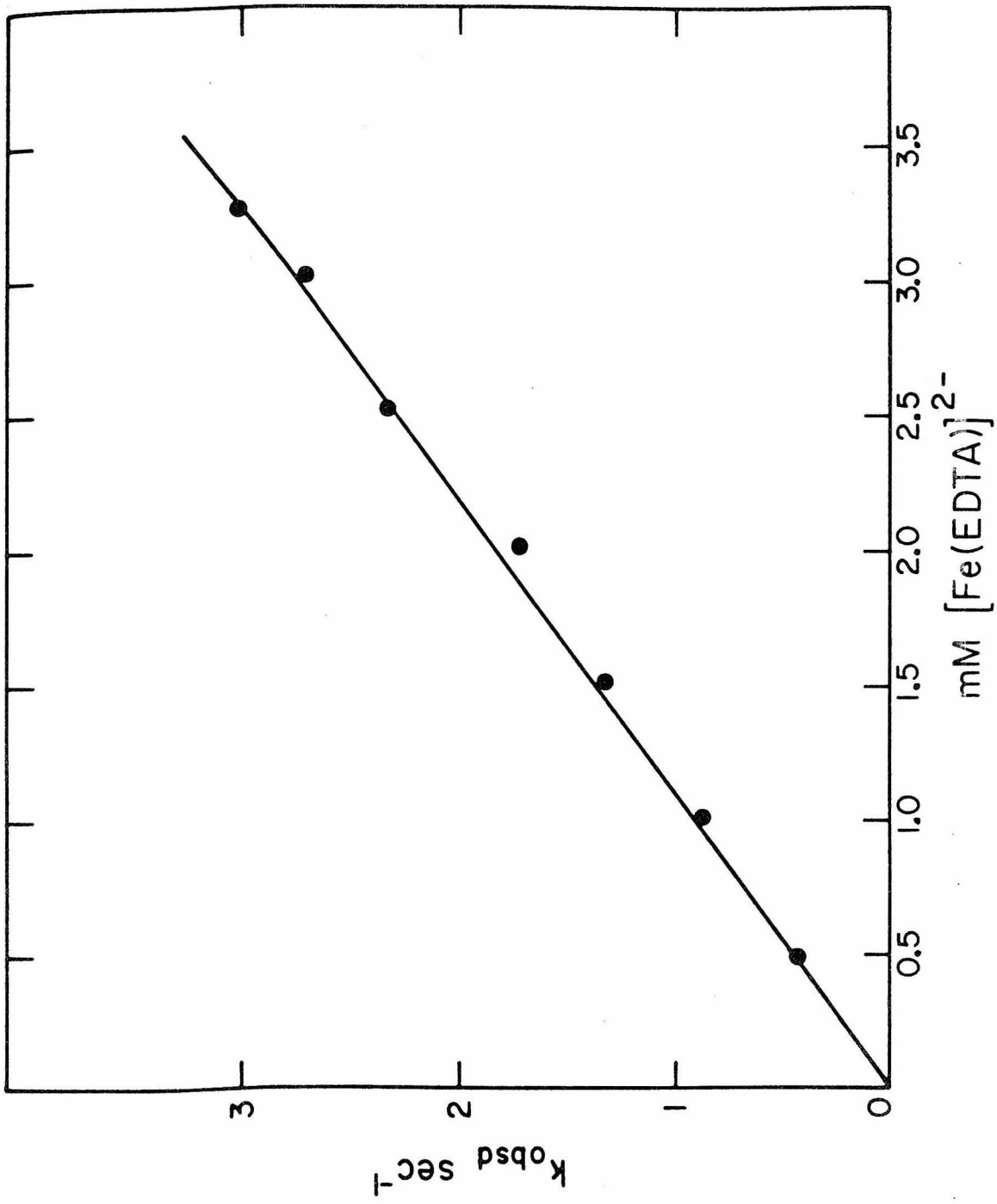
k_{obsd} sec^{-1}
0
1
2
3
0.5
1.0
1.5
2.0
2.5
3.0
3.5
mM $[Fe(EDTA)]^{2-}$

Figure 5. Eyring plot of rate data for the reduction of sulfite oxidase by $Fe(EDTA)^{2-}$ (pH 7 (phosphate), μ = 0.2).

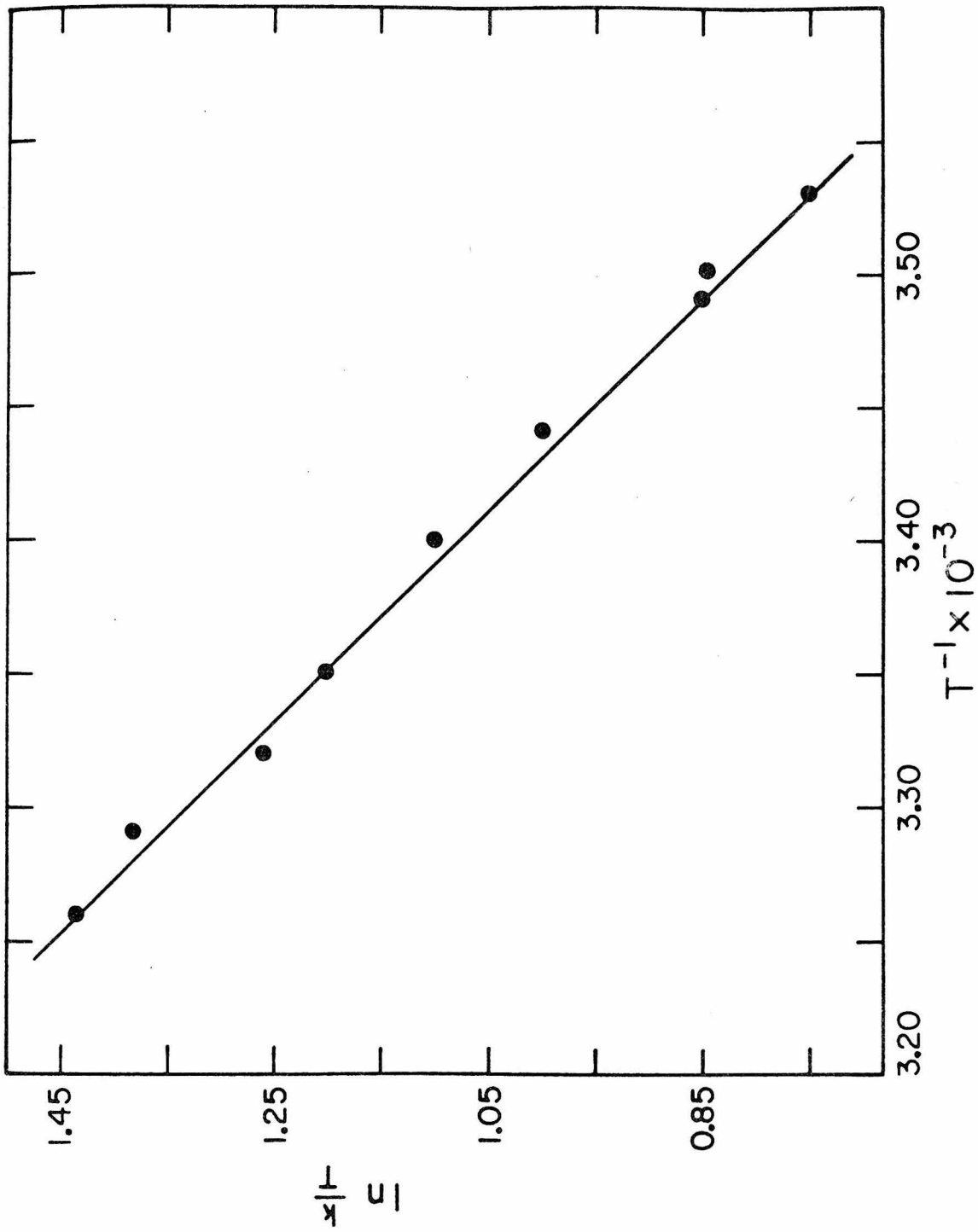
1.45
1.25
1.05
0.85
$\frac{H}{\chi}$
3.20
3.30
3.40
3.50
$T^{-1} \times 10^{-3}$

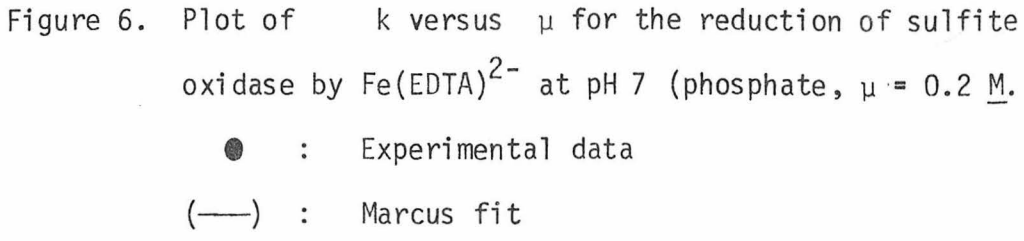
Figure 6. Plot of k versus μ for the reduction of sulfite
oxidase by Fe(EDTA)2- at pH 7 (phosphate, μ = 0.2 M.
● : Experimental data
(——) : Marcus fit

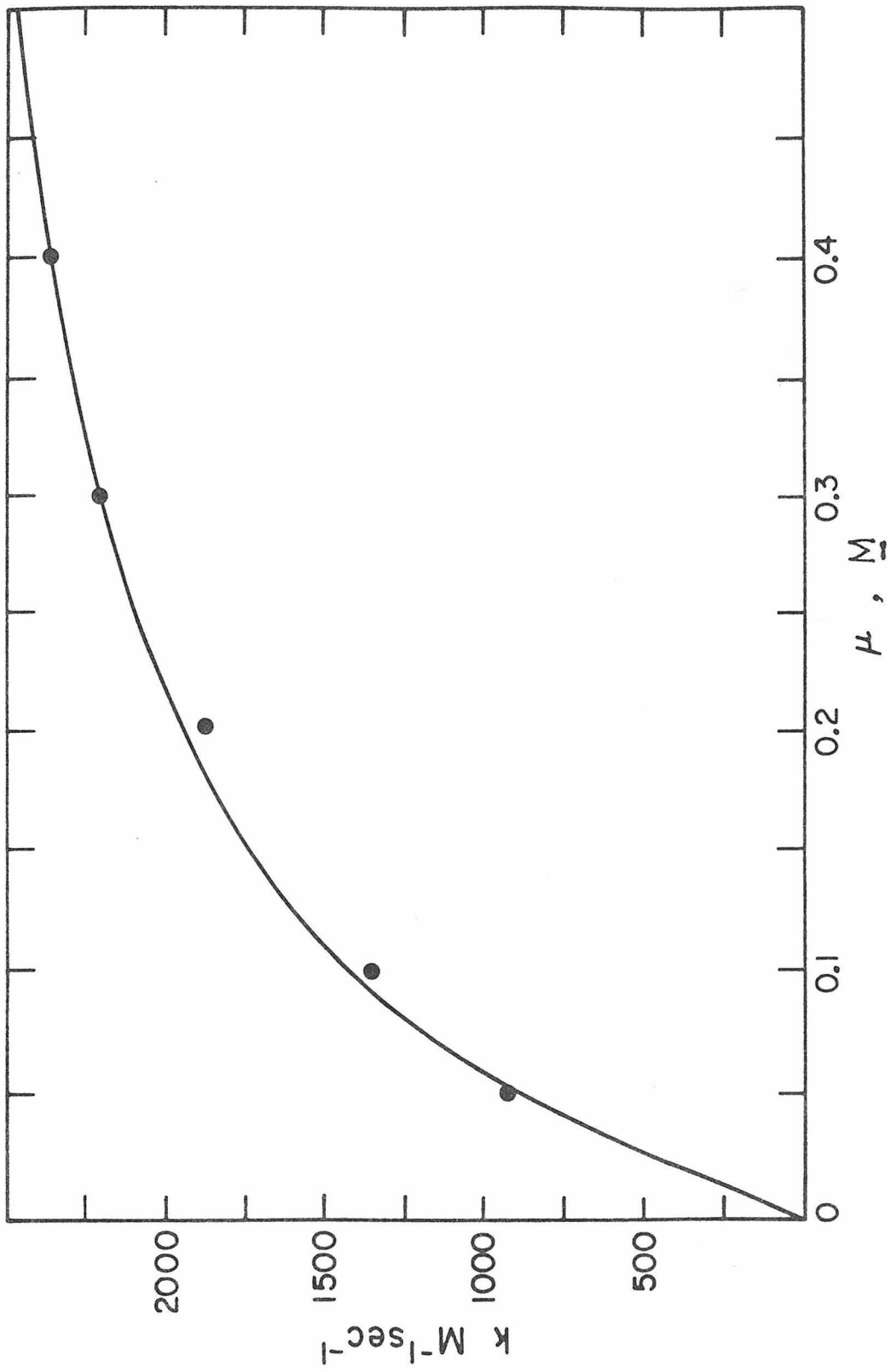
k M⁻¹sec⁻¹
2000
1500
1000
500
0
0.1
0.2
0.3
0.4
μ , M

mately the same within experimental error. The potential of the chicken enzyme is more positive than that of the beef enzyme. Several factors contributed to such a variation of the observed E^o values, one of which is the effect of anions present in the solution. It is possible that anions bind to various parts of the enzyme, thus causing a conformational change such that the E^o of the protein increases. This effect was also observed in the case of xanthine oxidase [19]. Furthermore, there is the possibility that the cleavage of the heme fragment caused a major conformational change such that the conformation of the heme fragment is greatly different from that of the intact enzyme.

However, it is interesting to compare these E^o values with those of cytochrome b_5 from various sources as the UV-visible absorption spectrum of sulfite oxidase is very similar to that of microsomal b_5, and there is also a strong similarity in amino acid sequence [10]. Inspection of the E^o values of cytochrome b_5 given in Table 2, shows that sulfite oxidase heme potentials are roughly 40-60 mV higher than those of microsomal b_5. Another similar protein, lactate dehydrogenase (flavocytochrome b_2), has a heme redox potential roughly 50-30 mV lower than microsomal b_5. It therefore appears that E^o values of these b_5-like hemes, i.e., heme containing bis-histidine iron protoporphyrin IX as prothetic group span over a range of more than 100 mV (from -28 to +84 mV). A wider range has been observed for cytochrome c system which ranges from +380 to -500 mV [20]. Such a wide variation of E^o values in cytochrome c has been accounted for in terms of a local heme environment of low dielectric constant [21]. The lower E^o value associates with

less hydrophobic environment of the heme center. Therefore, it is reasonable to propose that the heme environment in the sulfite oxidase is more hydrophobic than that of the microsomal b_5, as is evidenced from the kinetic studies of sulfite oxidase with inorganic reagent (see next section).

Table 2. Reduction potentials of enzymes containing b_5-like heme

Protein	E^o mV vs. NHE	References
cytochrome b_5	+ 20	a
microsomal cytochrome b_5 (intact)	-12 to -14	b
cytochrome b_T (mitochondrial)	-30	c

[a] S. F. Velick and P. Strittmatter, J. Biol. Chem. 221, 265 (1956).

[b] Y. Kawai, Y. Yoniyama, and H. Yoshikawa, Biochim. Biophys. Acta 67, 522 (1963).

[c] B. Hagihara, N. Sato, and T. Yamanaka, "The Enzymes," vol. XI, P. D. Boyer, ed. (1975), Ch. 8.

$Fe(EDTA)^{2-}$ Reduction Kinetics

The rate constant and the activation parameters for the $Fe(EDTA)^{2-}$ reduction of the heme of sulfite oxidase are very similar to those observed for electron transfer from $Fe(EDTA)^{2-}$ to ferricytochrome c ($k = 2.57 \times 10^4 M^{-1}s^{-1}$, $\Delta H^{\neq} = 6$ kcal mol^{-1}, $\Delta S^{\neq} = -18$ e.u. [22]. It has been proposed [23] that electron transfer to ferricytochrome takes

place at the partially exposed heme edge. Apparently, a similar type of electron transfer pathway is employed by the heme of sulfite oxidase. Furthermore, the calculated activation parameters are comparable to those for simple inorganic outer-sphere reactions. Electron transfer reactions of $Fe(EDTA)^{2-}/Fe(CDTA)^{-}$ and $Fe(CN)_6^{4-}/Fe(CN)_6^{3-}$ couples are associated with $\Delta H^{\neq}$ values of 4 and 3.6 kcal mol^{-1}, with $\Delta S^{\neq}$ values of -25 and -24 e.u., respectively [23,24]. Similarly, the $\Delta H^{\neq}$ and $\Delta S^{\neq}$ parameters observed for the reduction of $Ru(NH_3)_5py^{3+}$ by $Co(terpy)_2^{2+}$ are 6.2 kcal mol^{-1} and -23 e.u., respectively [17]. From these comparisons, it is clear that electron transfer mechanisms employed by sulfite oxidase do not involve any special enzyme effects. The $\Delta H^{\neq}$ value is consistent with an activation process requiring only minor nuclear positional rearrangements in the iron atom environment both in the oxidized and reduced enzymes.

The electron transfer reactivity of sulfite oxidase can be investigated further by applying the Marcus theory analysis to the data. As it has been established [18], the k_{11}^{corr} value calculated from the protein-$[Fe(EDTA)]^{2-}$ reactions can be used to compare electron transfer reactivities among proteins. Such treatment has been proven successful for a variety of proteins [18,19,25]. It is therefore interesting to compare the calculated k_{11}^{corr} value from the protein-$[Fe(EDTA)]^{2-}$ reaction with those of other low-spin heme containing proteins. The calculated k_{11}^{corr} is 2.73×10^2 $M^{-1}s^{-1}$, as compared to 2, 6, and 10^9 $M^{-1}s^{-1}$ for the corresponding k_{11}^{corr} for bacterial cytochrome c-551, horse heart cytochrome c, and a water-soluble low-spin iron porphyrin complex, respectively [26,27]. The parameters and work terms as defined in reference [19] that were used in the calculation are as follows:

$Fe(EDTA)^{2-}$, E^o = 120 mV, $k_{22} = 3 \times 10^4$ $M^{-1}s^{-1}$, R = 4 Å; sulfite oxidase E^o = 84 mV, R = 27.3 Å [28], Z = -20/-21, $k_{12} = 1.4 \times 10^3$ $M^{-1}s^{-1}$; w_{12} = 0.330, w_{21} = 0.173, w_{11} = 0.495, w_{22} = 0.493 kcal $mole^{-1}$.

It is impressive that the k_{11}^{corr} of these low spin hemes range over 9 orders of magnitude, with heme >> sulfite oxidase > cytochrome c ≃ cytochrome c-551. It is proposed that incorporation of a low-spin heme into either apo-sulfite oxidase or apo-cytochrome c vastly decreases the accessibility of the redox center to an external reagent in solution, thereby explaining the decrease in the rate electron transfer to the iron. The evidence suggests that the heme in sulfite oxidase is somewhat more accessible than the heme in cytochrome c.

Appendix 1. Supplementary data for the reduction of chicken liver sulfite oxidase by $Fe(EDTA)^{2-}$.

Concentration dependence (μ=0.2M)

$[Fe(EDTA)^{2-}]$ $\times 10^3$ M	k_{obsd} (sec^{-1})
0.5	0.474
1.0	1.22
1.5	1.82
2.27	2.46
2.5	3.01
3.0	3.53

Ionic strength dependence

μ (M)	k_{12} $M^{-1}sec^{-1}$
0.05	930
0.1	1362
0.2	1870
0.3	2222
0.4	2382

Temperature dependence

ln k/T	$1/T, \times 10^3 (K^{-1})$
1.44	3.26
1.38	3.29
1.26	3.32
1.21	3.35
1.11	3.40
0.99	3.44
0.85	3.49
0.84	3.50
0.75	3.53

REFERENCES

1. H. J. Cohen and I. Fridovich, J. Biol. Chem. 246, 359 (1971).
2. A. M. Charles, Arch. Biochem. Biophys. 129, 124 (1969).
3. R. M. Lyric and I. Suzuki, Can. J. Biochem. 48, 334 (1970).
4. O. Arrigoni, Ital. J. Biochem. 7, 181 (1959).
5. P. Fromageot, R. Vaillant, and H. Perez-Milan, Biochim. Biophys. Acta 44, 77 (1960).
6. I. Fridovich and P. Handler, J. Biol. Chem. 223, 321 (1956).
7. L. G. Howell and I. Fridovich, J. Biol. Chem. 243, 5941 (1968).
8. J. L. Johnson and K. V. Rajagopalan, J. Biol. Chem. 252, 2017 (1977).
9. D. R. Winge, W. M. Southerland, and K. V. Rajagopalan, Biochemistry 17, 1846 (1978).
10. B. Guiard and F. Laderer, Eur. J. Biochem. 74, 181 (1977).
11. H. J. Cohen and I. Fridovich, J. Biol. Chem. 246, 367 (1971).
12. M. Ikeda, T. Iizuki, H. Takao, and B. Hagihara, Biochim. Biophys. Acta 336, 15 (1974).
13. D. L. Kessler and K. V. Rajagopalan, J. Biol. Chem. 247, 6566 (1972).
14. S. P. Cramer, H. B. Gray, and K. V. Rajagopalan, J. Am. Chem. Soc. 101, 2772 (1979).
15. W. W. Cleland, Biochim. Biophys. Acta 67, 104 (1963).
16. H. L. Hodges, R. A. Holwerda, and H. B. Gray, J. Am. Chem. Soc. 96, 3132 (1974).
17. D. Cummins and H. B. Gray, J. Am. Chem. Soc. 99, 5158 (1977).
18. S. Wherland and H. B. Gray, "Biological Aspects of Inorganic Chemistry," D. Dolphin, ed. (John Wiley, New York, 1976).
19. R. Cammack, M. J. Barber, and R. C. Bray, Biochem. J. 157, 469 (1976).

20. G. R. Moore and R.J.P. Williams, FEBS Letters 79, 229 (1977).

21. R. J. Kassner, Proc. Natl. Acad. Sci. (USA) 69, 2263 (1972); J. Am. Chem. Soc. 75, 2674 (1973).

22. H. L. Hodges, R. A. Holwerda, and H. B. Gray, J. Am. Chem. Soc. 96, 3132 (1974).

23. R. G. Wilkins and R. E. Yelin, Inorg. Chem. 7, 2667 (1968).

24. R. Stasiw and R. G. Wilkins, Inorg. Chem. 8, 156 (1969).

25. S. Wherland and H. B. Gray, Proc. Natl. Acad. Sci. USA 73, 2950 (1976).

26. C. L. Coyle and H. B. Gray, Biochem. Biophys. Res. Comm. 73, 1122 (1976).

27. R. F. Pasternack and E. G. Spiro, J. Am. Chem. Soc. 100, 968 (1978).

28. Calculated from relation $R = 0.717\ M^{1/3}$ with M = 55,000.

Chapter 3

Spectroelectrochemical Studies of Polymer-Coated Graphite Transparent Electrodes

Introduction

Chemically transparent electrodes have been a subject of intense investigation since 1973 [1-73]. Such investigations are of interest for a variety of reasons; among them are the utilization of such electrodes in the electrocatalysis [26,28,43,49,75], the fabrication of electrodes for electroanalysis [16,28,31,36], the provision of a chiral electrode environment [2,5,6], and the development of catalytic electrodes for the study of photoelectrochemical processes [17,42,48, 50,56, 57,60,65,68]. Several approaches for attachment of electroactive species to the surface of various electrode materials have been studied. These approaches have included covalent bond formation [1-10, 12-15, 17-24, 26, 29-36, 38-44, 45,46, 48-50, 53-71), irreversible adsorption [11,16,25, 27,28] and polymeric coatings [37,44,47,49,51,52,72,73].

The coating of polymeric molecules on electrode surfaces is readily achieved by simply dipping the electrode material into a solution of the polymer [37,44,49,51,52,72,73]. This simple adsorption procedure allows modification of virtually any electrode surface and permits controllable amounts of polymer to be adsorbed. Miller et al. [44,52] have studied the adsorption of an electroinactive polyester onto platinum electrodes and found that such electrodes inhibited the electrochemical response of some electroactive couples. Bard et al. [37,51] reported the adsorption of electroactive poly(vinylferrocene) to platinum electrodes and covalently bound poly(methacryl chloride) to SnO_2 electrodes. Recently, Oyama and Anson[73,74,82]have reported the attachment of electroactive reagents Ru(edta)-, $Ru(NH_3)_5$-, and Cu(II)

to graphite electrodes coated with polymer containing sites for metal coordination. Such electrodes present opportunities for fundamentally new approaches to the study of electrochemical reactions including the possibility that such electrodes may have specific electrocatalytic properties. In their report, it was established that the polymer-coated electrodes were very durable and able to extract metal complexes from very dilute metal complex solutions. They also reported several electrochemical behaviors of the attached metal complexes.

In this chapter spectroelectrochemical studies of graphite optically transparent electrodes (GOTEs) coated with poly(4-vinylpyridine)(PVP) are presented. The studies allow one to quantitate the amount of polymer adsorbed on the electrodes. Furthermore, due to the difference in the characteristic spectra of Ru(edta) and Ru(edta)py, we have been able to observe the substitution reaction of the water molecules, occupied in the sixth position of the ruthenium in Ru(edta) complex by the pyridine group on the polymer backbone which was previously adsorbed onto the GOTE. The rates of substitution will be studied as a function of electrode potential and, where possible, will be compared with the corresponding homogeneous rate constants. Some experiments reported in this chapter were a result of collaborative work with Dr. N. Oyama.

Experimental

Apparatus. The one-inch square GOTEs were obtained from Lebow Company (Goleta, California). These electrodes were prepared by evaporating carbon with an electron beam technique onto ultraclean quartz surfaces. Electrodes with graphite film thickness ranging from 100 to

500 angstroms were used.

The design and assembly of a GOTE cell is shown in Figure 1. The cell was made from 7x4x1.2 cm clear lucite. Two tapered holes were drilled from the top of the block into the opening of the cell cavity to accommodate the reference electrode and for injecting solution into the cell. The cell cavity was formed in the lower half of the block cell in which a circular hole 1.5 cm in diameter was cut out. A quartz plate was glued in with epoxy to form the back of the cell. The GOTE was placed in front of the cell on a rubber o-ring and was held securely with another lucite plate and screws (see Figure 1). A small hole was drilled in from the side of the cell into the cell cavity to accommodate the platinum counter electrode. On one edge of GOTE, a piece of platinum wire was glued on with conducting epoxy (Tra-Con Inc., Medford, Massachusetts) for electrical contact. The exposed area of the OTE to the solution in the cell cavity was 2.54 cm^2. The optical pathlength of the cell is 1.3 cm. The reference electrode was a mini saturated calomel electrode (see Chapter 1). Its potential was 7 mV more positive than several commercial SCEs.

The spectroelectrochemical studies were performed using a Cary 219 spectrophotometer. Cyclic voltammograms and controlled potential coulograms were obtained with PAR (Princeton Applied Research) Model 174 and 173 instruments and an XYY recorder (Hewlett-Packard). Experiments were performed at room temperature, 22 ± 2°C.

Materials. Poly(4-vinylpyridine)(Borden Inc., Philadelphia, Pennsylvania) was recrystallized twice from methanol-diethylether. The average molecular weight (estimated viscometrically) of the sample was

Figure 1. Views of front, side and assembly of the optically transparent cell. Dimensions are in cm.
A: lucite plate, B: graphite cell, C: o-ring,
D: solution inlet port, E: reference electrode,
F: platinum counter electrode, G: screw,
H: cell cavity.

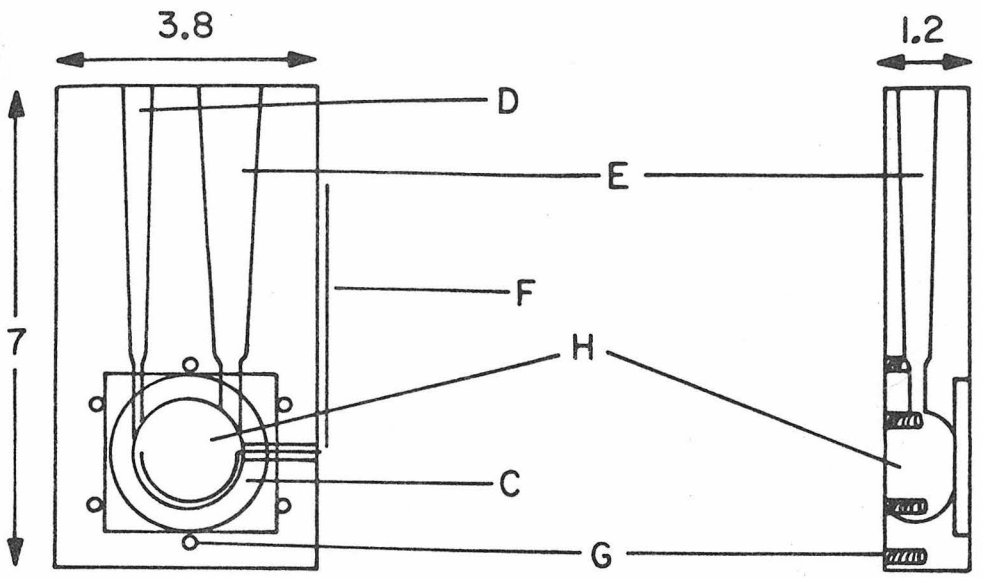
Front view
Side view
3.8
1.2
D
E
F
H
7
C
G

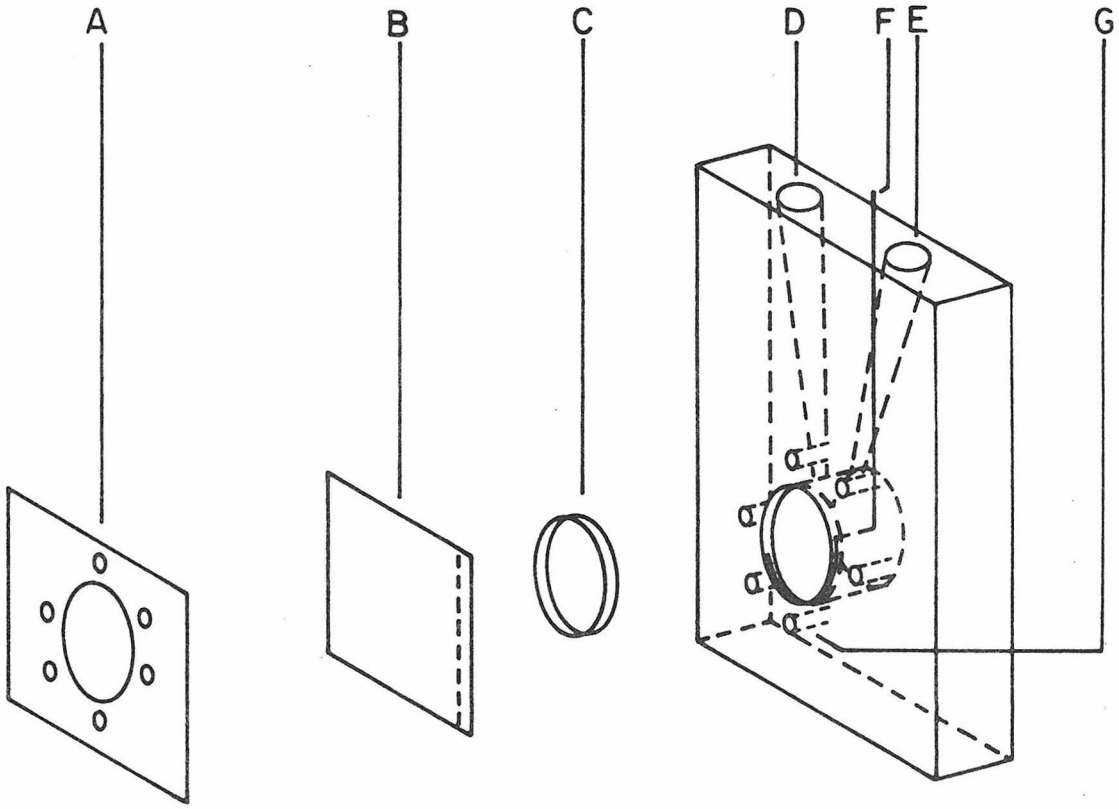
A
B
C
D
F
E
G

7.4×10^5 corresponding to about 7000 pyridine units per molecule of polymer.

Aquoethylenediaminetetraacetatoruthenium(III) was prepared from $RuCl_3$ as described by Mukaida et al. [76]. The chloride-free ruthenium complex was obtained according to a previously published technique [73].

The supporting electroylte for electrochemical measurements was 0.2M CF_3COONa adjusted to pH 7.1 with NaOH.

Electrode coating procedures. Adherent coatings of poly(4-vinylpyridine) were achieved by immersing the GOTE in either 0.2 or 0.5% solutions of the polymer in methanol for 10 to 30 minutes. The OTEs were then removed from the solutions, shaken to remove excess polymer solution and dried in air at room temperature for 15-20 minutes. After drying, the electrodes were soaked in pure methanol for a few minutes and dried in air. The electrode was then mounted in the electrochemical cell as indicated in Figure 1.

The formation of Ru^{III}(edta)py on the electrode surface was monitored spectroscopically at 290 nm in the cell containing Ru^{III}(edta) solution and an OTE which had previously been coated with the desired amount of polymer.

Results and Discussion

I. Spectrum characteristics of PVP and its adsorption onto GOTEs. The absorption spectra of PVP in methanol are shown in Figure 2. There is an intense absorption band at 257 nm with a molar extinction coefficient of 4.33×10^7 and a shoulder at 262 nm. The spectrum of PVP at lower pH where the pyridine nitrogen (pK_a = 2.37) is protonated [77] was also recorded. The 257 nm band of the deprotonated pyridine nitrogen shifted

Figure 2. Absorption spectra of 1.8×10^{-8}M poly(4-vinylpyridine) in methanol at pH 7.4(A) and 1.4(B) (adjusted to the pH with 0.2M CF_3COOH). pH of the solutions were estimated using pH meter.

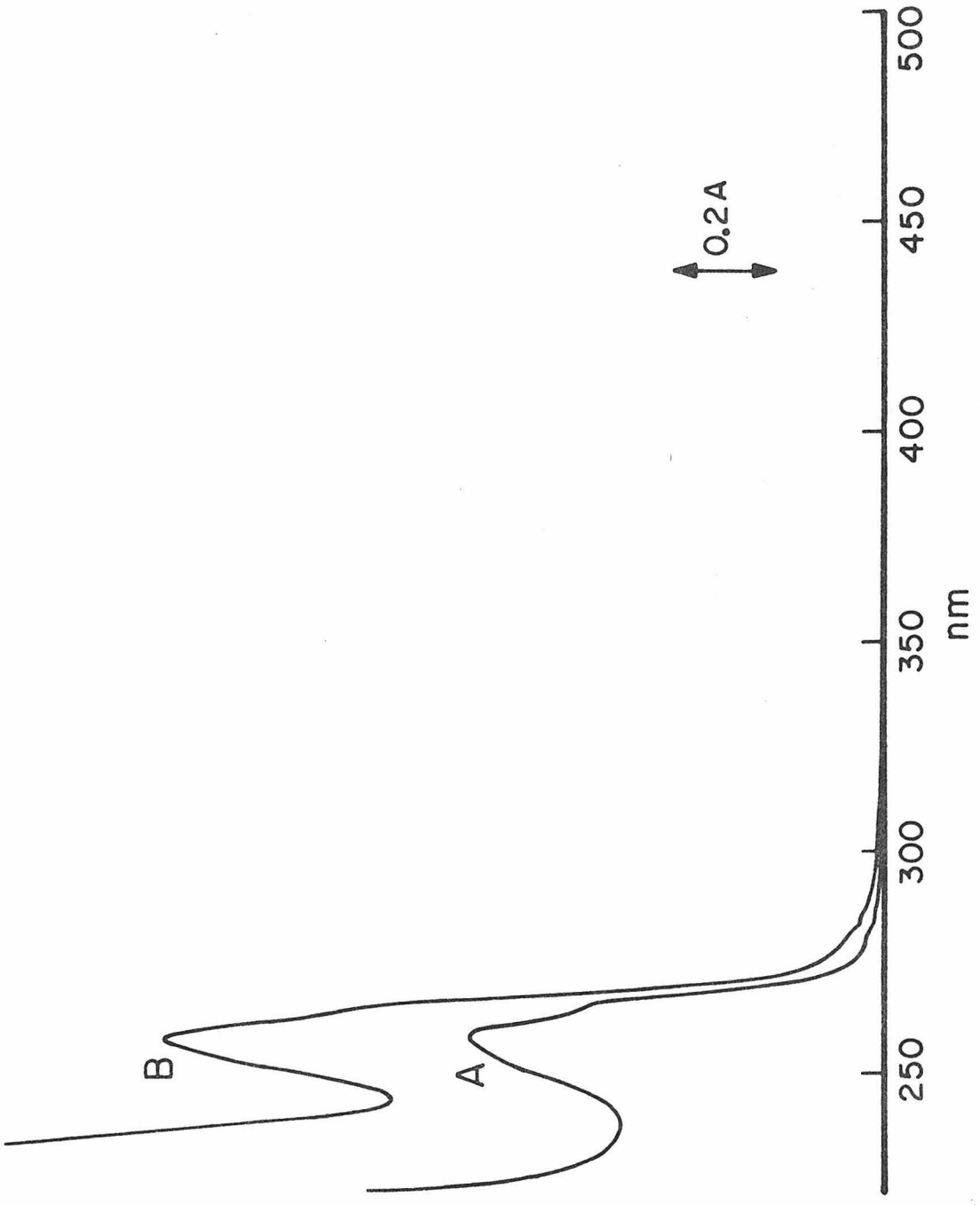
B
A
0.2A
250
300
350
400
450
500
nm

to 255 nm with a higher molar extinction coefficient of 7.50×10^7. The positions of the band and the shoulder observed are similar to those of free pyridine in which the bands have been attributed to transitions in the pyridine ring [78]. The increase in the band intensity as the pH of the PVP solution decreases is also observed in the spectrum of pyridine in acid solution [78,80]. (The observation has been attributed to the increase in the dipole moment of the protonated pyridine nitrogen which in turn increases the oscillator strength resulting in an increase in the band intensity [79,80]).

The adhesive of GOTEs coated with PVP showed absorption spectra in the presence of 0.2M CF_3COONa pH 7.1 very similar to those of homogeneous solutions of the polymer (Figure 3). By assuming that the molar extinction coefficient at 257 nm was the same for attached and unattached polymer, i.e., $4.33 \times 10^{10} mole^{-1} cm^2$ at pH 7.4, the quantity of polymer adsorbed on the GOTE could be estimated. It is important to note here that the uncoated GOTE exhibited no absorption band between 550 and 245 nm.

Cyclic voltammograms of the PVP-coated and uncoated electrodes were indistinguishable (Figure 4) as similarly observed for pyrolytic graphite electrodes [73]. The polymer film seemed to absorb strongly on the electrode surface; continuous cycling of a coated electrode between +700 and -700 mV caused negligible changes in the absorption intensity at 257 nm. Furthermore, in the coulometric experiment in which the potentials of the coated electrode were maintained at +500 and -500 mV for at least 1.5 to 2 hours, the absorbance at 257 nm showed at least 90% of the polymer remaining on the electrode surface.

Figure 3. Absorption spectra of PVP coated on the graphite OTE. Spectrum was recorded in the presence of supporting electrolyte: 0.2M CF_3COONa (pH 7.1).

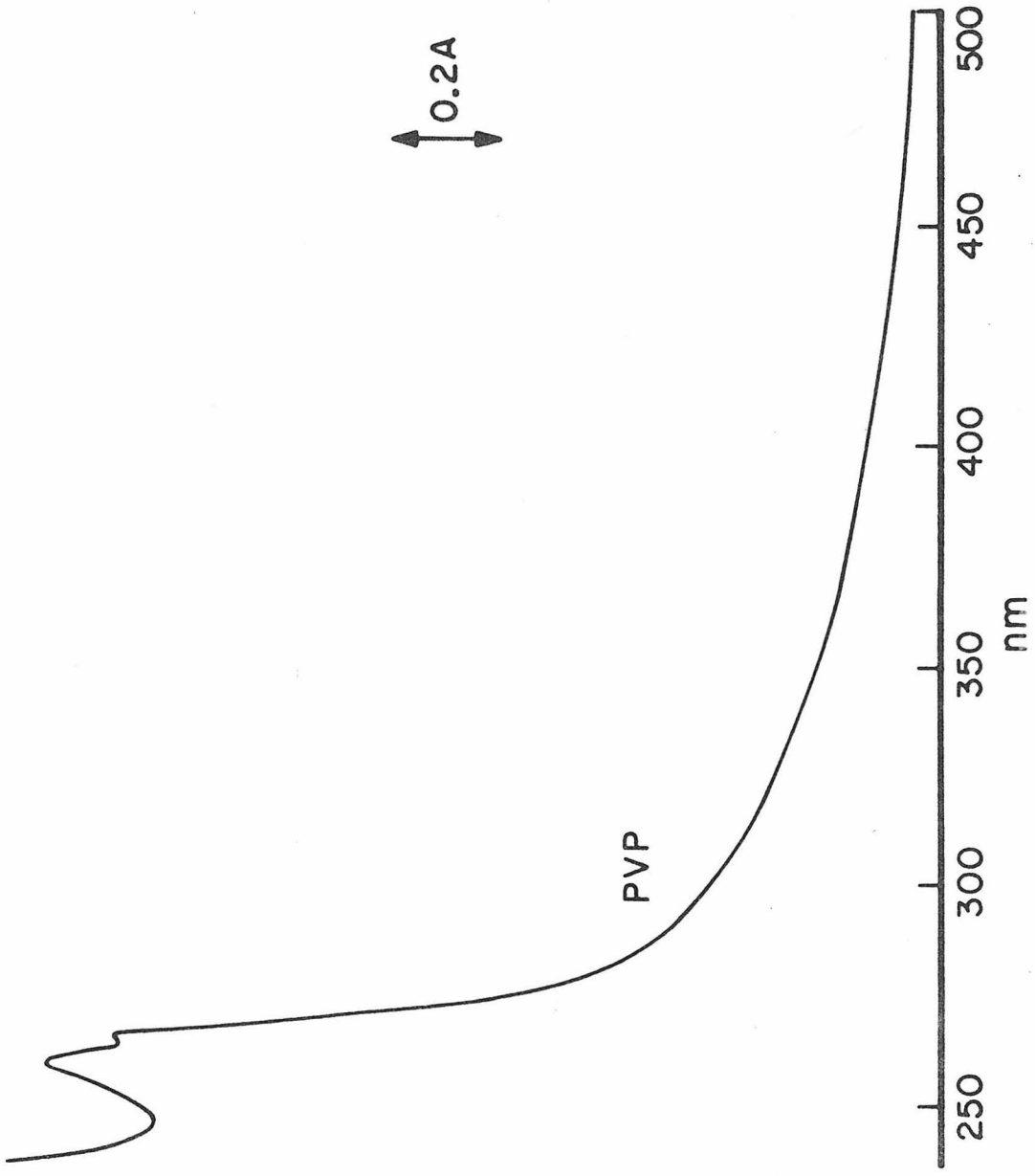
0.2A
PVP
250
300
350
400
450
500
nm

Figure 4. Cyclic voltammograms of GOTE prior(A) and after(B) adsorption of 3.5×10^{-7} mole cm^{-2} PVP on the surface. Voltammograms were recorded in the presence of 0.2M CF_3COONa (pH 7.1), scan rate 200 mV sec^{-1}.

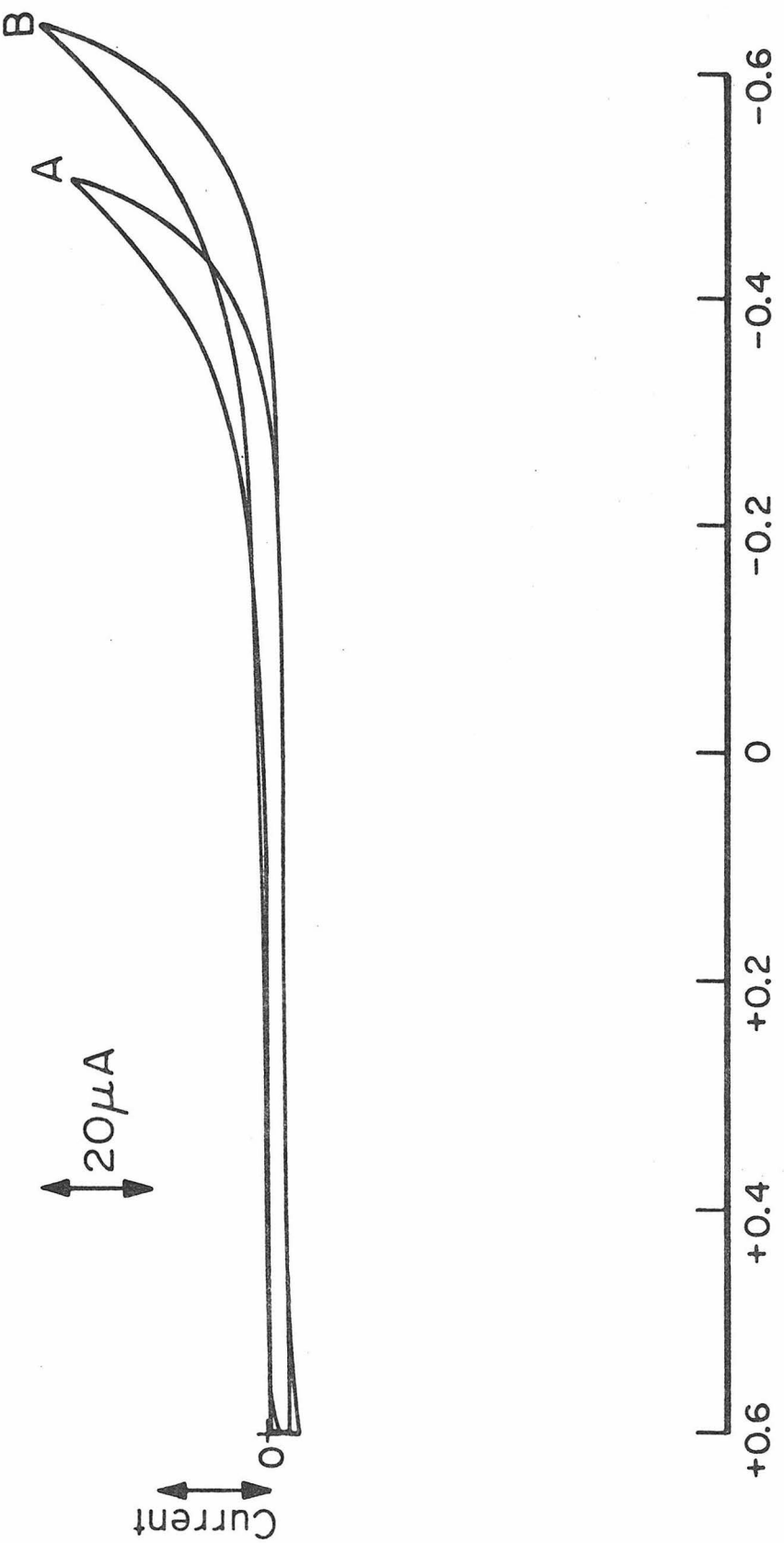
B
A
20μA
Current
0
+0.6
+0.4
+0.2
0
-0.2
-0.4
-0.6
E vs. SSCE

The adsorption and stability of PVP on the electrode surface was insensitive to the thickness of the graphite film; e.g., it was found that no difference in time was required to immerse the OTE in the polymer solution to obtain approximately the same coverage. However, they are sensitive to the pH of the polymer solution used to adsorb PVP on the electrode surface. When the polymer solution of pH 4.2 was used, approximately 50% of the adsorbed polymer came off in 5 minutes as detected by absorbance at 257 nm in the presence of 0.2M CF_3COONa (pH 7.1). We found nonuniformity of the PVP film as evidenced from the difference of the coverages calculated from the absorbances at 257 nm measured at different sections of the electrode surface. In addition, we also observed a discrepancy in the surface coverage calculated from the known amount of PVP dried on a fixed surface area and those from absorption intensity of the same electrode.

II. Coordination of Ru^{III}(edta) to PVP-coated GOTEs.

The facile attachment of Ru^{III}(edta) to the pyridine group on the PVP backbone which was previously adsorbed onto graphite electrodes has already been documented [73]. We also observed similar rapid binding process using GOTEs. Figure 5i shows steady-state cyclic voltammograms at various scan rates for the electrode surface obtained by dip-coating from a 0.5% of methanolic PVP solution, followed by excessive washing with methanol and exposure to an aqueous solution of 0.5 mM Ru^{III}(edta) for 15 minutes. The electrode was then washed with water and assembled to form an OTE cell where the voltammograms were recorded in the presence of 0.2M CF_3COONa pH 7.1. The average of the anodic and

cathodic peak potentials, -0.11 V is virtually the same as the value reported earlier [73] which corresponded to the Ru(edta)py complex. The peak-to-peak potential separation (ΔE_p) obtained was larger than ordinary graphite electrodes owing to the greater resistance of GOTE, e.g., a resistance of 3.5 KΩ was measured for a 200Å thick GOTE. A plot of square root of potential scan rates versus peak current for the voltammograms in Figure 5i is shown in Figure 5ii. Normally, one expects a linear dependence of peak current on the potential scan rate for reactants attached to electrode surfaces [25]. However, a linear plot similar to Figure 5ii was also obtained by electrodes coated with 10^{-7}mole cm^{-2} or greater quantities of PVP [82]. They have attributed the effect of the thickness of polymer layer to limitations of the movement of counter ions into the polymer film to balance the ionic charge during the electroreduction of attached complexes.

III. Attachment kinetics of Ru^{III}(edta) to PVP-coated GOTEs. Employing the OTE, it is possible to monitor spectrally the substitution reaction of the water molecule coordinated to Ru^{III}(edta) complex by the pyridine group of the PVP polymer. Homogeneous absorption spectra of Ru^{III}(edta) and Ru^{III}(edta)py measured in methanolic aqueous solutions pH 7, 25°C are shown in Figure 6i. At wavelengths greater than 280 nm, Ru^{III}(edta)py exhibits similar absorption spectra to thoseof Ru^{III}(edta). However, the molar absorptivity of the former is significantly larger than that of the latter with the difference between the molar absorption coefficients of $3.0x10^3$ at 290 nm. By contrast, the absorption spectra of Ru^{II}(edta)py (Figure 6ii) (prepared from reduction

Figure 5. i: Steady-state cyclic voltammograms for Ru(edta) attached to PVP-coated graphite OTE. Surface concentraion of pyridine = 2.75×10^{-7} mole cm^{-2}. Voltammograms were recorded in the presence of 0.2M CF_3COONa (pH 7.1). Scan rate, mV sec^{-1} are given in each curve.

ii: Peak currents vs. (scan rate)$^{1/2}$ for the curves in i.

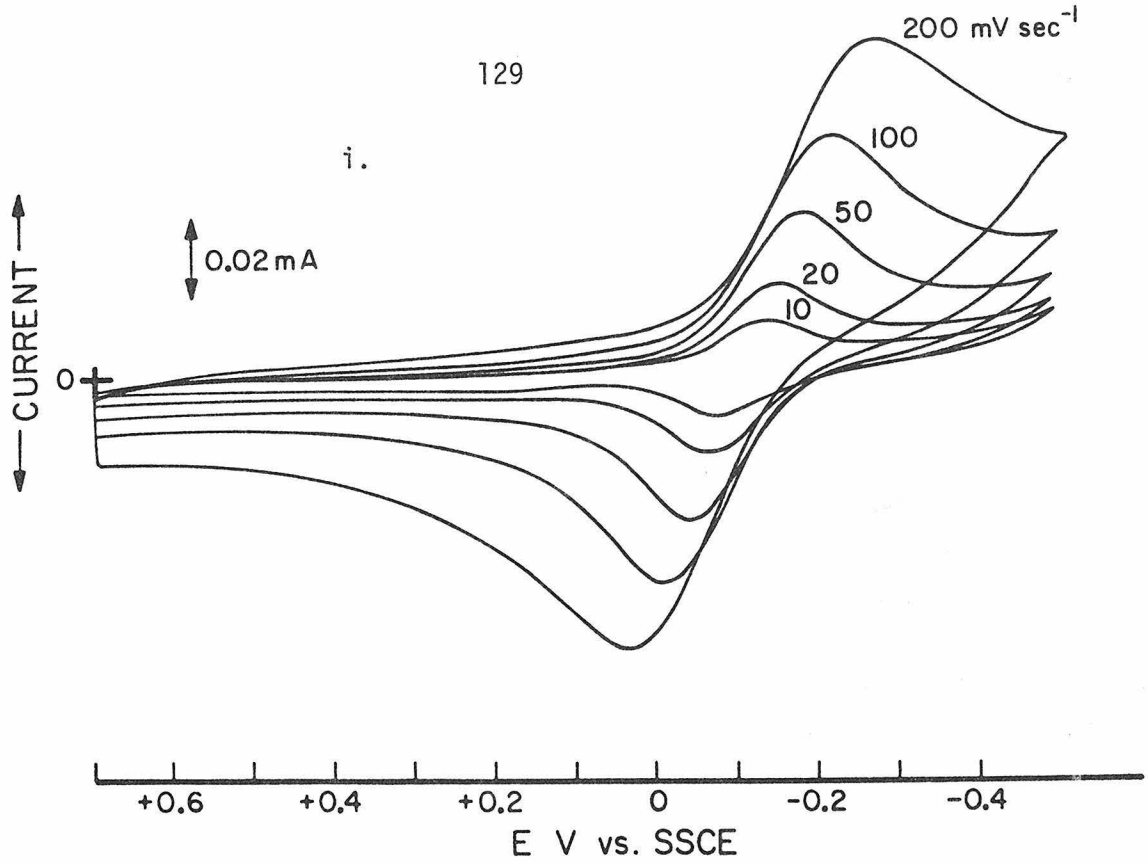
i.
200 mV sec⁻¹
100
50
20
10
0.02 mA
CURRENT
0
+0.6
+0.4
+0.2
0
-0.2
-0.4
E V vs. SSCE

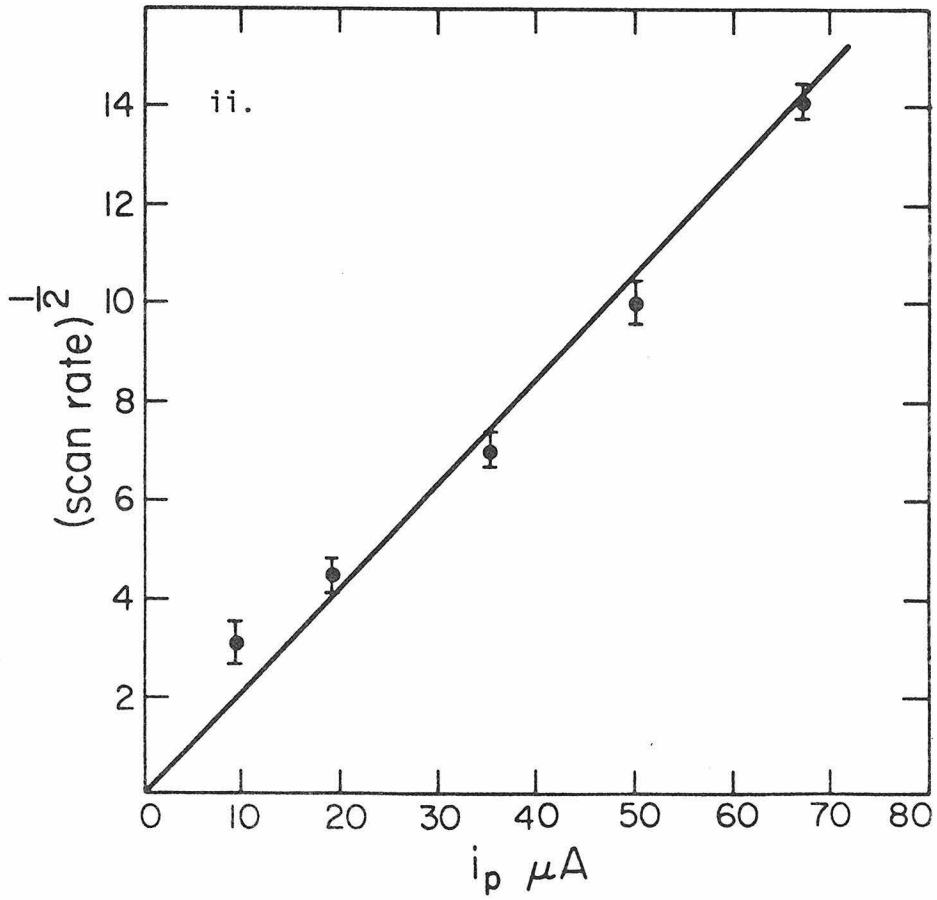
ii.
14
12
10
8
6
4
2
(scan rate)^-1/2
0
10
20
30
40
50
60
70
80
ip μA

Figure 6. Homogeneous absorption spectra of

i: A: 5.0×10^{-5}M Ru^{III}(edta)py

B: 5.0×10^{-5}M Ru^{III}(edta)

C: 1.8×10^{-8}M PVP

ii: A: 5.0×10^{-5}M Ru^{II}(edta)py

B: 5.0×10^{-5}M Ru^{II}(edta)

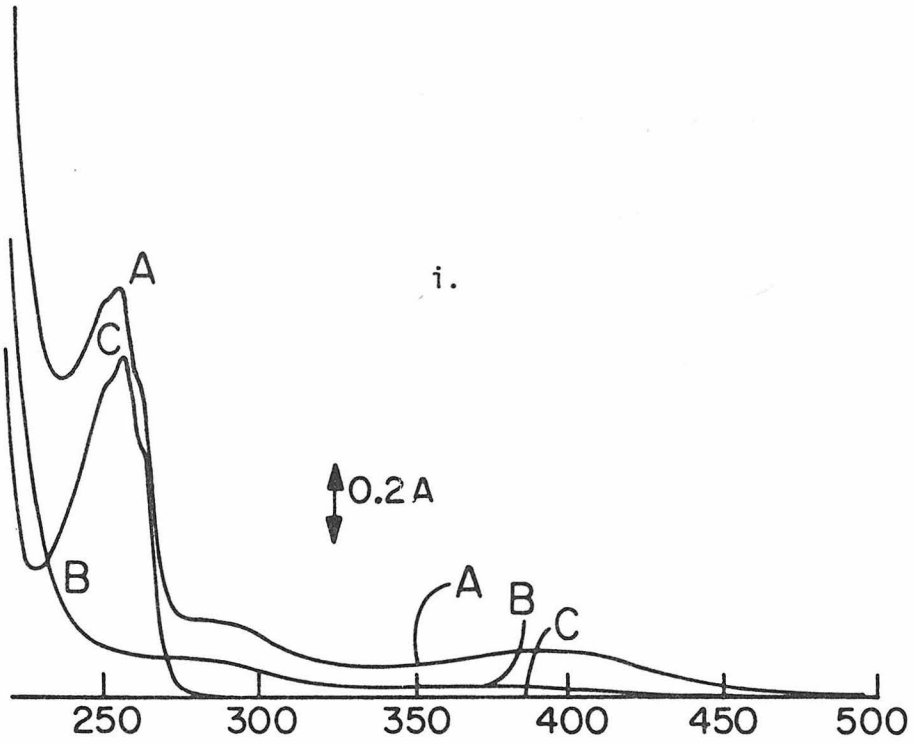
i.
A
C
B
0.2 A
A
B
C
250
300
350
400
450
500

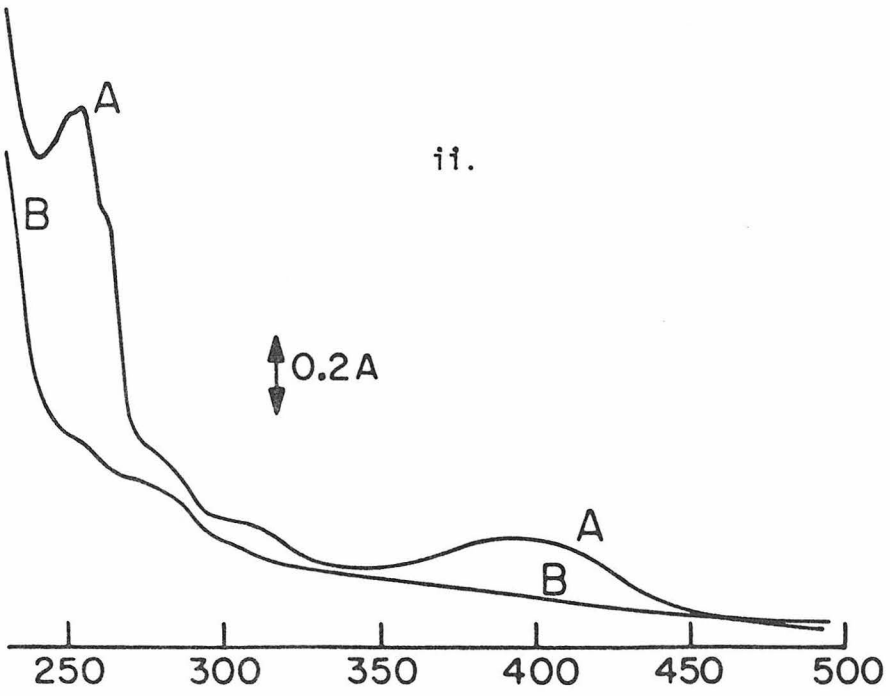
ii.
A
B
0.2 A
A
B
250
300
350
400
450
500

of Ru^{III}(edta)py by amalgamated zinc under argon atmosphere for three hours) exhibits a broad absorption band at 390 nm with the molar extinction coefficient of 8.4×10^3.

We have studied the substitution kinetics of Ru(edta) with the pyridine group on PVP backbone which was previously adsorbed on GOTE. The extent of the reaction was followed spectrally at 290 nm in an OTE cell employing PVP-coated GOTE. The cell contained 2×10^{-4} M of Ru^{III}(edta) solution in 0.2 M CF_3COONa, pH 7.1. Absorbance increased as a result of the formation of Ru^{III}(edta)py on the electrode surface. Figure 7 shows the amount of Ru^{III}(edta)py formed as calculated from the increase in absorptivity at 290 nm as a function of time. Initially, the quantity of Ru^{III}(edta)py increased linearly with time and then leveled off, presumably because equilibrium was attained. Such behavior has also been observed with pyrolytic graphite electrodes [73]. From the intial linear portion of the plot in Figure 7, the rate of the substitution reaction was calculated. The rates obtained increased as the concentrations of pyridine groups on the electrode surfaces increased as given in Table 1.

Figure 7. Time dependence of the attachment of Ru^{III}(edta) to PVP-coated electrode from $2x10^{-4}$ M solution of Ru^{III}(edta) in 0.2 M CF_3COONa (pH 7.1). Surface concentration of py = $5.98x10^{-8}$ mole-cm^{-2}. Initial rate calculated to be $7.50x10^{-11}$ mole-cm^{-2}-sec^{-1}.

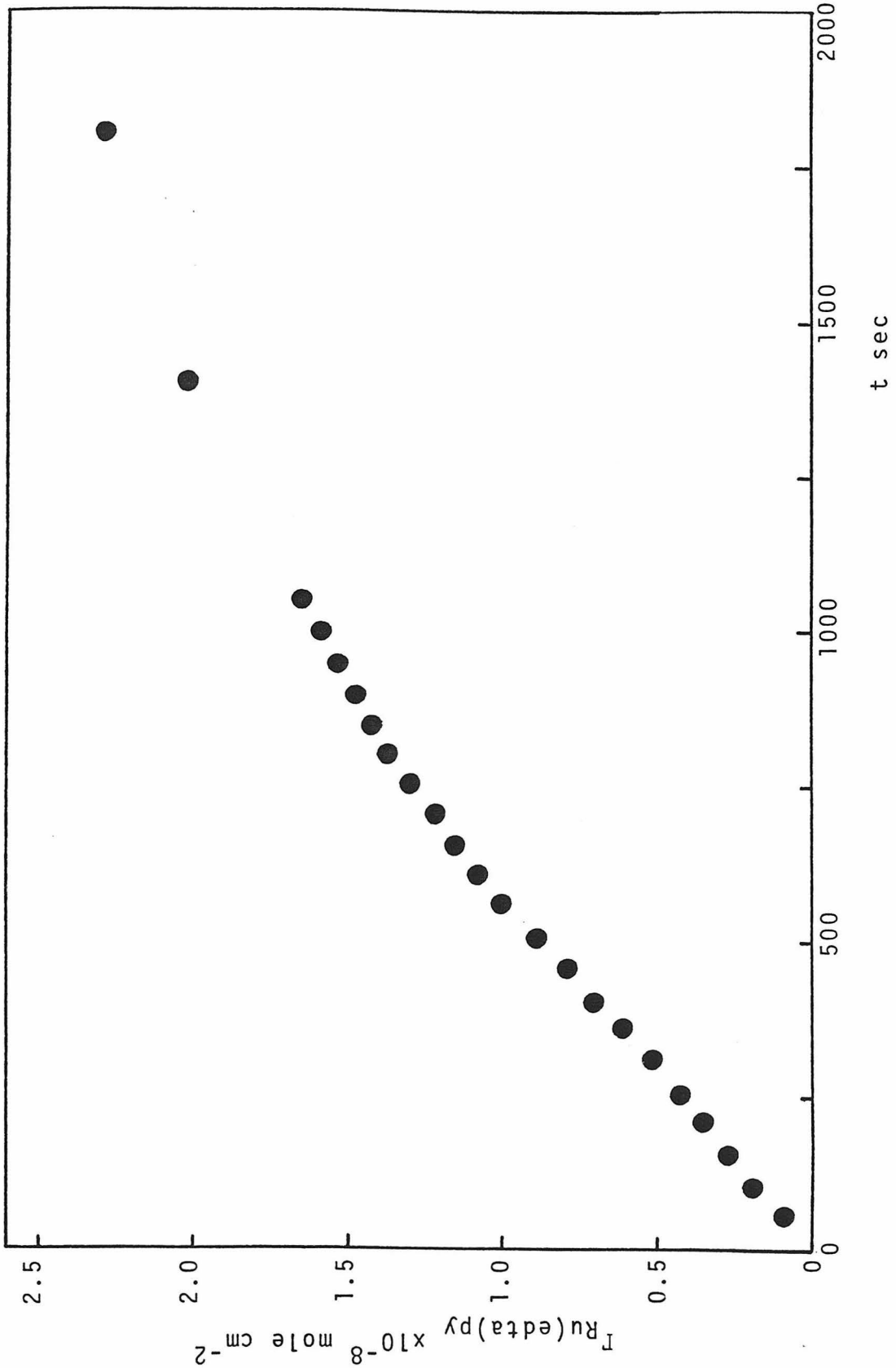
2.5
2.0
1.5
1.0
0.5
0
0
500
1000
1500
2000
t sec
$\Gamma_{Ru(edta)py}$ x10^{-8} mole cm^{-2}

Table 1. Initial rates of formation of Ru^{III}(edta)py on GOTE surfaces at different pyridine surface concentrations.

Γ_{py} mole/cm^2	$d\Gamma_{Ru}/dt$ mole/cm^2-sec
5.33×10^{-8}	6.66×10^{-11}
5.98×10^{-8}	7.50×10^{-11}
9.86×10^{-8}	1.32×10^{-10}

A plot of pyridine surface concentrations versus initial rates of formation of Ru^{III}(edta)py on graphite OTE surfaces gives a linear relationship. The second order rate constant for the substitution reaction on the electrode surface was not calculated, due to the fact that it is difficult to estimate actual Ru^{III}(edta) concentration as "seen" by the electrode surface.

The initial rate constants were also studied as a function of the electrode potential. The experiment was performed in a manner similar to

Figure 8. Plot of $d\Gamma_{Ru(edta)py} / dT$ vs. $[PVP]_{surface}$.

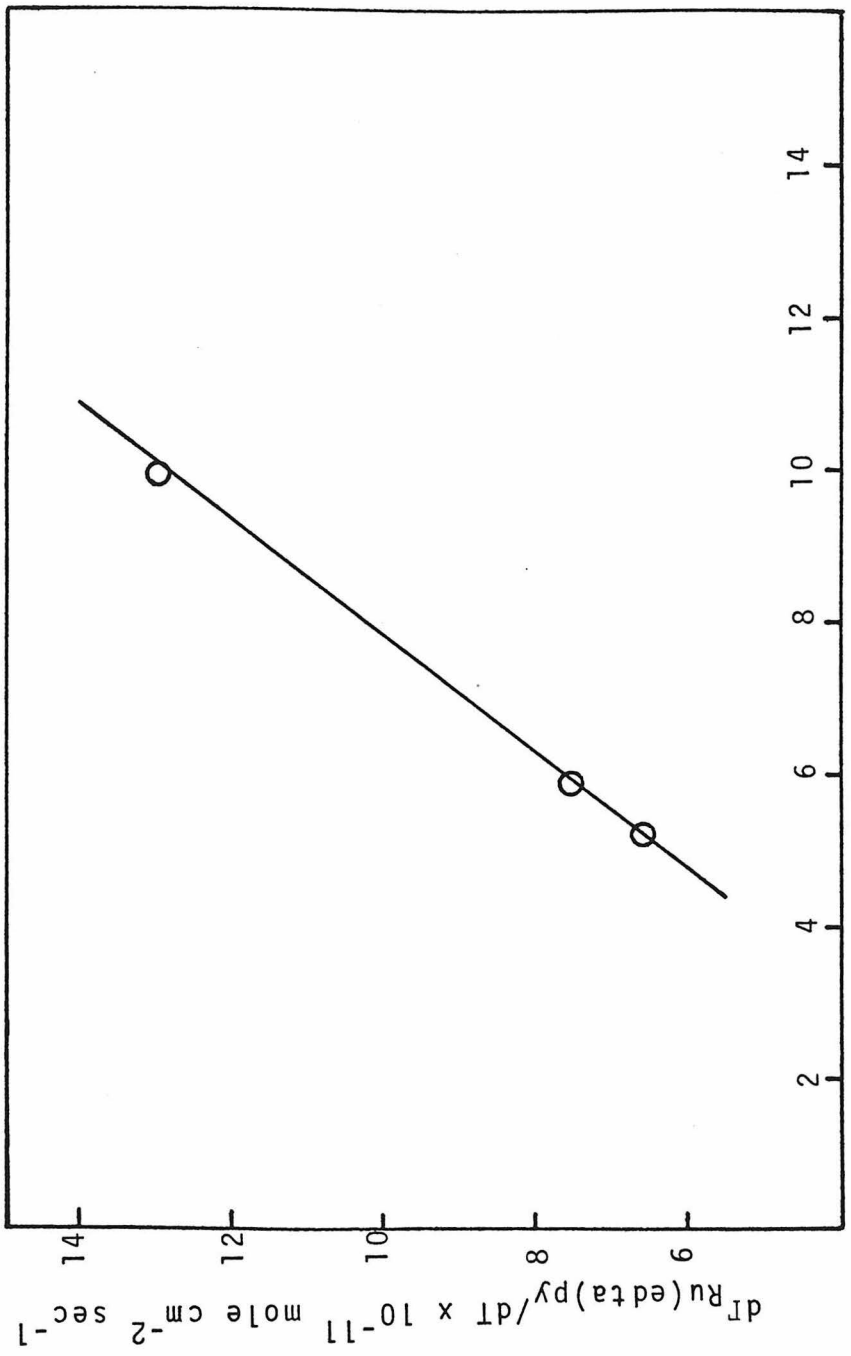
$d\Gamma_{Ru(edta)py}/dt \times 10^{-11}$ mole cm^{-2} sec^{-1}
14
12
10
8
6
2
4
6
8
10
12
14
$\Gamma_{Py} \times 10^{-8}$ mole cm^{-2}

those for the studies of the attachment of Ru^{III}(edta) to PVP-coated OTE except that the potential of the electrode was cycled from open circuit to +700 and +500 mV and maintained at each potential for 3 minutes. The plot of absorptivity versus time was linear for about 15 minutes before it then leveled off. This linearity implied that the rate of attachment was independent of the electrode potential. The thickness of the PVP layer employed in this study was in the order of 10^5 Å, which was at least three or four orders of magnitude thicker than the double layer [83]. Therefore, any change in the charge density at the electrode surface probably has negligible or no effect on complexes at a distance outside the double layer, thus resulting in independence of the rate of attachment with the electrode potential.

It was noted earlier [73] that large quantities of Ru^{III}(edta) could be attached by employing more concentrated Ru^{III}(edta) solutions to bind the complex to PVP-coated electrodes. The attachment isotherm of two different concentrations of pyridine on the electrode surfaces, 1.10×10^{-6} and 3.30×10^{-7} mole cm^{-2} (Figure 9) were studied. The electrode was initially exposed to a low concentration of Ru^{III}(edta) solution and the increase in 290 nm absorption was followed until no further increase was observed, then a solution with higher concentration was used, and vice versa. After the absorption using one concentration of Ru(edta) reached saturation, the spectrumof the Ru^{III}(edta)py attached on the electrode was recorded in the presence of supporting electrolyte. Maximum amounts of Ru^{III}(edta)py that can be formed employing a fixed concentration of Ru^{III}(edta) to bind the complex to PVP-coated electrodes were plotted as a function of Ru^{III}(edta) concentrations as shown in

Figure 9. Attachment isotherm of the PVP-coated GOTEs.

A: $\Gamma_{py} = 1.10\times10^{-6}$ mole cm^{-2}

B: $\Gamma_{py} = 3.30\times10^{-7}$ mole cm^{-2}.

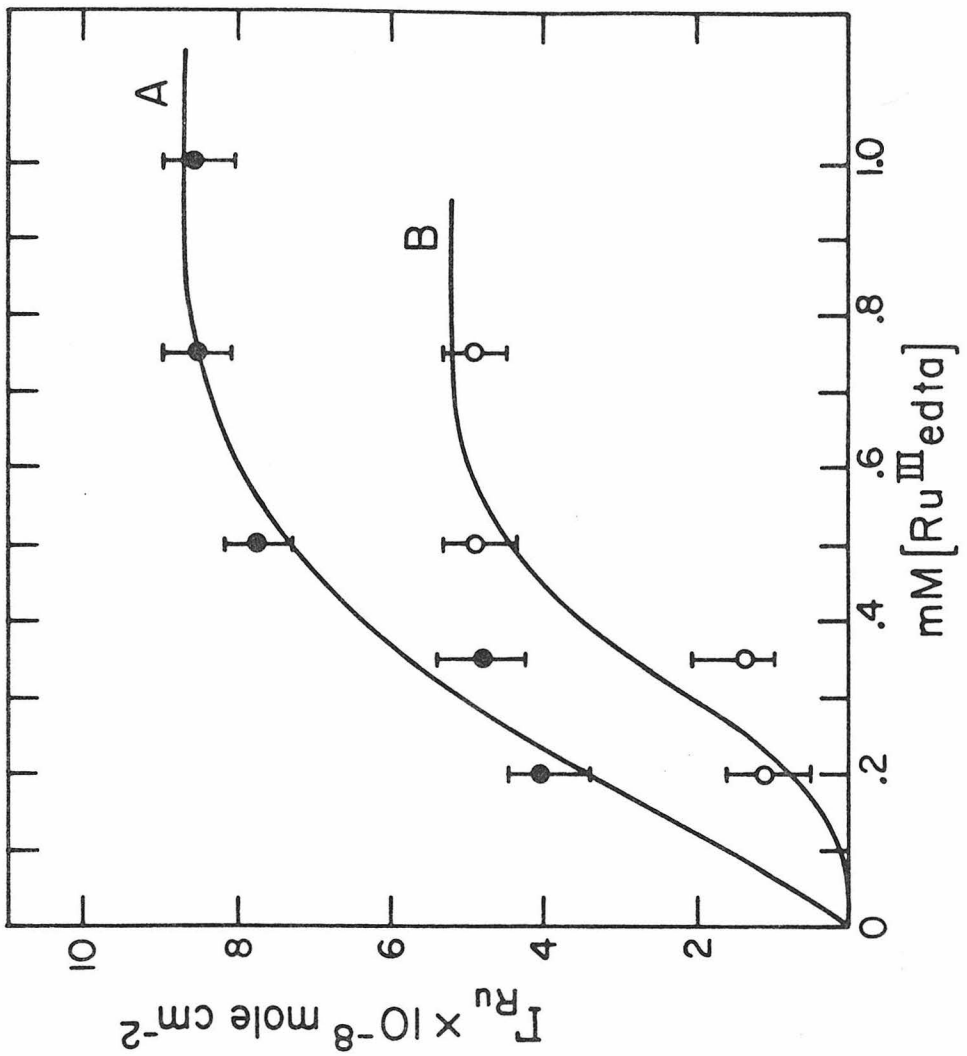
A
B
0
.2
.4
.6
.8
1.0
2
4
6
8
10
mM[Ru^III edta]
Γ_Ru x 10^-8 mole cm^-2

Figure 9. Note that the maximum amounts of Ru^{III}(edta)py formed were well below the amount of available pyridine ligands. For the pyridine concentration of 1.10×10^{-6} and 3.30×10^{-7} mole cm^{-2} the maximum amounts of Ru^{III}(edta)py that can be formed were 8.50×10^{-8} and 5.00×10^{-8} mole cm^{-2}, respectively. In both cases approximately 10% of the total pyridine concentration on the surface was available for coordination with Ru^{III}(edta) complex.

IV. Detachment kinetics of Ru^{III}(edta)py from PVP-coated GOTEs When the GOTE, to which Ru^{III}(edta) was bound by coordination to previously attached PVP, was monitored spectrally in the presence of 0.2M CF_3COONa (pH 7.1), the intensity of 290 nm absorption band decreased slowly as the pyridine-ruthenium bond was broken [73]. At the same time the band at 257 nm corresponding to the free pyridine groups on the surface increased in intensity. Figure 10 shows a first order plot of typical spectral data for the detachment process. The plot was linear for at least 80% of the reaction. The rate constants obtained from the slopes of plots similar to Figure 9 at two different values of initial Ru^{III}(edta)py concentrations are given in Table 2.

Table 2. Rate of detachment of Ru^{III}(edta) from PVP-coated GOTEs at different initial amounts of Ru^{III}(edta)py on the electrode surfaces. Rates were measured in the presence of 0.2M CF_3COONa (pH 7.1).

Γ_{Ru} on GOTE mole cm^{-2}	k sec^{-1}
4.82×10^{-8}	3.47×10^{-4}
3.25×10^{-8}	3.60×10^{-4}

Figure 10. Time dependence of the detachment of Ru^{III}(edta) from the PVP-coated GOTE. Initial concentration of Ru^{III}(edta)py formed on the surface = 4.82×10^{-8} mole cm^{-2}. The kinetics was followed spectroscopically at 290 nm in the presence of 0.2M CF_3COONa (pH 7.1).

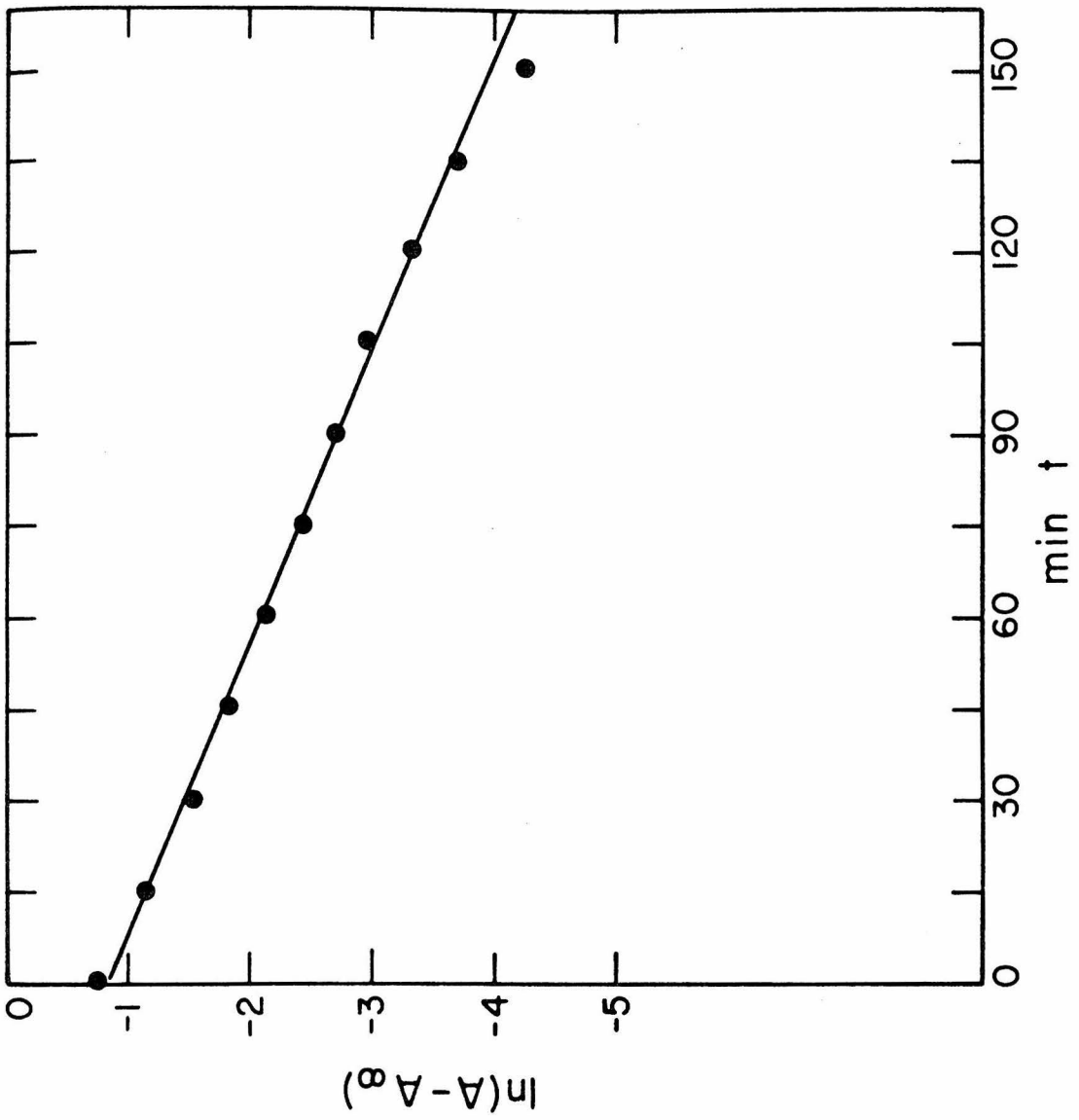
0
-1
-2
-3
-4
-5
ln(A - A∞)
0
30
60
90
120
150
min t

The rates were almost invariant to the initial Ru^{III}(edta)py concentrations. The results suggested that the breaking of ruthenium-nitrogen bond was not influenced by the concentration of the complex on the surface. It is reasonable to visualize that even at the highest Ru^{III}(edta)py on the PVP backbone, they are well separated from each other, such that sterically hindrance was not expected to occur on the surface. The rates of detachment were also found to be independent of the electrode potential in the range where ruthenium is in the oxidized form (+500 and +700 mV). We attributed this observation to the effect of the thick layer of polymer on the electrode, as previously discussed for the attachment case.

Comparison of the detachment rate obtained with that of the corresponding homogeneous rate ($k_{-1} = 6.1x10^{-2}sec^{-1}$) [81] shows that breaking the ruthenium-nitrogen bond is easier when the complex can move freely in the solution than when it is attached to the surface. By attaching the complex to the electrode surface, a more stable ruthenium-nitrogen bond was obtained.

In the attempt to determine the quantities of the ruthenium complex formed on the surface, we found that the values calculated from the triangular area under the cathodic peak [83] of a cyclic voltammogram of the attached complex were less than those detected by absorption intensity at 290 nm and coulometry. The last two gave approximately the same values. The discrepancy between the coverages calculated from cyclic voltammogram and coulometry was also observed for pyrolytic graphite electrodes as well [73,82]. The cause of such behavior was not the nature of the electrodes, but rather the thickness of the polymer

coating on them. Note that in the experiments studied in this chapter and those by Oyama and Anson[82], the surface pyridine concentrations were in the order of 10^{-7} mole cm^{-2}. At this relatively high coverage, it is reasonable to expect that the complexes formed near the electrode surface were relatively inaccessible from the solvent and supporting electrolyte. Therefore, the slowest time scale of cyclic voltammetry (10 mV sec^{-1}) employed seemed to be insufficient for counter ion to diffuse into the inner part of the polymer layer necessary for the charge neutralization upon reduction. Hence, the coverage calculated from the current observed during cyclic voltammetry corresponded to only a fraction of the complex on the surface. Furthermore, it was observed that at faster cyclic voltammetry sweep rates, the amount of ruthenium available for electroreduction as detected by the absorbance at 290 nm reduced considerably; e.g., at 200 mV sec^{-1} scan rate, only 20% of the ruthenium present was reduced. However, controlled potential electrolysis of the Ru^{III}(edta)py showed approximately the same amount of the complex as detected by absorption intensity at 290 nm, indicating that all of the complex formed on the surface was available for electroreduction. We also observed that a longer time was required to reduced the attached complex with a high pyridine concentration than for those with a lower one. The controlled potential reduction of Ru^{III}(edta)py was monitored spectroscopically at 290 nm. Figure 11i shows the plot of such absorbance and integrated charge passed through during the reduction process as a function of time. The linear dependence of the charge and absorption intensity is shown in Figure 11ii. From the slope of the plot, the effective electrode area of 4.36 cm^{-2} was calculated (Q/A =

Figure 11. i: Plots of charge(Q) and absorbance(A_{290}) at 290 nm during controlled potential reduction (-500 mV) of Ru^{III}(edta)py on the electrode surface.

ii: Linear relation between Q and A_{290}.

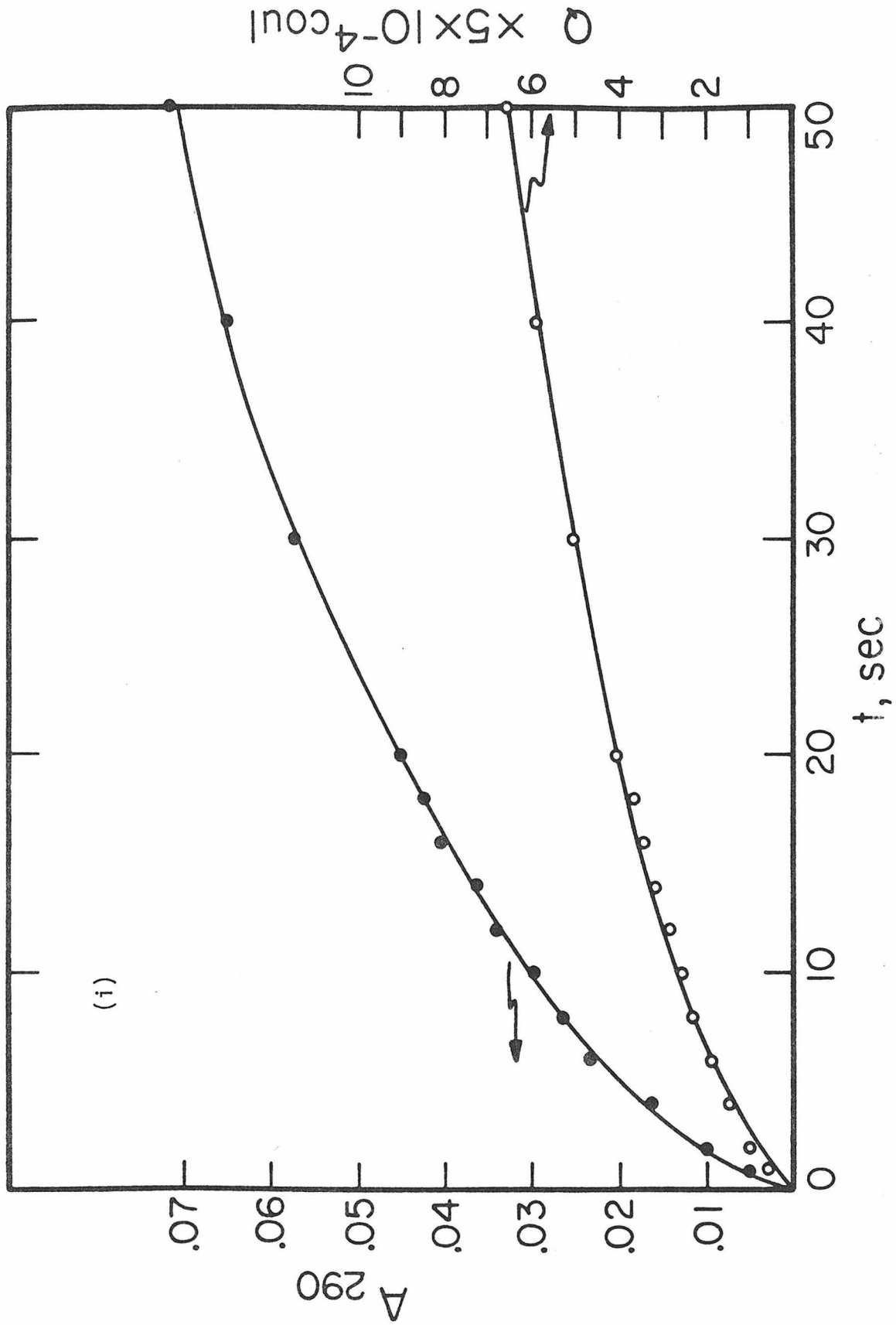
A 290
.01
.02
.03
.04
.05
.06
.07
0
10
20
30
40
50
t, sec
Q ×5×10⁻⁴coul
2
4
6
8
10
(i)

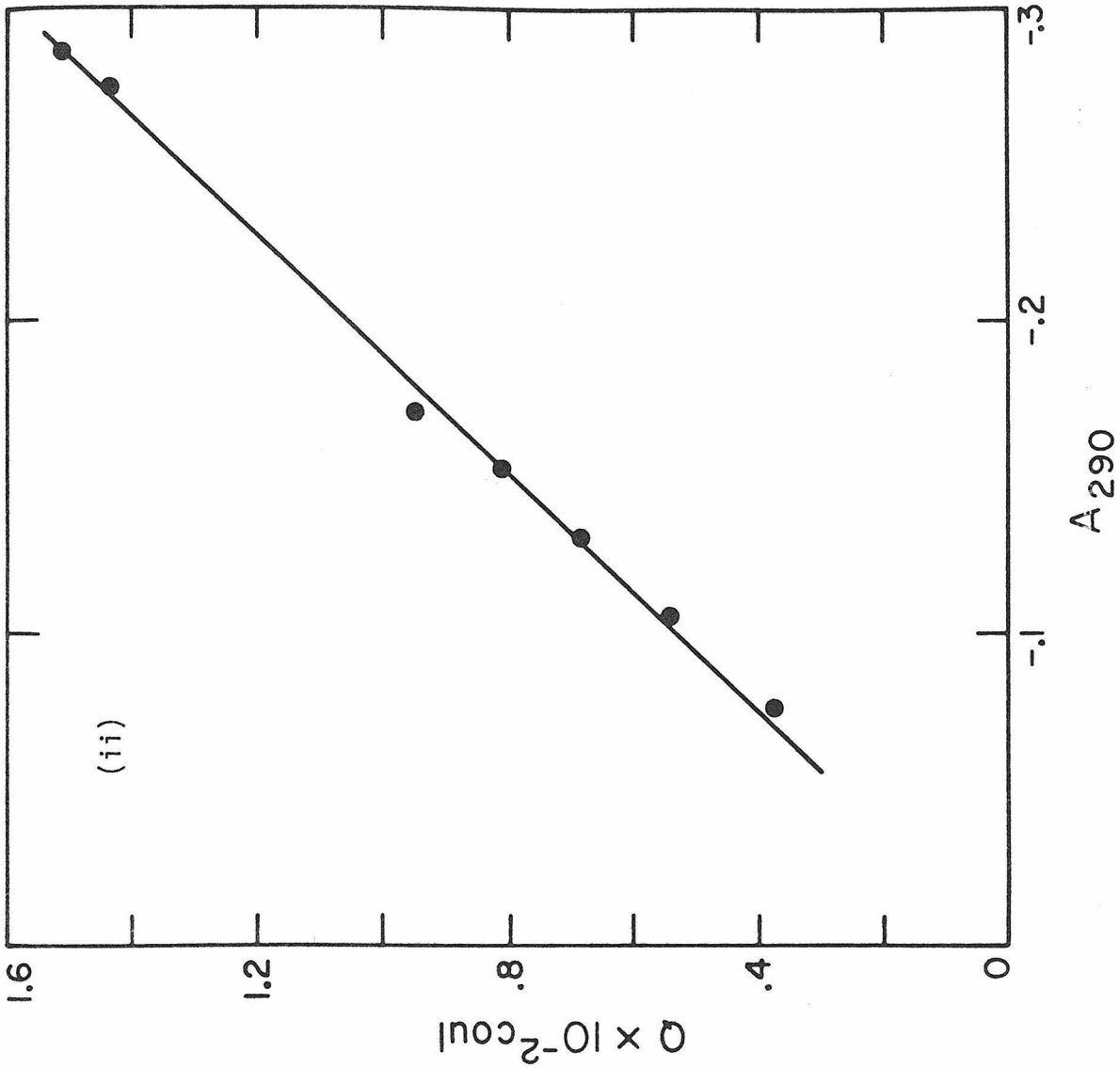
(ii)
Q x 10⁻²coul
1.6
1.2
.8
.4
0
-.3
-.2
-.1
A290

$5x10^{-2}$ coul = [F x area]/ε_{290}, ε_{290} = $8.41x10^{6}$ mole cm^{-2}). The calculated area was about 1.8 times larger than the value measured for the GOTE surface prior adsorption of the PVP (2.54 cm^2), suggesting that the PVP adsorbed on the electrode surface was non-uniform.

Conclusion

We have demonstrated in this study the usefulness of spectroelectrochemical technique as applied in order to allow one to quantitatively determine the quantities of electro-inactive specie by means of absorption intensity. The study also presents some evidence suggesting the significance of the charge transport in the polymer film, especially at high surface coverage, in order to undergo electron transfer process.

References

1. R. F. Lane and A. T. Hubbard, J. Phys. Chem. 77, 1401, 1411 (1973).
2. B. F. Watkins, J. R. Behling, E. Kariv, and L. L. Miller, J. Am. Chem. Soc. 97, 3549 (1975).
3. P. R. Moses, L. Wier, and R. W. Murray, Anal. Chem. 98, 7435 (1975).
4. M. Fujihira, T. Matsue, and T. Osa, Chem. Lett., 875 (1976).
5. B. E. Firth and L. L. Miller, J. Am. Chem. Soc. 98, 8272 (1976).
6. B. E. Firth, L. L. Miller, M. Mitani, T. Rogers, J. Lennox, and R. W. Murray, J. Am. Chem. Soc. 98, 8271 (1976).
7. C. M. Elliott and R. W. Murray, Anal. Chem. 48, 1247 (1976).
8. R. J. Burt, G. J. Leigh, and C. J. Pickett, J. Chem. Soc. Chem. Comm.,940 (1976).
9. N. R. Armstrong, A.W.C. Lin, M. Fujihira, and T. Kuwana, Anal. Chem. 48, 741 (1976).
10. T. Osa and M. Fujihira, Nature (London) 264, 349 (1976).
11. A. P. Brown, C. A. Koval, and F. C. Anson, J. Electroanal. Chem. 72, 379 (1976).
12. H. L. Landrum, R. T. Salmon, and F. M. Hawkridge, J. Am. Chem. Soc. 99, 3154 (1977).
13. S. Mazur, T. Matusinovic, and K. Cammann, J. Am. Chem. Soc. 99, 3888 (1977).
14. A. F. Diaz, U. Hetzler, and E. Kay, J. Am. Chem. Soc. 99, 6780 (1977).
15. V. S. Srinivasan and W. J. Lamb, Anal. Chem. 49, 1639 (1977).
16. D. G. Davis and R. W. Murray, Anal. Chem. 49, 194 (1977).
17. M. Fugihira, N. Ohishi, and T. Osa, Nature (London) 268, 226 (1977).
18. J. F. Evans and T. Kuwana, Anal. Chem. 49, 1632 (1977).

19. J. A. Schoeffel and A. T. Hubbard, Anal. Chem. 49, 2330 (1977).

20. P. R. Moses and R. W. Murray, J. Electroanal. Chem. 77, 393 (1977).

21. J. C. Lennox and R. W. Murray, J. Electroanal. Chem. 78, 395 (1977).

22. D. F. Untereker, J. C. Lennox, L. M. Wier, P. R. Moses, and R. W. Murray, J. Electroanal. Chem. 81, 309 (1977).

23. A.W.C. Lin, P. Yeh, A. M. Yacynych, and T. Kuwana, J. Electroanal. Chem. 84, 411 (1977).

24. G. J. Leigh and C. J. Pickett, J. Chem. Soc. (Dalton), 1797 (1977).

25. A. P. Brown and F. C. Anson, Anal. Chem. 49, 1589 (1977).

26. J. F. Evans, T. Kuwana, M. T. Henne, and G. T. Roger, J. Electroanal. Chem. 80, 409 (1977).

27. A. P. Brown and F. C. Anson, J. Electroanal. Chem. 83, 203 (1977).

28. J. Zagal, R. K. Sen, and E. Yeager, J. Electroanal. Chem. 83, 207 (1977).

29. A. F. Diaz and T. Kuwana, J. Electroanal. Chem. 86, 441 (1977).

30. M. Fugihira, A. Tamura, and T. Osa, Chem. Lett., 361 (1977).

31. G. T. Cheek and R. F. Nelson, Anal. Lett. 5, 393 (1978).

32. C. A. Koval and F. C. Anson, Anal. Chem. 50, 223 (1978).

33. A. M. Yacynych and T. Kuwana, Anal. Chem. 50, 640 (1978).

34. P. R. Moses, L. M. Wier, J. C. Lennox, H. O. Finklea, J. R. Lenhard, and R. W. Murray, Anal. Chem. 50, 576 (1978).

35. C. F. Kolpin and H. S. Swofford Jr., Anal. Chem. 50, 916 (1978).

36. D. C. Tse and T. Kuwana, Anal. Chem. 50, 1315 (1978).

37. K. Itaya and A. J. Bard, Anal. Chem. 50, 1478 (1978).

38. J. F. Stargardt, F. M. Hawkridge, and H. L. Landrum, Anal. Chem. 50, 930 (1978).

39. A. F. Diaz and K. K. Kanazawa, J. Electroanal. Chem. 86, 441 (1978).

40. M. S. Wrighton, R. G. Austin, A. B. Bocarsly, J. M. Bolts, O. Haas, K. D. Legg, L. Nadjo, and M. C. Palazzotto, J. Electroanal. Chem. 87, 429 (1978).

41. G. Hagen, B. S. Glavaski, and E. Yeager, J. Electroanal. Chem. 88, 269 (1978).

42. M. Fugihira, T. Osa, D. Hursh, and T. Kuwana, J. Electroanal. Chem. 88, 285 (1978).

43. T. Kuwana, M. Fugihira, K. Sunakawa, and T. Osa, J. Electroanal. Chem. 88, 299 (1978).

44. L. L. Miller and M. R. Van De Mark, J. Electroanal. Chem. 88, 437 (1978).

45. A. P. Brown and F. C. Anson, J. Electroanal. Chem. 92, 133 (1978).

46. C. P. Andrieux and J. M. Saveant, J. Electroanal. Chem. 93, 163 (1978).

47. R. Nowak, F. A. Schultz, M. Umana, H. Abruna, and R. W. Murray, J. Electroanal. Chem. 94, 219 (1978).

48. D. D. Hawn and N. R. Armstrong, J. Phys. Chem. 82, 1288 (1978).

49. L. L. Miller and M. R. Van De Mark, J. Am. Chem. Soc. 100, 639 (1978).

50. M. S. Wrighton, R. G. Austin, A. B. Bocarsly, J. M. Bolts, O. Haas K. D. Legg, L. Nadjo and M. C. Palazzotto, J. Am. Chem. Soc. 100, 1602 (1978).

51. A. Merz and A. J. Bard, J. Am. Chem. Soc. 100, 3222 (1978).

52. M. R. Van De Mark and L. L. Miller, J. Am. Chem. Soc. 100, 3223 (1978).

53. J. C. Lennox and R. W. Murray, J. Am. Chem. Soc. 100, 3710 (1978).

54. H. Tachikawa and L. R. Faulkner, J. Am. Chem. Soc. 100, 4379 (1978).

55. J. R. Lenhard, R. Rocklin, H. Abruna, K. Willman, K. Kues, R. Nowak, and R. W. Murray, J. Am. Chem. Soc. 100, 5213 (1978).

56. J. M. Bolts and M. S. Wrighton, J. Am. Chem. Soc. 100, 5257 (1978).

57. T. Miyasaka, T. Watanabe, A. Fujishima, and K. Honda, J. Am. Chem. Soc. 100, 6657 (1978).

58. M. S. Wrighton, M. C. Palazzotto, A. B. Bocarsly, J. M. Bolts, A. B. Fischer, and L. Nadjo, J. Am. Chem. Soc. 100, 7264 (1978).

59. J. R. Lenhard and R. W. Murray, J. Am. Chem. Soc. 100, 7870 (1978).

60. I. Haller, J. Am. Chem. Soc. 100, 8050 (1978).

61. N. Oyama, A. P. Brown, and F. C. Anson, J. Electroanal. Chem. 87, 435 (1978).

62. N. Oyama and F. C. Anson, J. Electroanal. Chem. 88, 289 (1978).

63. M. Sharp, M. Peterson, and K. Edstrom, J. Electroanal. Chem. 95, 123 (1979).

64. H. O. Finklea and R. W. Murray, J. Phys. Chem. 83, 353 (1979).

65. Y. Umezawa and T. Yamamura, J. Electroanal. Chem. 95, 113 (1979).

66. M. F. Dantartas, J. F. Evans, and T. Kuwana, Anal. Chem. 51, 104 (1979).

67. J. F. Evans and T. Kuwana, Anal. Chem. 51, 358 (1979).

68. K. Pool and R. P. Buck, J. Electroanal. Chem. 95, 241 (1979).

69. D. F. Smith, K. Willman, K. Kuo, and R. W. Murray, J. Electroanal. Chem. 95, 217 (1979).

70. N. Oyama and F. C. Anson, J. Am. Chem. Soc. 101, 1634 (1979).

71. H. S. White and R. W. Murray, Anal. Chem. 51, 236 (1979).

72. F. B. Kaufman and E. M. Engler, J. Am. Chem. Soc. 101, 547 (1979).

73. N. Oyama and F. C. Anson, J. Am. Chem. Soc. 101, 739 (1979).

74. N. Oyama and F. C. Anson, J. Am. Chem. Soc. 101, 3450 (1979).

75. Y. Umezawa and T. Yamamura, J. Chem. Soc. Chem. Comm., 1106 (1978).

76. H. Mukaida, H. Okuno, and T. Ishimori, Nippon Kagaku Zushi. 86, 56 (1965).

77. T. Matsubara and C. Creutz, J. Am. Chem. Soc. 100, 6255 (1978).

78. P. Ford, De F. P. Rudd, R. Gaunder, and H. Taube, J. Am. Chem. Soc. 90, 1187 (1968).

79. H. H. Jaffe and M. Orchin, "Theory and Applications of Ultraviolet Spectroscopy" (John Wiley, New York, 1962), p. 361.

80. H. P. Stephenson, J. Chem. Phys. 22, 1077 (1954).

81. T. Matsubara and C. Creutz, J. Am. Chem. Soc., in press.

82. N. Oyama and F. C. Anson, J.Electrochem.Soc., submitted for publication.

83. P. Delahay, "Double Layer and Electrode Kinetics" (Interscience, New York, 1965).

Abstracts of Propositions

Proposition 1. Kinetics of sulfite oxidase with its physiological oxidant(cytochrome c), reductant(sulfite), and inorganic reagents in order to elucidate electron transfer mechanism employed by the enzyme is proposed.

Proposition 2. Kinetics studies of modified cytochrome c with sulfite oxidase is proposed. The studies should enable one to understand the nature of the electron pathway in and out of cytochrome c.

Proposition 3. Photoacoustic spectroscopic technique is proposed to be applied to the elucidation of the photosynthetically active units in vivo of green plants.

Proposition 4. The ^{13}C nuclear magnetic resonance studies of π back-bonding of metalloporphyrins are proposed.

Proposition 5. Photochemical and photophysical studies of some derivatives of polypyridine ruthenium are proposed.

Proposition 6. The determination of the origin of the cyanolysable sulfur in molybdenum iron/sulfur flavin hydroxylases using the Extended X-ray Absorption Fine Structure (EXAFS) technique is proposed.

Proposition 1

Electron transfer mechanism employed by sulfite oxidase

This proposition is concerned with the elucidation of electron transfer mechanisms employed by sulfite oxidase in: 1) determination of the reduction of sulfite oxidase by its physiological reductant, sulfite; 2) determination of the oxidation of the enzyme by its physiological oxidant, cytochrome c; and 3) determination of the electron transfer mechanism of the enzyme with inorganic reagants. Sulfite oxidase is a molybdenum and heme containing enzyme which catalyzes the oxidation of sulfite to sulfate, with cytochrome c as the ultimate physiological electron acceptor [1]. Sulfite is oxidized at the molybdenum site, which is in turn reoxidized by the b_5-like heme [2]. The enzyme thereby couples the two-electron oxidation of sulfite with two one-electron reductions of cytochrome c. The enzyme from beef [3], chicken [4], or rat [5] liver has a molecular weight of about 110,000 and exists as a dimer of 55,000 dalton units, each containing a molybdenum and heme prosthetic group. Ever since the first successful purification of the enzyme from beef liver eight years ago [3], several interesting studies have emerged including the cleavage of the native enzyme into two functional domains [6], metal substitution of demolybdoenzyme [7,8], electron paramagnetic spectroscopic studies of the molybdenum site of the enzyme [4,9], and X-ray absorption spectroscopic studies [10].

It has been established from EPR experiments that upon reduction of the enzyme with sulfite, the low-spin ferric heme (Soret band at 413 nm) was reduced to low-spin ferrous heme with a Soret band at 423 nm [3] and a Mo(V) EPR signal appears at $g = 1.97$ [9] (Mo has an oxidation state of +6 in the native form).

Sulfite oxidase is an essential enzyme in sulfur metabolism. Patients with sulfite oxidase deficiency are abnormal at birth and have many neurologic abnormalities [11]. Biochemical investigation revealed the presence of increased amounts of sulfite in the urine. Therefore, it is important that the catalytic role of this enzyme be understood. As a first step toward a long range goal, it is proposed that the electron transfer mechanism employed by this enzyme be studied.

The electron transfer reactions of sulfite oxidase were studied briefly by Fridovich [3] and Rajagopalan [4] in which the initial velocity studies were performed by determining the relative velocities using varying concentrations of sulfite and fixed variable concentrations of cytochrome c and vice versa. The electron transfer mechanism employed by the enzyme was proposed to be of the ping-pong mechanism as given in the scheme below:

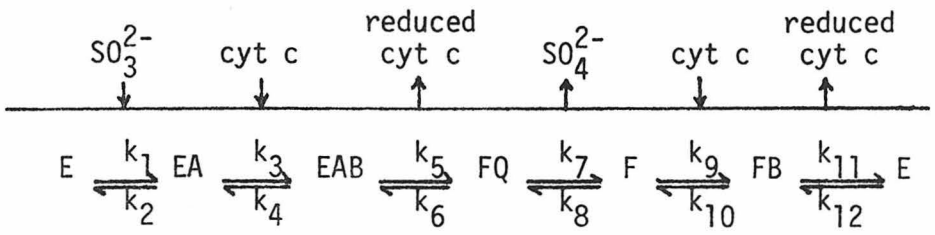

However such studies do not give a clear cut picture of the interaction of the enzyme with substrates. Furthermore, the detailed electron transfer pathway employed by the enzyme cannot be sought out. Therefore, dividing the turn-over kinetics into two separate experiments should enable the experimenter to obtain detailed electron transfer pathways employed by the enzyme.

The preliminary kinetic studies of reduction of sulfite oxidase by sulfite (followed at 423 nm) have been performed. The absorbance showed biphasic behavior for both chicken and beef enzymes. The initial fast phase is about 80% of the total absorbance change. Plots of observed rate constants versus sulfite concentrations are shown in Figures 1a and 1b for chicken and beef enzymes respectively. It is seen that the fast phases approach saturation limit at high concentrations of sulfite, while the slow phases appear to be independent of sulfite concentrations. The plots of the fast phases were fitted with the rate equation:

$$k_{obs} = \frac{kK[SO_3^{2-}]}{1 + K[SO_3^{2-}]} \qquad (1)$$

The first order rate constants for the fast phase were calculated to be 200, 105 sec^{-1} with equilibrium constants of 8.6×10^3, $7.5 \times 10^4 mol^{-1}$ for chicken and beef enzymes, respectively. The slow phase of the 423 nm absorbance change were calculated to be 8.0×10^{-2} and 3.5×10^{-2} sec^{-1} for chicken and beef enzymes, respectively.

The fact that fast phase approach to saturation limit with increasing sulfite concentration is a common phenomenon in enzyme-substrate kinetics [12] is consistent with a mechanism involving rapid pre-equilibrium enzyme substrate complex formation. One possible mechanism would be the following:

$$SO_3^{2-} + Mo^{VI}Fe^{III} \rightleftharpoons SO_3^{2-}\cdots Mo^{VI}Fe^{III} \quad (2)$$

$$SO_3^{2-}\cdots Mo^{VI}Fe^{III} \xrightarrow{k} SO_4^{2-}\cdots Mo^{IV}Fe^{III} \quad (3)$$

$$SO_4^{2-}\cdots Mo^{IV}Fe^{III} \longrightarrow SO_4^{2-} + Mo^{IV}Fe^{III} \quad (4)$$

$$Mo^{IV}Fe^{III} \longrightarrow Mo^{V}Fe^{II} \quad (5)$$

where k is the rate-limiting step, and $SO_3^{2-}\cdots Mo^{VI}Fe^{III}$ represents the enzyme-substrate procursor complex. However, it is possible that equation (5) would be the rate-limiting step, i.e., the intramolecular electron transfer from molybdenum to iron. These mechanisms could be sought out by performing exactly the same experiments as in these preliminary studies, but monitoring the disappearance of sulfite which has a maximum absorbance at 212.5 nm. If one observes the same behavior as when the reaction is monitored at 425 nm, i.e., biphasic and first order rate constant is the same, then it is possible that the first mechanism applies (reaction (3) is the rate-limiting step). Furthermore, the existence of the slow phase has been attributed to the presence of non-active enzyme in the purified sample [4]. The slow phase observed, therefore, corresponds to the interconversion of the non-active enzyme into active form. This proposal could be proved or disproved by performing the experiments with different batches of enzyme preparations, since the ratio of active to non-active enzyme should vary from one preparation to another, thus reflecting in the ratio of absorbance change of fast and slow phases.

The next series of experiments is proposed to examine the oxidation of sulfite-reduced enzyme with cytochrome c. These experiments will

either disprove that the intramolecular electron transfer is non-observable under the experimental conditions if the rate of electron transfer is not very much different from the rate of reduction of the enzyme, or will support it. Furthermore, the electron transfer mechanism of this enzyme could be studied via the redox reactions with inorganic redox agents, e.g., $Co(phen)_3^{3+}$, $Ru(NH_3)_5py^{3+}$, and $Ru(NH_3)_6^{3+}$. These experiments should enable one to determine the mechanism of reduction and oxidation of the enzyme by inorganic reagents in addition to providing information concerning the accessibility of the redox center [13,14].

Figure 1. Plots of observed rate constants versus sulfite concentrations monitored at 423 nm at 25^{o}, pH 9 (Tris), ionic strength = 0.05 M for:

a. Chicken liver enzyme

b. Beef liver enzyme

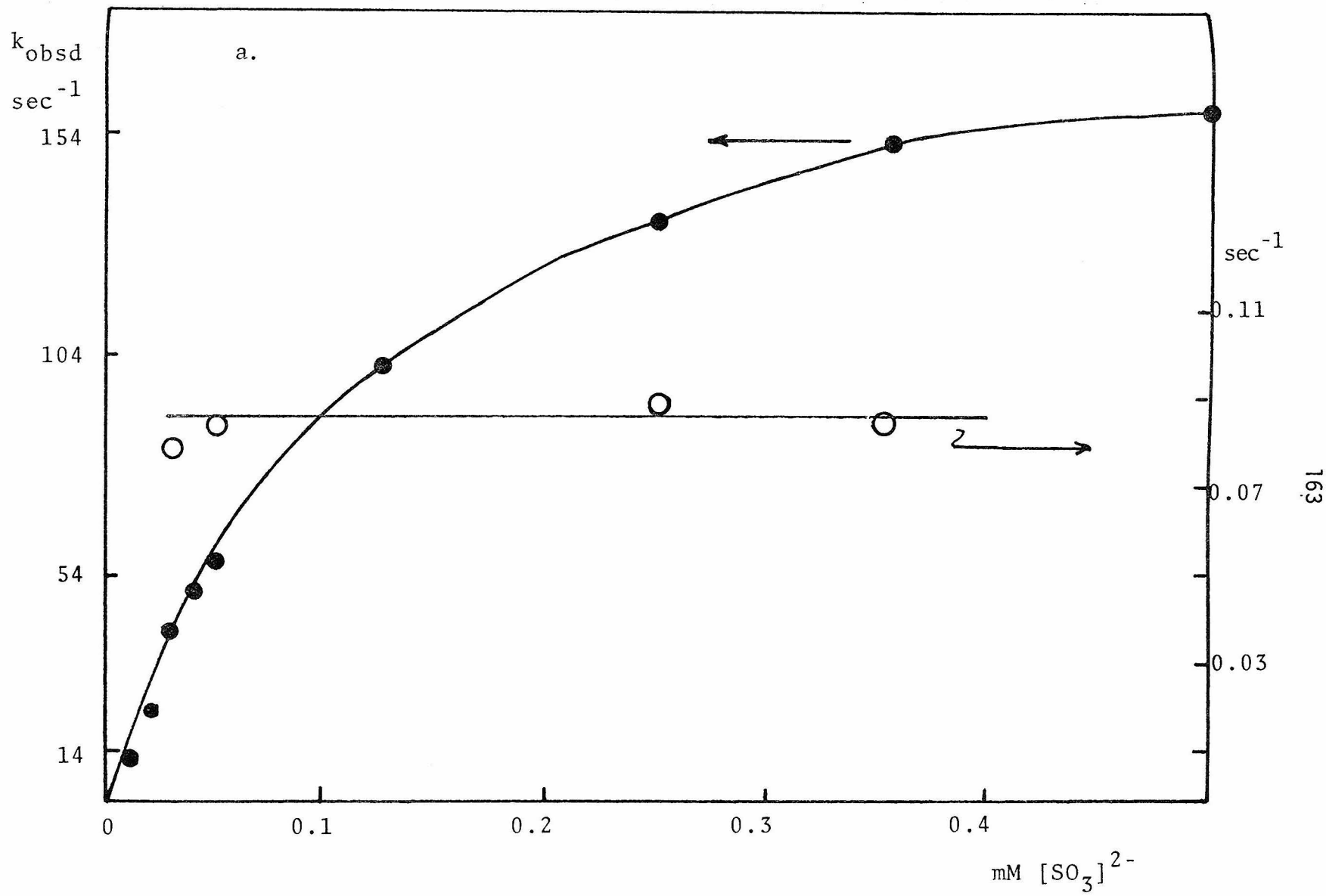
k_{obsd}
sec^{-1}
a.
154
104
54
14
0
0.1
0.2
0.3
0.4
mM $[SO_3]^{2-}$
sec^{-1}
0.11
0.07
0.03
2

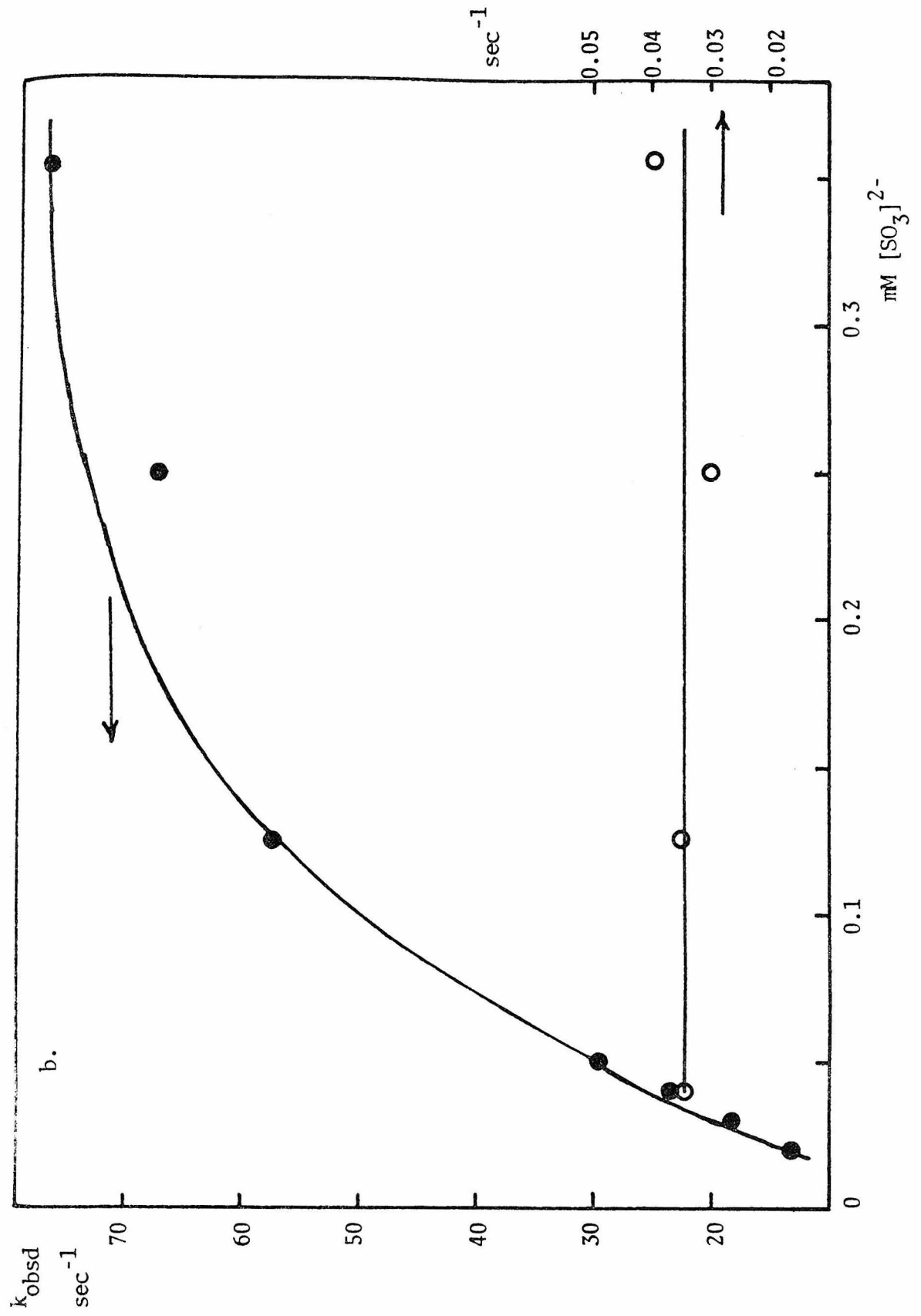
b.
k_{obsd} sec^{-1}
70
60
50
40
30
20
sec^{-1}
0.05
0.04
0.03
0.02
0
0.1
0.2
0.3
mM $[SO_3]^{2-}$

References

1. a) H. J. Cohen, S. Betcher-Lange, D. Kessler, and K. V. Rajagopalan, J. Biol. Chem. 247, 7759 (1972).
b) N. Oshino and B. Chance, Arch. Biochem. Biophys. 170, 514 (1975).
2. J. L. Johnson and K. V. Rajagopalan, J. Biol. Chem. 251, 5505 (1976).
3. H. J. Cohen and I. Fridovich, J. Biol. Chem. 246, 359 (1971).
4. D. L. Kessler and K. V. Rajagopalan, J. Biol. Chem. 247, 6566 (1972).
5. D. L. Kessler, J. L. Johnson, H. J. Cohen, and K. V. Rajagopalan, Biochem. Biophys. Acta 334, 86 (1974).
6. J. L. Johnson and K. V. Rajagopalan, J. Biol. Chem. 252, 2017 (1977).
7. H. P. Jones, J. L. Johnson, and K. V. Rajagopalan, J. Biol. Chem. 252, 4988 (1977).
8. J. L. Johnson, H. P. Jones, and K. V. Rajagopalan, J. Biol. Chem. 252, 4994 (1977).
9. H. J. Cohen, I. Fridovich, and K. V. Rajagopalan, J. Biol. Chem. 246, 374 (1971).
10. S. P. Cramer and H. B. Gray, J. Am. Chem. Soc. 101, 2772 (1979).
11. V. E. Shih, I. F. Abrams, J. L. Johnson, M. Carney, R. Mandell, R. M. Robb, J. P. Cloherty, and K. V. Rajagopalan, New England J. Med. 297, 1022 (1977).
12. K. E. Plowman, "Enzyme Kinetics" (McGraw-Hill, New York, 1972) ,Ch.1.
13. S. Wherland and H. B. Gray, "Biological Aspects of Inorganic Chemistry", D. Dolphin, ed. (John Wiley, New York, 1976).
14. D. Cummins and H. B. Gray, J. Am. Chem. Soc. 99, 5158 (1977).

Proposition 2

Kinetic studies of (modified cytochrome *c*) with sulfite oxidase

Despite the fact that a wide variety of techniques have been used to study the reduction of cytochrome c by cytochrome c reductase and its oxidation by cytochrome oxidase, little is known about the mechanisms of these processes at the molecular level. The location of the reaction sites on cytochrome c for cytochrome c reductase and cytochrome oxidase is the subject of some controversy, particularly as to whether the sites are the same or different. A number of chemical modification and antibody binding studies indicate that the binding sites may be different [1-4], while Salemme et al. [5] have suggested that both the oxidase and the reductase bind at the same site on the front of cytochrome c over the heme crevice.

Since the binding interaction of cytochrome c with its oxidase and reductase is known to involve the positively charged lysines on cytochrome c [6-8], one way to study the location of the binding sites is to measure how modification of specific lysine groups affects the reactivity of cytochrome c with the reductase and oxidase. A large number and wide variety of reagents have been used to chemically modify lysine residues of cytochrome c, e.g., acetic anhydride [9], ethylthiotrifluoroacetate [10], gladiolic acid [11], trinitrobenzene sulfonate [12], and fluorescein isothiocyanate [13]. Studies of these modified cytochrome c's indicate that modification of only a small number of the lysines result in loss of most of the respiratory chain electron transfer activities of the protein. However, these reagents do not provide good yields of singly substituted products and make it very difficult to separate them in a completely pure form. In fact, several of the studies

result in modified cytochrome c with many residues substituted [8,4]. Therefore, from comparison of their activities, it is not possible to identify unambiguously which area of the protein is involved in the interaction with the oxidase and reductase.

Recently, selective chemical modification of single lysine residues on the cytochrome c molecule became possible. Staudenmayer et al. [10,15] reported on the preparation of five derivatives with single trifluoro acetylated lysine residues at positions 13, 22, 25, 55, and 99. In their preliminary report, Brautigan et al. [16] identified three mono-4-carboxy-2,6-dinitrophenyllysine 13, 60, and 72 cytochrome c. Smith et al. [17] reported the preparation of six trifluoromethylphenylcarbamoyl (TFC) derivatives of cytochrome c at positions 8, 13, 27, 72, 79, and 100. Kinetic studies of these derivatives with cytochrome oxidase [17], succinate cytochrome reductase [18] indicated that the only modifications that decreased the reaction rate were those of lysines immediately surrounding the heme crevice (lysines 8, 15, 25, 27, 72, and 79 for reactions with cytochrome oxidase, and lysines 8, 13, and 72 for reaction with succinate cytochrome reductase). These results indicated that the binding site on cytochrome c for cytochrome c_1 (succinate cytochrome reductase) overlaps considerably with that for cytochrome oxidase. It was suggested [18] that cytochrome c might undergo some type of rotational diffusion during the electron transport process.

Recently, it has been established that liver mitochondria sulfite oxidase is a reductase for cytochrome c [19]. The cytochrome c reductase activity of sulfite oxidase is a native property of the enzyme, and becomes observable on release of the enzyme from mitochondria by gentle

hypotonic treatment [20]. The location of sulfite oxidase in the intermembrane space of mitochondria provides ready access to cytochrome c located on the outer surface of the inner membrane [21]. Thus studies of the interaction of cytochrome c and sulfite oxidase is of considerable interest. Therefore, it is proposed that kinetic studies of sulfite oxidase with modified cytochrome c be studied. Since the binding site of sulfite oxidase to cytochrome c is via the b_5-like heme of the former, comparison of the results with those of cytochrome c_1 in succinate cytochrome reductase should provide further insight into the mechanism of entry of electrons into cytochrome c.

The experiment to be proposed involves the preparation of specific trifluoroacetylated (TFA) and trifluoromethylphenylcarbamyl (TFC) lysine derivatives of cytochrome c [10,11,17]. Sulfite oxidase could be purified from chicken liver according to the method of Kessler and Rajagopalan [22]. Reduced sulfite oxidase could be obtained from the reduction of the enzyme with excess dithionite. Excess reductants are removed by dialyzing against buffers used in an anaerobic condition. Once the modified cytochrome c has been prepared, reduction kinetics of each modified cytochrome c by reduced sulfite oxidase can be studied. The reactions would be studied in tris buffer, pH 9 and followed at 550 nm (ε = 28 mM cm^{-1}). The rate of reduction of modified cytochrome c's with sulfite oxidase would be compared on the basis of the position of the substituted lysyl residues and the domain of interaction with the enzyme could be identified. The rate of the reactions with TFC and TFA modification could be compared, since TFC is relatively bulky, to TFA. Therefore, if there is a significant difference between the two rates, it

would imply that there is a steric interference in the electron transfer mechanism. If this is not the case, then the difference in the reaction rate of sulfite oxidase with TFC (TFA) modified cytochrome c from those with native cytochrome c would indicate the significance of that particular lysine residue upon binding with sulfite oxidase.

In summary, it is proposed that a series of reduction kinetics of sulfite oxidase with modified cytochrome c be studied, careful examination and comparison of reactivities of modified cytochrome c with cytochrome oxidase [17] and succinate cytochrome reductase [18] would enable us to understand the nature of the electron pathway in and out of cytochrome c.

References

1. T. Takano, O. B. Kallai, R. Swanson, and R. E. Dickerson, J. Biol. Chem. 248, 5235 (1973).

2. E. Margoliash, S. Ferguson-Miller, J. Tulloss, C. H. Kang, B. A. Feinberg, D. L. Brautigan, and E. Morrison, Proc. Natl. Acad. Sci. USA 70, 3245 (1973).

3. L. Smith, H. C. Davies, M. Reichlin, and E. Margoliash, J. Biol. Chem. 248, 237 (1973).

4. L. Smith, H. C. Davies, and M. E. Nava, Biochemistry 15, 5827 (1976).

5. F. R. Salemme, J. Kraut, and M. D. Kamen, J. Biol. Chem. 248, 7701 (1973).

6. P. Nichalls, Arch. Biochem. Biophys. 106, 25 (1964).

7. C. A. Yu, L. Yu, and T. E. King, J. Biol. Chem. 250, 1383 (1975).

8. S. Ferguson-Miller, D. L. Brautigan, and E. Margoliash, J. Biol. Chem. 251, 1104 (1976).

9. K. Wada and K. Okunuki, J. Biochem. (Tokyo) 66, 263 (1969).

10. N. Staudenmayer, S. Ng, M. B. Smith, and F. Millett, Biochemistry 16, 600 (1977).

11. G. A. White and W. B. Elliott, Biochem. Biophys. Res. Commun. 47, 1186 (1972).

12. K. Wada and K. Okunuki, J. Biochem. (Tokyo) 66, 249 (1969).

13. S. Ferguson-Mill er, D. L. Brautigan, and E. Margoliash in "The Porphyrins," D. Dolphin, ed. (Academic Press, New York, 1977).

14. S. Ferguson-Miller, D. L. Brautigan, and E. Margoliash, J. Biol. Chem. 253, 130, 140, 149 (1978).

15. N. Staudenmayer, M. B. Smith, H. T. Smith, F. K. Spies Jr., and F. Millett, Biochemistry 15, 3198 (1976).

16. D. L. Brautigan and S. Ferguson-Miller, Fed. Proc., Fed. Am. Soc. Exp. Biol. 35, abstract #1219.

17. H. T. Smith, N. Staudenmayer, and F. Millett, Biochemistry 16, 4971 (1977).

18. A. J. Ahmed, H. T. Smith, M. B. Smith, and F. Millett, Biochemistry 17, 2479 (1978).

19. D. L. Kessler and K. V. Rajagopalan, Biochim. Biophys. Acta 370, 389 (1974).

20. H. J. Cohen, S. Betcher-Lange, D. L. Kessler, and K. V. Rajagopalan, J. Biol. Chem. 247, 7759 (1972).

21. C. Lee, "Probes of Structure and Function of Macromolecules and Membranes," B. Chance, ed., vol. 1 (Academic Press, New York, 1971), pp. 417-426.

22. D. L. Kessler and K. V. Rajagopalan, J. Biol. Chem. 247, 6566 (1972).

Proposition 3

Elucidation of the photosynthetically active units *in vivo* of green plants by photoacoustic spectroscopy

Photoacoustic spectroscopy (PAS) is a spectroscopic technique for the investigation of solids, semisolids, and liquids. It has proven to be a valuable method for the optical investigation of samples that cannot be studied by other conventional spectroscopic techniques due to their physical properties, e.g., powder, amorphous, gel, etc. [1,2]. The photoacoustic effect was first studied by Alexander Graham Bell in 1881. The effect occurs when a gas in an enclosed cell is illuminated with chopped or periodically interrupted light. Any energy absorbed by the gas is converted entirely or partially into kinetic energy of the gas molecules, thereby giving rise to pressure fluctuations within the cell. In 1881 the pressure fluctuations were detected as audible sound through a hearing tube.

The photoacoustic effect in gases has been used fairly extensively since then, until recently when Kreuzer and Patel [3] demonstrated that the use of a sensitive microphone and a tunable laser can impart to the photoacoustic effect a very high sensitivity. In a modern typical photoacoustic spectroscopic experiment, a sample is placed inside a closed chamber filled with inert gas. The sample is then illuminated by light modulated at an acoustic frequency. Any light absorbed by the sample is converted in part or in whole into heat by nonradiative de-excitation processes within the sample. The resultant periodic heat flows from the sample absorber to the surrounding gas, creating pressure fluctuations in the chamber which are detected by the microphone. Detailed review articles of PAS are available [1,2].

The principal advantage of this technique is that it enables one to obtain spectra similar to optical absorption spectra [1] on any type

of sample. Furthermore, since only the absorbed light is converted to sound, light scattering presents no difficulties in PAS. PAS has proven to be a powerful technique to study the optical and thermal properties of solids and solutions [1,4,5]. However, less attention has been given to using the technique for the study of energy conversion processes for which it is very well suited, as it measures directly the thermal energy generated upon absorption of radiation by the sample [6]. The naturally occurring energy conversion process is photosynthesis in which this thermal energy is the wasted part (together with fluorescence) of the absorbed radiation. Therefore, the photoacoustic and the optical absorption spectra of photosynthetically active samples should differ by the amount of absorbed energy that is converted into chemical energy. Also, inhibited photosynthetic samples should give photoacoustic signals larger than those obtained with normal samples, because in the latter case there is no photochemical loss.

This proposition concerns the PAS studies of light-harvesting pigments in photosynthetic membranes. The light-harvesting pigments are thought to be organized in units of 300-400 pigment molecules [7,8]. Each unit contains chlorophyll a_{II} in photosystem II units and chlorophyll a_{I} in photosystem I units) in association with a number of accessory pigments (chlorophyll b and carotenoids in green algae and higher plants) and a specialized reaction center. Although chlorophyll appears to be the primary photosynthetic pigment in all plants, its organization in green plants is less understood. Evidence accumulated strongly points to an organization in which the chlorophyll molecules are specifically conjugated with a relatively few but different polypeptide chains (the ratio of protein:

pigment molecules $\simeq$ 1: $<$10) [9].

The mechanism by which these chlorophylls aggregate and bind to the protein *in vivo* is much less understood, due to the unavailability of techniques to study the membrane bound sample. Furthermore, the attempt to study the system *in vitro* under conditions similar to those *in vivo* is often unsuccessful, due to the fact that the composition of the protein-chlorophyll complexes varies with the method of isolation and purification [10]. Therefore, in a much simpler manner, the studies of protein-chlorophyll complexes *in vivo* can be achieved by means of PAS.

Measurements of the photoacoustic spectra of membrane bound protein-chlorophyll complexes are proposed. The visible and infrared spectra of aggregated chlorophyll species, predicted to be present by absorption spectra of purified sample, can be compared to the photoacoustic spectra measured for species identification. The preparation of membrane-bound photosynthetic units from green plants has been described [11-14]. The absorption spectral data of the proposed aggregated chlorophyll species are given in Table I. The actual use of PAS with membrane-bound samples, either in the form of suspension or dried, has been described previously [15].

Therefore, the PAS studies should enable one to identify the manner of association of the chlorophyll molecules with each other and with other components of the photosynthetic unit *in vivo*. Furthermore, upon comparison of the magnitude of the photoacoustic and optical absorption spectra of the purified aggregated chlorophyll species, one should be able to identify the species which are responsible for the photochemical reaction. Information gained through this study is a short step

toward a long range goal, that is to say, it is better to understand first how nature converts light into chemical energy, after which man-made energy conversion devices should be within easy reach.

Table 1. Spectral data for aggregated chlorophyll species[1]

Species	Medium	Spectral Band peaks (nm)
$(Chl\ a)_2$	CCl_4	665, 682
	benzene	667, 682
$(Chl\ b)_2$	CCl_4	647, 664
	3-methyl pentane	641, 659
$(Chl_2 \cdot pyr)_n$	dodecane	690
$(Chl \cdot bipyr)_n$	dedecane	715
$(Chl \cdot H_2O)_n$	dedecane	743

[1] From G. R. Seely, in "Primary Processes of Photosynthesis," J. Barber, ed. (Elsevier, New York, 1977), Ch. 1.

References

1. R. Rosenewaig, Anal. Chem. 47, 592A (1975).

2. W. R. Harshbarger and M. B. Robin, Acc. Chem. Res. 6, 329 (1973).

3. L. B. Kreuzer and C.K.N. Patel, Science 173, 45 (1971).

4. M. J. Adams, B. C. Beadle, A. A. King, and G. F. Kirkbright, Analyst 101, 553 (1976).

5. M. J. Adams, B. C. Beadle, and G. F. Kirkbright, ibid. 102, 281, 569 (1977).

6. A. Fujishima, G. H. Brilmeyer, and A. J. Bard, in "Semiconductor Liquid-Junction Solar Cells," A. Heller, ed. (The Electrochem. Soc. Proc., Vol. 77-3, 1977), pp. 172-177.

7. J. Myers and J. Graham, Plant Physiol. 48, 282 (1971).

8. J. Myers and J. Graham, ibid. 55, 686 (1975).

9. J. P. Thornber, R. S. Alberti, F. A. Hunter, J. A. Shiozawa, and K. S. Kan, in "Chlorophyll-Proteins, Reaction Centers, and Photosynthetic Membranes," J. M. Olson, ed., report (Brookhaven Symposium, New York, 1976), p. 132.

10. B. Kok and R. Radner, in "Chemical Mechanisms in Bioenergetics," D. Rao Sanadi, ed. (ACS, New York, 1976), Ch. 5.

11. P. Massini and G. Vooru, Biochim. Biophys. Acta 153, 589 (1968).

12. J. Szabad, E. Lehoezki, L. Szalay, and K. Csatarday, Biophys. Struct. Mech. 1, 65 (1974).

13. S. D. Kung and J. P. Thornber, Biochim. Biophys. Acta 253, 285 (1971).

14. K. Apel, in "Chlorophyll-Proteins, Reactions Centers, and Photosynthetic Membranes," J. M. Olson, ed., report (Brookhaven Symposium, New York, 1976), p. 149.

15. D. Cahen, H. Garty, and S. Roy Caplan, FEBS Lett. 91, 131 (1978).

Proposition 4

^{13}C NMR studies of π back-bonding of metalloporphyrins

Development of a means for obtaining quantitative information concerning the nature of metal-to-ligand π bonding is of wide interest. ^{19}F NMR of some phosphene complexes of Ni(II), Pd(II), and Pt(II) have demonstrated that the ^{19}F nucleus, especially when in the para position, is a reasonable probe of electron density changes [1]. ^{1}H and ^{13}C NMR chemical shifts of pyridine and substituted pyridine complexes of Fe(II) [2-5] have been studied. These studies demonstrate that chemical shift changes, especially for ^{19}F and ^{13}C nuclei, are a promising means of directly observing π back-bonding effects which have been previously deduced by other means (e.g., infrared [6,7], electronic [7,8], Mossbauer [8]). Figard et al. [5] and Lavallee et al. [4] studied ^{13}C NMR chemical shifts of pentacyanoferrate(II) and cobaltate(III)complexes of unsaturated nitrogen heterocyclic ligands, and they found ^{13}C shift changes are considerably larger than solvent effects, especially shifts at the γ position, which appear to correlate most strongly with chemical evidence for π back-bonding. They have suggested that electron density changes may be the most important parameter in determining shift changes at this position, since effects of the anisotropy of the bound moiety and electric field effects should be least. Furthermore, the symmetry about the γ-carbon atom should minimize anisotropy of binding electrons.

It is therefore proposed that ^{13}C NMR be applied to study π back-bonding in metalloporphyrins. Several studies of the axial ligation reactions of Fe(III) porphyrins have already been reported [9-13]. The data available concerned studies of equilibrium constants for addition of imidazoles, pyridines, and their derivatives to tetraphenylporphyrin

complexes of chloroiron(III). Satterlee and LaMar [14] studied proton nuclear magnetic resonance of imidazole-iron bonding in porphyrin complexes and observed contact shifts in which they concluded that it arises primarily from iron(d_π) → imidazole π^* charge transfer. Normally porphyrin ligands will donate charge (probably mainly through σ-symmetry orbitals) to the metal ion [15], therefore electron donor capabilities of the metal ion depend upon the kinds of porphyrins. It would be very useful to be able to compare charge donating abilities among various porphyrins. The porphyrins of interest are tetraphenylporphyrin and its derivatives, octaethylporphyrin, mesoporphyrin, deuteroporphyrin, hematoporphyrin, and protoporphyrin IX. The structures of these porphyrins are given in Table 1. The deduction of a scale of charge donating ability of the porphyrin complexes will be through the ^{13}C shifts, as previously described. It is proposed to study initially the γ-carbon shift of bis-pyridine Fe(II) and Co(III) complexes of the previously mentioned porphyrin ligands. The complexes can be prepared according to literature methods [12,16,17]. The ^{13}C NMR spectra will be studied in a common solvent, e.g., CH_3Cl or benzene. It may be useful to use ^{13}C-enriched pyridine to aid in the identification of the coordinated pyridine resonances. It would also be helpful to study the mixed-ligand systems, e.g., one of the axial ligands can be CN^- or CO. It may provide additional information concerning π back-bonding, especially if the ^{13}CO or $^{13}CN^-$ resonances are also shifted as the electron donating characteristics of the porphyrin ligand are varied.

Finally, if ^{13}C shifts of the γ-carbon of pyridine proves successful to evaluate the degree of $d_{\pi} \rightarrow \pi^*$ electron delocalization, then it is proposed that the study be extended to the imidazole derivatives. It would be interesting to see if a similar conclusion can be deduced.

Table 1. Various porphyrin ligands

i

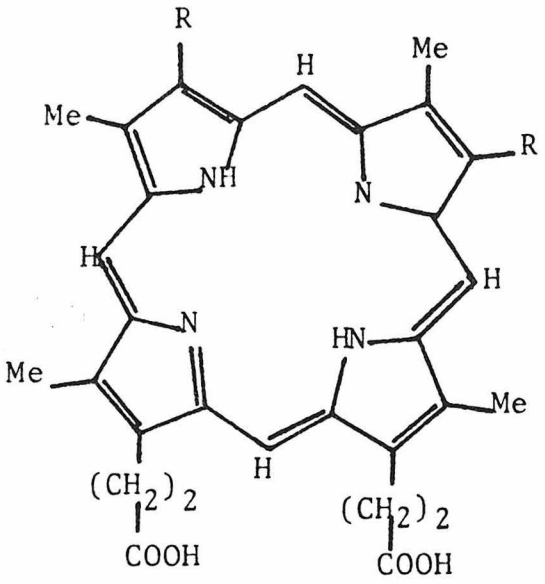

R = -CH = CH_2	protoporphyrin IX
= $-OCH_3$	hematoporphyrin
= $-CH_2-CH_3$	mesoporphyrin
= -H	deuteroporphyrin

ii

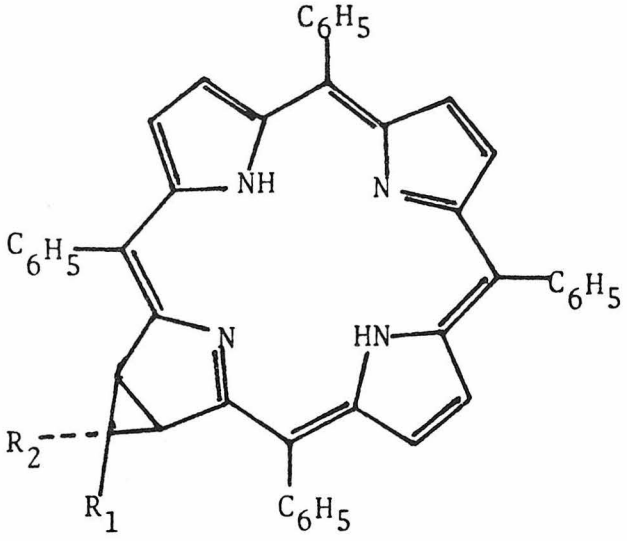

$R_1 = R_2 = H$ tetraphenylporphyrin

$R_1 = H$, $R_2 = COOCH_3$

$R_1 = COOCH_3$, $R_2 = H$

$R_1 = R_2 = COOCH_3$

iii

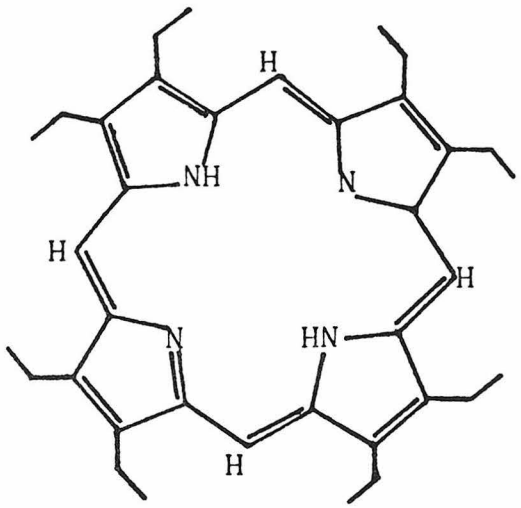

octaethylporphyrin

References

1. G. W. Parshall, J. Am. Chem. Soc. 96, 2360 (1974).

2. D. K. Lavallee and E. B. Fleischer, J. Am. Chem. Soc. 94, 2583 (1972).

3. J. M. Malin, C. F. Schmidt, and H. E. Toma, Inorg. Chem. 14, 2924 (1975).

4. D. K. Lavallee, M. D. Baughman, and M. P. Phillips, J. Am. Chem. Soc. 99, 718 (1977).

5. J. E. Figard, J. V. Pankstelis, E. F. Byrne, and J. D. Petersen, J. Am. Chem. Soc. 99, 8417 (1977).

6. F. A. Cotton and E. Wilkinsons, "Advanced Inorganic Chemistry," 3rd ed. (John Wiley, New York, 1972), Ch. 22.

7. J. A. Olabe and P. J. Aymonino, J. Inorg. Nucl. Chem. 38, 225 (1976).

8. H. E. Toma and J. M. Malin, Inorg. Chem. 12, 1039 (1973).

9. C. L. Coyle, P. A. Rafson, and E. H. Abbott, Inorg. Chem. 12, 2007 (1973).

10. E. H. Abbott and P. A. Rafson, J. Am. Chem. Soc. 96, 7378 (1974).

11. F. A. Walker, D. Boroiz, and K. M. Kadish, J. Am. Chem. Soc. 98, 3484 (1976).

12. F. A. Walker, M. Lo, and M. T. Ree, J. Am. Chem. Soc. 98, 5552 (1976).

13. J. M. Duclos, Bioinorg. Chem. 2, 263 (1973).

14. J. D. Satterlee and G. N. LaMar, J. Am. Chem. Soc. 98, 2804 (1976).

15. F. Adar, "The Porphyrins," vol. III, part A, D. Dolphin, ed. (Academic Press, New York, 1978), Ch. 2.

16. J. E. Falk, "Porphyrins and Metalloporphyrins" (Elsevier, New York, 1964).

17. J. H. Fuhrhop, "The Porphyrins," vol. II, part B., D. Dolphin, ed. (Academic Press, New York, 1978), Ch. 5.

Proposition 5

Photochemical and photophysical studies of some derivatives of polypyridine ruthenium

Photoelectrochemical cells have been proposed for the direct conversion of solar energy to electricity or chemical fuel [1]. These cells can be classified as photovoltaic and photogalvanic. The operation of the photovoltaic cell depends upon the generation of an electromotive force as a result of the absorption of light, whereas the photogalvanic depends on the excitation of photoactive species in solution by electromagnetic radiation which induces a faradaic process at the electrode. The best known example of photogalvanic cells is the iron-thionine system [2-4], in which the photoinduced reduction of thionine by ferrous ions takes place in the bulk solution. Unfortunately, because of their low efficiencies, they have not been considered seriously as a practical means of converting light into electricity. However, due to the recent development of semiconductor electrodes and thin layer devices there is a possibility of increasing the efficiency of such cells [5-7].

Recently, the quenching of tris(2,2'-bipyridine) ruthenium(II) luminescence by various inorganic and organic substrates is a subject of much interest [8,9]. The attractive properties of $Ru(bipy)_3^{2+}$, are that it absorbs light appreciably in the visible region, has a relatively long-lived charge transfer triplet state [10], and has large difference in ground and excited state potentials [11] which makes it a promising complex for the application to solar energy conversion and storage. Because most of the studies have been concentrated on the application to solar energy storage, little progress has been made on the photogalvanic effect.

The potential of $Ru(bipy)_3^{2+}$ for use in solar energy conversion was first recognized by Lin and Sutin [12]. They observed the generation of

photogalvanic potential on illumination of $Ru(bipy)_3^{2+}$–Fe^{3+} system in a cell consisting of two identical compartments separated by a sintered glass disk. A schematic representation of the proposed mechanism for such a system is shown below

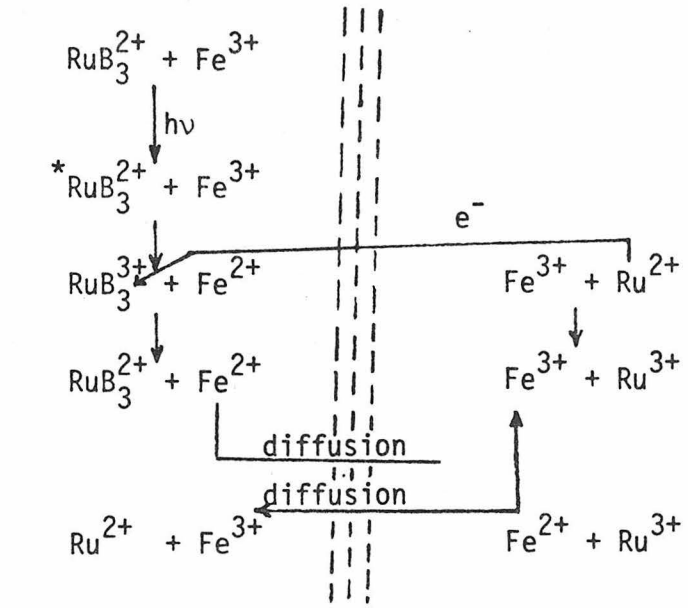

Upon illumination of the left side, an excited state $*Ru(bipy)_3^{2+}$ is generated which is capable of reducing Fe^{3+}:

$$*Ru(bipy)_3^{2+} + Fe^{3+} \rightleftharpoons Ru(bipy)_3^{3+} + Fe^{2+} \qquad (1)$$

In the right half cell, the equilibrium of equation (1) lies far to the left. The effect of radiation is thus to produce an endoenergetic state in which the Fe^{2+} and $Ru(bipy)_3^{3+}$ exceed their equilibrium values.

Therefore, upon connecting the cell to an external high impedance voltmeter, it is possible to utilize this free energy gain. The photogalvanic potentials from this type of cell can be estimated according to Lin and Sutin [12] as

$$\Delta U = \log \frac{[Ru(II)]_{dark}}{[Ru(III)]_{dark}} - \log \frac{[Ru(II)]_{light}}{[Ru(III)]_{light}} \qquad (2)$$

From this equation, the value of the first term depends on the reduction potential of Ru(III) complex, while the second term depends on the lifetime of the Ru(II) complex's excited state and the efficiency of electron transfer to the quencher. Thus the efficiency of the photogalvanic cell can be improved by means of changing the substituents on the polypyridine rings of the ruthenium complexes, thereby affording the possibility of increasing the lifetime of the emitting state of Ru(II) and/or lowering the reduction potential of the Ru(III).

While only the electron transfer process is desirable in photogalvanic cell, it is generally found that energy transfer processes occur with equal efficiency. Energy transfer processes lead back to the ground state of the starting Ru(II). One approach to reduce the energy transfer process is to incorporate the system in a favorable microenvironment which will increase the rate of photoinduced electron transfer such that it is much more favorable than the energy transfer process. The effect of micelles [13] and of polyelectrolyte [14] on the photo-initiated electron transfer from $Ru(bipy)_3^{2+}$ to Cu^{2+} ions has been reported. In both cases, a strong enhancement of the quenching rate of the charge transfer

state of $Ru(bipy)_3^{2+}$ by Cu^{2+} ions has been observed. Recently, Matheson et al. [15] reported enhancement of the rate of electron transfer from $*Ru(bipy)_3^{2+}$ to Fe^{3+} ions in the system containing polyvinylsulfate. The effect of polyvinylsulfate on the rate was shown to be mainly a volume effect, whereby the positively charged reactants were "condensed" in the negative potential field of the microenvironment. Furthermore, Whitten et al. [9] have synthesized a series of water-soluble complexes in which the polar charged $Ru(bipy)_3^{2+}$ core is surrounded by aliphatic groups of varying size. They also reported the increase in photoinduced electron transfer from these hydrophobic complexes to organic quenchers such as paraquat and N,N-dimethylaniline.

This proposition concerns photochemical and photophysical studies of the systems consisting of derivatives of $Ru(bipy)_3^{2+}$ and Fe^{3+} ions. The Ru complexes are given in Table 1. The experiments to be studied include the following 1) Determination of emission lifetimes of Ru complexes in Table 1 by laser flash spectroscopy [16]. The flash photolysis experiments will be done in a way similar to those for $Ru(bipy)_3^{2+}$ by Rabani et al. [17]. The absorbance versus time oscillograms will be collected immediately after the exciting flash at the wavelengths corresponding to emission wavelengths of each Ru complex. They are given in Table 1. From these studies the lifetimes of the emission of Ru complexes can be obtained. 2) Oxidative quenching of the Ru complexes with Fe^{3+} ions. The emission intensity of the system Ru^{2+}/Fe^{3+} will be measured as a function of concentration of Fe^{3+} ion. The Stern-Volmer constants (K_{SV}) can be calculated from the relation

$$(I_o/I)_{cor} = 1 + K_{SV}[Q]$$

where $$(I_o/I)_{corr} = \left(\frac{I_{ref}}{I}\right) \frac{[D]}{[D_{ref}]}$$

I_{ref} and I are the observed emission intensities without and with quencher present, respectively, $[D_{ref}]$ and [D] are the donor concentrations of an unquenched and quenched sample, respectively, and [Q] is the concentration of quencher. From K_{SV} the rate constant of the quenching reactions (k_q) is deduced from $K_{SV} = k_g\sigma_o$ where σ_o is the unquenched emission lifetime obtained from the flash experiments. Lastly, it is proposed that the photogalvanic effects of the system Ru^{2+}/Fe^{3+} be studied. The experiments will be done in the presence of polyvinylsulfate for the reason previously described. The electrochemical cell to be used will be of the type given below

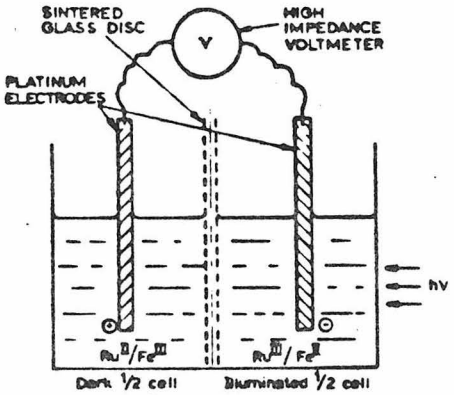

A photogalvanic cell containing $[Ru(bipy)_3]^{2+}$, Fe^{3+} and H_3O^+ in which the ruthenium complex functions as an electron donor

One compartment will be exposed to tungsten projection lamp (range 400-500 nm), while the other is kept in the dark. The potential will be determined by means of a high impedance voltmeter. It would be interesting to study the potential as a function of concentration of Ru and Fe^{3+} complexes, and of acid.

It is hoped that information gained from this study will not only increase the understanding of these newly synthesized Ru complexes, but also aid in the design and optimization of a more practical photogalvanic cell.

Table 1. Polypyridine complexes of ruthenium

Complexes	E^o (V vs. NHE)	λ_{max}, nm absorption	λ_{max}, nm emission
$[Ru(PTPI)]^{2+}$	-1.17	552	345
		496	400
$[Ru(bpy)_2(bpyrm)]^{2+}$	-1.29	420	600
$[Ru(bpy)_2(4,4'\text{-}Me_2bpyrm)]^{2+}$	-1.25	442	598
$[Ru(bpy)_2(2,9\text{-}Me_2phen)]^{2+}$	-1.18	452	588
		378	
$[Ru(bpy)_2(biimH_2)]^{2+}$	-0.93	448	595

PTPI ≡ 2-p-tolylpyridinecarboxaldimine,

bpyrm ≡ 2,2'-bipyrimidine,

$biimH_2$ ≡ 2,2'-biimidazole,

Taken from E. V. Dose and L. J. Wilson, Inorg. Chem. 17, 2660 (1978).

References

1. G. Porter and M. D. Archer, Interdiscip. Sci. Rev. 1, 119 (1976).

2. E. Robinowitch, J. Chem. Phys. 8, 351, 560 (1940).

3. R. Gomer, Electrochim. Acta 20, 13 (1975).

4. D. E. Hall, J. A. Eckert, N. N. Lichtin, and P. D. Wildes, J. Electrochem. Soc. 123, 1705 (1976).

5. H. T. Tien and J. M. Mountz, J. Electrochem. Soc. 125, 885 (1978).

6. K. Shigehara, M. Nishimura, and E. Tsuchida, Electrochim. Acta 23, 855 (1978).

7. D. E. Hall, P. D. Wildes, and N. N. Lichtin, J. Electrochem. Soc. 125, 1365 (1978).

8. N. Sutin and C. Creutz, Adv. Chem. Ser. 168, 1 (1978) and references cited therein.

9. P. J. Delaive, J. T. Lee, H. Abruna, H. W. Sprintschnik, T. J. Meyer, and D. G. Whitten, Adv. Chem. Ser. 168, 28 (1978) and references cited therein.

10. R. Bensasson, C. Salit, and V. Balzani, J. Am. Chem. Soc. 98, 3723 (1976).

11. R. C. Young, J. K. Nagle, T. J. Meyer, and D. G. Whitten, J. Am. Soc. 100, 4773 (1978).

12. C. T. Lin and N. Sutin, J. Phys. Chem. 80, 97 (1976).

13. G. L. Gaines, Jr., P. E. Belinken, and S. J. Valenty, J. Am. Chem. Soc. 100, 6549 (1978).

14. D. Meyerstein, J. Rabani, M. S. Matheson, and D. Meisel, J. Phys. Chem. 82, 1879 (1978).

15. D. Meisel, J. Rabani, D. Meyerstein, and M. S. Matheson, J. Phys. Chem. 82, 985 (1978).

16. M. A. West, in "Creation and Detection of the Excited State," W. R. Ware, ed., vol. 4 (Marcel Dekker, New York, 1976), Ch. 5.

17. D. Meisel, M. S. Matheson, W. A. Mulac, and J. Rabani, J. Phys. Chem. 81, 1449 (1977).

Proposition 6

The determination of the origin of the cyanolysable sulfur in molybdenum iron/sulfur flavin hydroxylases by xray absorption spectroscopy

Xanthine oxidase, xanthine dehydrogenase, and aldehyde oxidase contain similar prosthetic groups, namely molybdenum, iron-sulfur centers, and FAD in the same proportions [1-3]. They also have similar molecular weights and absorption spectra in both their native and deflavo forms [4]. The only difference among them is the substrate specificity as their name indicate . Inactivation of these enzymes by treatment with cyanide results in the extraction from these enzymes of sulfur which is eliminated as thiocyanate. Treatment of desulfoenzyme [5] with sulfide effects partial restoration of activity [1,2,6]. Under the reactivation conditions, the incorporation of $^{35}S^{2-}$ has been demonstrated, as has the release of $^{35}SCN^{-}$ on subsequent treatment with cyanide [1].

As for the origin of this cyanolysable sulfur in these enzymes, there are three possibilities: iron-sulfur prosthetic groups, cysteine residues, or persulfide groups present in these enzymes. The iron-sulfur chromophores have been ruled out by the fact that little difference in spectral properties in the visible absorption spectra upon cyanide inactivation is observed [1,2]. Furthermore, analysis of iron-sulfur chromophores for sulfur in both native and cyanide-inactivated enzymes shows identical amounts of sulfur present [1]. Massey and Edmonson [1] studied inactivation of xanthine oxidase with cyanide and arsenite in both aerobic and anaerobic experimental conditions, and proposed that the sulfur atoms released following cyanide treatment originated from a persulfide group that is present at the active centers of fully functional enzymes as shown below:

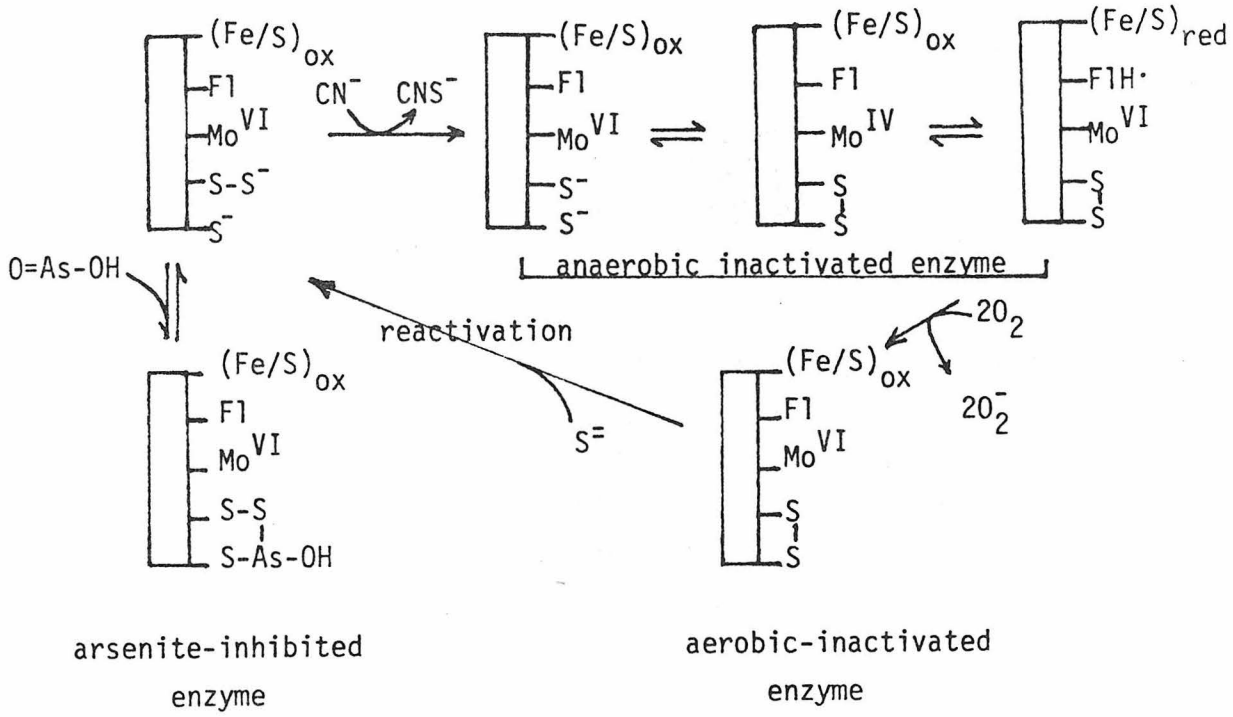

arsenite-inhibited enzyme

aerobic-inactivated enzyme

The presence of a disulfide bridge in enzymes has been documented earlier [7].

Recently, Caughlan [8] argued that an active center cysteine residue could equally well be considered as the source of cyanolysable sulfur. He proposed the following mechanism:

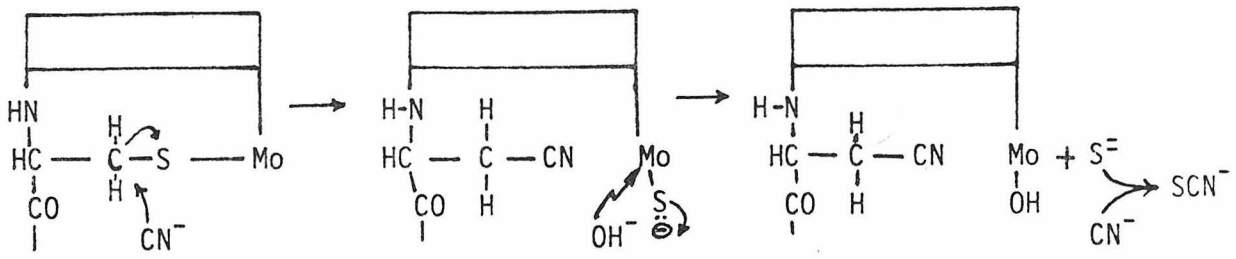

His mechanism is concentrated on the formation of cyanoalanine, that is, using $^{14}CN^-$ (assuming the cyanoalanine is stable), one should observe the fixation of 1 mol $^{14}CN^-$ and release of 1 atom sulfur, as $^{14}CNS^-$ per functional active site. This is indeed so in the cases of xanthine oxidase [9] and xanthine dehydrogenase [10]. Moreover, they also found that the presence of substrate or of competitive inhibitor reduced the amount of $^{14}CN^-$ bound, which is consistent with the binding of cyanide to the active site [9,10].

Therefore, it is proposed that the validity of these two mechanisms be tested by xray absorption spectroscopic studies (EXAFS) of these three molybdo-enzymes.

Extended xray absorption fine structure (EXAFS) is a very attractive technique for studying the structure-function relationship of large metalloproteins [11]. It has an advantage over xray diffraction studies due to the fact that it can be used equally well for systems in solution and in crystalline form. Structural information for several metalloproteins has appeared for the past three years, including

rubredoxin [12], hemoglobin [13], cytochrome P450 [14], nitrogenase [15], azurin [16], and sulfite oxidase [17]. The theory, instrumental considerations, and data analysis of EXAFS have been reviewed previously [18,19].

Basically xrays are absorbed by matter according to the formula $I = I_0 e^{-\mu x}$, where μ is the absorption coefficient, I_0 and I are the incident and transmitted xray intensities, respectively, and x is the thickness of the absorber. The xray absorption spectrum of a substance is characterized by several absorption edges which result from abrupt increases in μ at photon energies just sufficient to liberate an inner-shell electron from an atom. Rather than a gradual monatomic fall-off at photon energies above the value at the edge, the absorption spectrum of most substances is characterized by the presence of fine structure (see figure below).

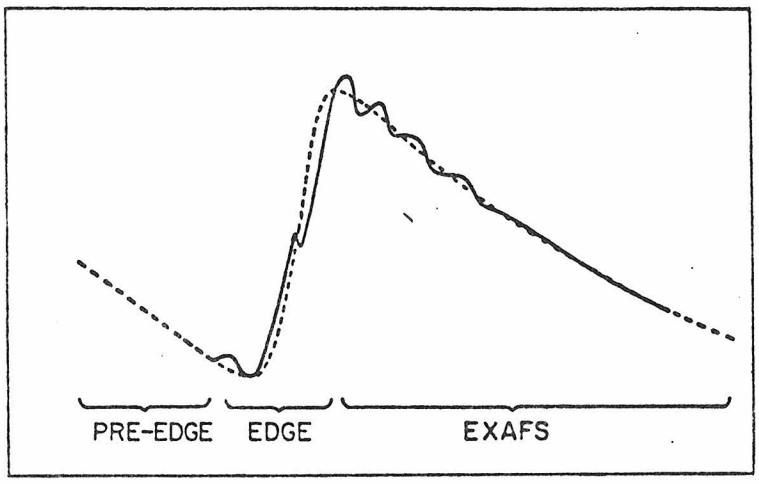

Figure 1. Schematic representation of a typical x-ray absorption spectrum. The edge region extends over 25-50 eV and the EXAFS is typically observable over several hundred to a thousand eV. The transition region between the edge structure and the EXAFS region remains ill-defined and poorly understood.

This fine structure is generally understood as occurring from interference of the low energy photoelectron scattering from neighbors surrounding the absorbing atom. Therefore, analysis of absorption edges and EXAFS fine structure (oscillations) can provide information about the metal site and its surrounding ligands.

The experiments which are proposed involve the collection of xray absorption spectra of both native and cyanide inactivated xanthine oxidase [20], xanthine dehydrogenase, and aldehyde oxidase. Once the spectra are obtained, treatment of the spectra including isolation of EXAFS from the absorption spectra, Fourier transform analysis, and curve fitting analysis could be done. The detailed considerations of data analysis have been reviewed elsewhere [19]. By comparing the results with those of model compounds [19], the validity of both mechanisms can be concluded. If the persulfide mechanism is valid, then the effect of sulfur on the EXAFS data in native enzyme should be expected to be different from that in the cyanide treated enzyme. On the contrary, if the second mechanism is valid, there should be no effect of sulfur observed in the cyanide treated enzyme.

References

1. W. Massey and D. Edmonson, J. Biol. Chem. 245, 6595 (1970).

2. W. F. Cleere and M. P. Caughlan, Biochem. J. 143, 331 (1974).

3. U. Branzoli and V. Massey, J. Biol. Chem. 249, 4346 (1974).

4. V. Branzoli and V. Massey, J. Biol. Chem. 249, 4339 (1974).

5. R. C. Bray, The Enzymes 12B, 299 (1975).

6. D. Edmonson, V. Massey, G. Palmer, L. M. Beacham, and G. B. Elion, J. Biol. Chem. 247, 1597 (1972).

7. D. Cavallini, G. Frederici, and E. Barboni, Eur. J. Biochem. 14, 169 (1970).

8. M. P. Caughlan, FEBS Lett. 81, 1 (1977).

9. I. Fridovich and P. Handler, J. Biol. Chem. 231, 899 (1958).

10. K. V. Rajagopalan and P. Handler, J. Biol. Chem. 242, 4097 (1967).

11. B. M. Kincaid, P. Eisenberger, K. O. Hodgson, and S. Doniach, Proc. Natl. Acad. Sci. USA 72, 2340 (1975).

12. R. G. Shulman, P. Eisenberger, W. E. Blumberg, and N. A. Stombaugh, Proc. Natl. Acad. Sci. USA 72, 4003 (1975).

13. P. M. Eisenberger, R. G. Shulman, G. S. Brown, and S. Ogawa, Proc. Natl. Acad. Sci. USA 73, 491 (1976).

14. S. P. Cramer, J. H. Dawson, K. O. Hodgson, and L. P. Hager, J. Am. Chem. Soc. 100, 7282 (1978).

15. S. P. Cramer, K. O. Hodgson, W. O. Gillum, and L. E. Mortenson, J. Am. Chem. Soc. 100, 3398 (1978).

16. T. D. Tullins, P. Frank, and K. O. Hodgson, Proc. Natl. Acad. Sci. USA 75, 4069 (1978).

17. S. P. Cramer, H. B. Gray, and K. V. Rajagopalan, J. Am. Chem. Soc., 101, 2772 (1979).

18. P. Eisenberger and B. M. Kincaid, Science 200, 1441 (1978).

19. S. P. Cramer and K. O. Hodgson, Proc. Inorg. Chem., submitted for publication.

20. The EXAFS of xanthine oxidase has just been completed by K. O. Hodgson's group, and the results revealed that Mo is coordinated by 2 oxo groups, 2 short Mo-S bonds and 1 medium Mo-S bond. Therefore, only cyanide inactivated form is to be studied in this proposition.